April 1984
Vol. 63 No. 4

AT&T
BELL LABORATORIES

TECHNICAL JOURNAL

A JOURNAL OF THE AT&T COMPANIES

Antenna Sidelobe Suppression

Mobile Radio

Channel-Bank Spectrometer Data

Interframe Cross-Connect System

Multipriority Stock-Order Assignment

AT&T BELL LABORATORIES TECHNICAL JOURNAL (ISSN0005-8580) is published by AT&T, 550 Madison Avenue, New York, NY 10022; C. L. Brown, Chairman and Chief Executive Officer; W. M. Ellinghaus, President; V. A. Dwyer, Vice President and Treasurer; T. O. Davis, Secretary.

The Journal is published ten times each year. The Computing Science and Systems section and the special issues are included as they become available. Subscriptions: United States—1 year $35; 2 years $63; 3 years $84; foreign—1 year $45; 2 years $73; 3 years $94. A subscription to the Computing Science and Systems section only is $10 ($12 foreign). Single copies of most issues of the Journal are available at $5 ($6 foreign). Payment for foreign subscriptions or single copies must be made in United States funds, or by check drawn on a United States bank and made payable to the Technical Journal and sent to AT&T Bell Laboratories, Circulation Dept., Room 1E335, 101 J. F. Kennedy Pky, Short Hills, NJ 07078.

Comments on the technical content of any article or brief are welcome. These and other editorial inquiries should be addressed to the Editor, AT&T Bell Laboratories Technical Journal, Room 1J319, 101 J. F. Kennedy Pky, Short Hills, NJ 07078. Comments and inquiries, whether or not published, shall not be regarded as confidential or otherwise restricted in use and will become the property of AT&T. Comments selected for publication may be edited for brevity, subject to author approval.

Printed in U.S.A. Second-class postage paid at Short Hills, NJ 07078 and additional mailing offices. Postmaster: Send address changes to the AT&T Bell Laboratories Technical Journal, Room 1E335, 101 J. F. Kennedy Pky, Short Hills, NJ 07078.

AT&T Bell Laboratories

Technical Journal

VOL. 63 APRIL 1984 NO. 4

AT&T BELL LABORATORIES TECHNICAL JOURNAL
Vol. 63, No. 4, April 1984
Printed in U.S.A.

An Experimental Investigation of Wide-Angle Sidelobe Suppression in a Pyramidal Horn-Reflector Antenna

by C. A. SILLER, JR.*

(Manuscript received September 22, 1983)

An experimental investigation into the suppression of wide-angle radiation from a pyramidal horn-reflector antenna is reported in this study. We show that lining the sidewalls or diffracting edges of this antenna with microwave absorber in the region of the visible aperture can lead to a marked reduction in sidelobe energy when the antenna is transversely polarized. Specifically, sidelobe reductions of as much as 10 dB are attainable over angular regions 40 degrees or more from the main beam. Though the described absorber treatment reduces wide-angle radiation, it can simultaneously increase and distinctly modify the character of near-in sidelobe structure. Data reported in this study are related to those of a recently published paper on selective near-in sidelobe reduction for a pyramidal horn-reflector antenna.

I. INTRODUCTION

The judicious application of microwave absorber as a method to modify reflector antenna sidelobe levels is a well-known and powerful technique. The approach is especially useful in the design of large-aperture antennas for terrestrial radio communications, where RF interference into or from other radio links is of paramount and increasing concern.

In a recent paper, R. A. Semplak[1] presented data from an experimental investigation of selective near-in sidelobe reduction of a pyram-

* AT&T Bell Laboratories.

idal horn-reflector antenna. That work is especially important for those interference situations occurring at small angles from the antenna beam, where the antenna discrimination is naturally less than that at large angles. On the other hand, wide-angle antenna radiation often limits the number of converging routes into a microwave radio station, a potentially acute situation at metropolitan junctions. For the pyramidal horn-reflector antenna, this latter problem was ameliorated for longitudinal polarization* by modifying radome attachment methods[3] and for transverse polarization by attaching multiple-edge blinders to the sidewalls of the antenna.[4,5] This paper is related to Semplak's, in that we also report the results of an experimental investigation into sidelobe suppression in a pyramidal horn-reflector. Unlike Semplak's investigation, however, our focus is on broadband, wide-angle sidelobe suppression. We show, as Semplak did, that sidelobe suppression is dependent on where the absorber is specifically situated, some locations being preferable to others. Additionally, our findings highlight the fact that radiation from this antenna is not completely modeled in prior analytic studies, since they fail to completely predict the radiation patterns of this antenna.

Pyramidal horn-reflector antennas, one generic type in a family of horn-reflectors, are of considerable practical significance.[6] They are widely deployed throughout the world, with domestic use alone exceeding more than 10,000. In Semplak's study a scaled-down precision antenna was measured at 30 GHz. For this study we used a precision, fiberglass antenna specifically designed for line-of-sight operation in the 4-, 6-, and 11-GHz common carrier bands.[7] This antenna stands approximately 16 feet high, has a 70-inch offset paraboloid illuminated by a 29-degree radial pyramidal horn, and is equipped (for a portion of this study) with 17-edge blinders.[8] A photograph of this antenna appears in Fig. 1. Though this fiberglass antenna has an aperture area only 60 percent that of the standard pyramidal antenna used in the AT&T Communications network (with a 90-inch focal length), it affords uncommonly good wide-angle sidelobe suppression. Indeed, in some cases this antenna provides far-out sidelobe levels lower than that of the larger pyramidal horn-reflector. These last observations are noteworthy since we demonstrate in this paper that the wide-angle radiation can be further suppressed by as much as 10 dB using absorber on the sidewalls of the antenna aperture. Unfortunately, this absorber

* We use the conventional definitions for longitudinal and transverse polarizations for this antenna.[2] For terrestrial applications, the pyramidal horn axis is perpendicular to the local plane of the earth, and longitudinal polarization corresponds to aperture electric fields perpendicular to that horizontal plane, while transverse polarization corresponds to electric fields parallel to the earth's surface. All patterns are measured in the transverse plane, an azimuthal plane parallel to the earth's surface.

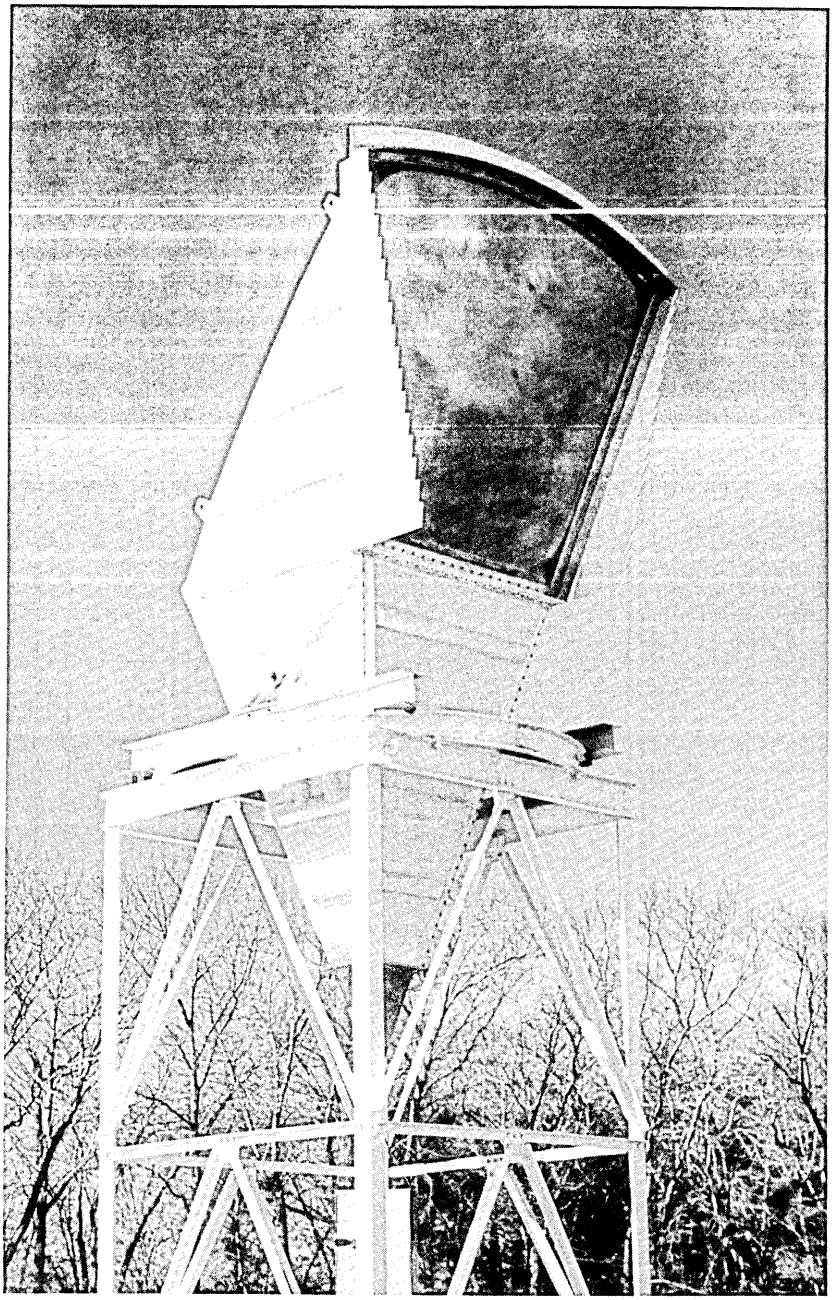

Fig. 1—Fiberglass, pyramidal, horn-reflector antenna equipped with multiple-edge blinders.

treatment simultaneously increases the near-in radiation lobes. It may well be that a combination of Semplak's methods, with selected microwave absorber placement like that described herein, could suppress sidelobe energy throughout major regions of the antenna's azimuthal radiation plane.

II. EXPERIMENTAL MEASUREMENTS AND INTERPRETATION

The experimental measurements reported in this study were carried out in two phases. In the first phase the antenna was equipped with 17-edge blinders, and the interior sidewalls in the region of the visible aperture were covered with 2-inch-thick, hair-type absorber. This absorber has a near-normal, specular power reflection coefficient less than 0.01 at 4 GHz, with an even smaller reflection at the higher frequencies used for part of this study. Absorber installation in the antenna is schematically illustrated in Fig. 2, where the multiple-edge blinders are omitted for clarity. In the second phase of the study, the blinders were removed, and a 3.5-inch strip of 2-inch-thick absorber was recessed and placed adjacent to the side diffracting edges. This situation, illustrated in Fig. 3, will be deferred for subsequent discussion.

2.1 Absorber-lined antenna interior

For this first phase of the investigation, complete principal and cross-polarized patterns were measured at a single frequency in each

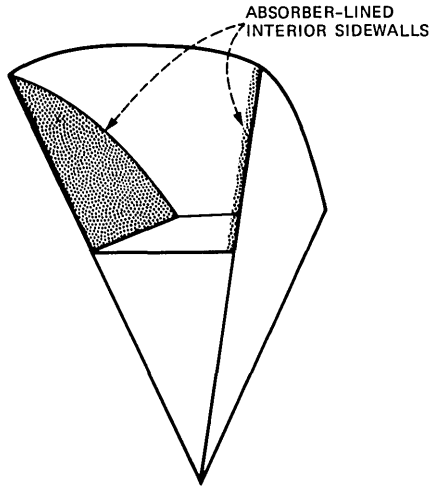

Fig. 2—Absorber installation on sidewalls of antenna. Edge blinders omitted for clarity.

of the 4-, 6-, and 11-GHz common carrier bands. Typical radiation pattern measurements, with and without absorber modification, are presented in Figs. 4 and 5, respectively. Complete 360-degree azimuthal plane patterns are measured in two stages. For radiation near the main beam, a 30-dB RF attenuator is used to limit power into the RF receiver. In the vicinity of 10 degrees, where the power is significantly lower, the attenuator is removed and the remainder of the pattern is measured. Patterns like those in Figs. 4 and 5, therefore, appear

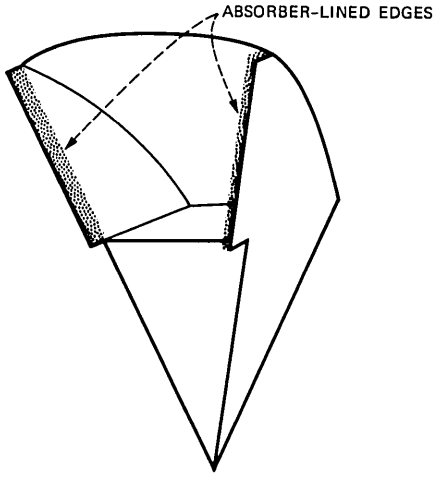

Fig. 3—Absorber installation along exterior, recessed, side diffracting edges. Edge blinders omitted for this portion of study.

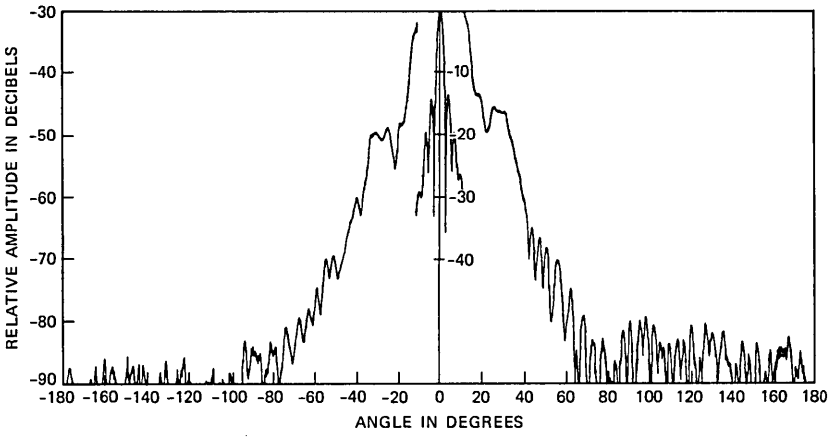

Fig. 4—Radiation pattern of antenna equipped with sidewall absorber and multiple-edge blinders. Transverse polarization, transverse (azimuthal) measurement plane; 3.95 GHz. (Note 30-dB change in ordinate scale near ±10 degrees.)

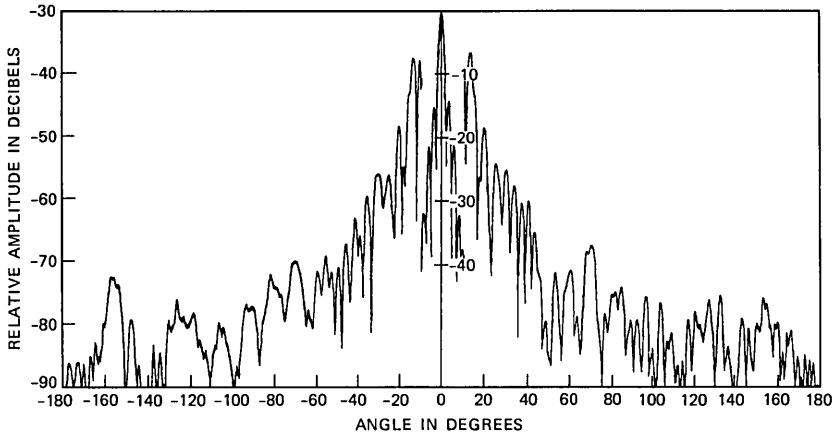

Fig. 5—Radiation pattern of antenna equipped with multiple-edge blinders but without absorber. Transverse polarization, transverse measurement plane; 3.95 GHz. (Note 30-dB change in ordinate scale near ±10 degrees.)

discontinuous with a corresponding 30-dB change in the ordinate. Because the absorber differentially affects near-in and wide-angle radiation sidelobes, results are most conveniently presented in separate subsections.

2.1.1 Absorber-lined antenna interior: effect on near-in sidelobes

Figures 6 and 7 present typical near-in sidelobe performance for 3.95-GHz longitudinal and transverse polarization. These figures also include comparative patterns for the antenna without absorber. The presence of absorber has little effect for longitudinal polarization (Fig. 6), while it notably raises the sidelobe levels and changes the character of sidelobe structure for transverse polarization (Fig. 7).

It will be remembered that the projected aperture fields for this antenna correspond closely to the illumination provided by dominant mode square waveguide. For longitudinal polarization, aperture fields are tangent to, and therefore vanish at, the antenna sides. Thus, for this polarization state, the aperture fields are unperturbed and hardly affect the near-in pattern except for a very slight decrease in aperture width (approximately 5.4 percent).

For transverse polarization, aperture electric fields are normal to the sidewalls and are greatly affected by the presence of absorber. Though one might initially think that the absorber attenuates and, therefore, acts to taper the aperture field, giving rise to reduced near-in sidelobes, Fig. 7 indicates this is not the case. This somewhat unexpected result could be attributable to aperture phase errors or blockage. Aperture phase errors tend to dominantly fill in the first

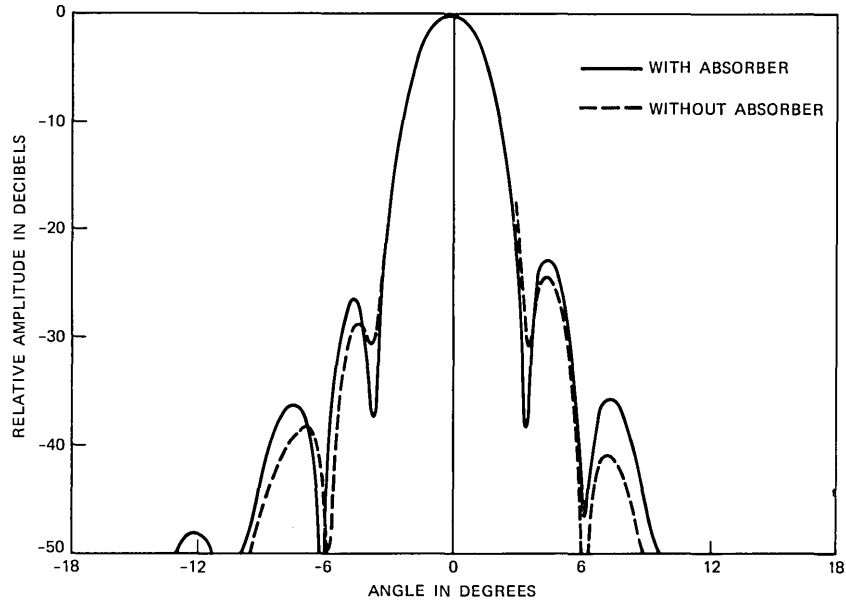

Fig. 6—Near-in radiation pattern. Antenna equipped with multiple-edge blinders. Longitudinal polarization, transverse measurement plane; 3.95 GHz.

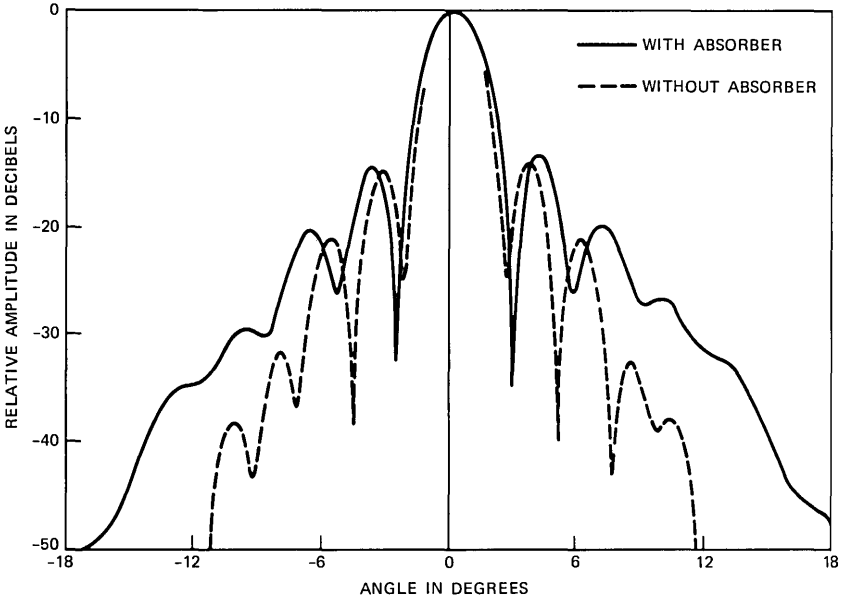

Fig. 7—Near-in radiation pattern. Antenna equipped with multiple-edge blinders. Transverse polarization, transverse measurement plane; 3.95 GHz.

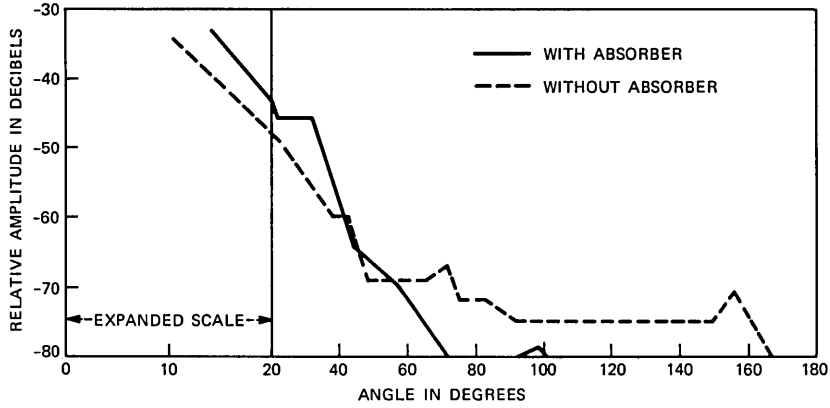

Fig. 8—Smoothed radiation pattern. Antenna equipped with blinders. Transverse polarization, transverse measurement plane; 3.95 GHz.

radiation null, with secondary nulls only secondarily affected.[9] Our measurements indicate that the first null is invariably preserved, with filling in occurring beyond that point. Moreover, phase errors could cause beam shifting in the longitudinal (vertical) plane, an effect not observed in these measurements. A more likely explanation is the excitation of certain higher-order modes, since the absorber was not recessed but partially blocked the aperture. (This effect would be minimal for longitudinal polarization since the fields are already low along the antenna sides.) This hypothesis is difficult to confirm without recessing the absorber, an impossibility in this particular design and an almost intractable problem from an analytic standpoint. It is worth noting though, that even radiation from the higher-order modes should be insignificant beyond several beamwidths (e.g., see Ref. 10), suggesting that the absorber fundamentally causes increased sidelobe levels in the approximate 15- to 40-degree region. This point is discussed further in Section III.

2.1.2 Absorber-lined antenna interior: effect on wide-angle sidelobes

Figures 4 and 5 show that absorber can significantly affect wide-angle sidelobe levels, especially for transverse polarization. This point is further illustrated in Figs. 8 through 11, which present smoothed* directivity patterns for 3.95-GHz principal and cross-polarized operation. Note that when the antenna receives a transversely polarized

* Smoothed radiation patterns are prepared by the widely accepted technique of drawing an envelope across *peaks* in the antenna radiation pattern. We show a 180-degree envelope that represents the worst sidelobe performance over the full 360-degree transverse measurement plane.

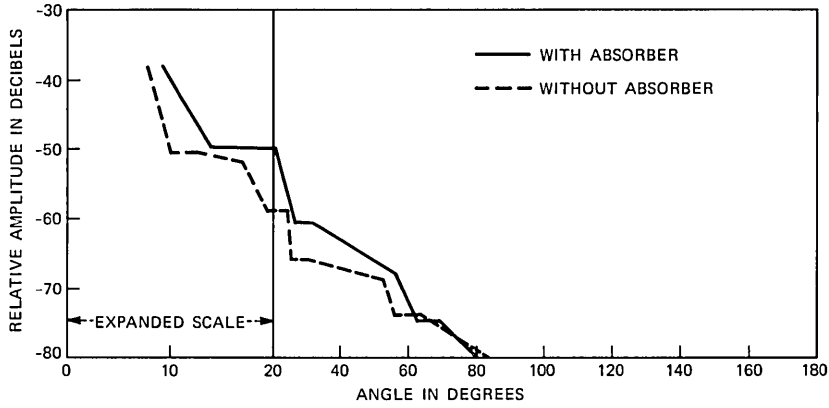

Fig. 9—Smoothed radiation pattern. Antenna equipped with blinders. Longitudinal polarization, transverse measurement plane; 3.95 GHz.

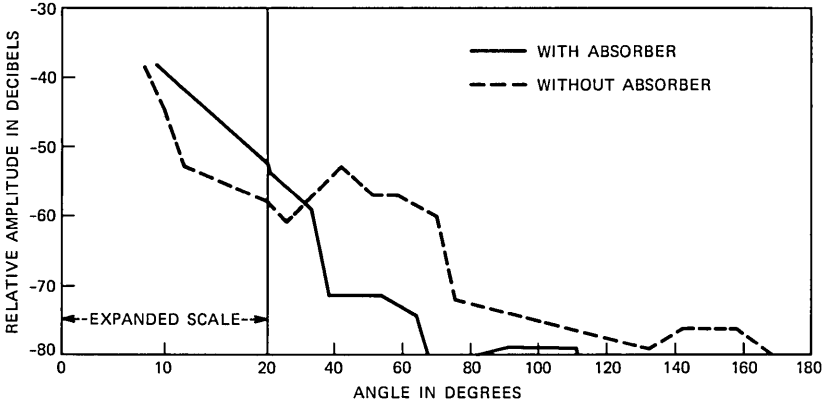

Fig. 10—Smoothed radiation pattern. Antenna equipped with blinders. Transverse polarization response of longitudinal polarization illumination, transverse measurement plane; 3.95 GHz.

signal (co- or cross-polarized), sidelobes beyond approximately 40 degrees are generally reduced, sometimes by 10 dB or more. Even for longitudinally polarized reception, some improvement can be attained, though the differences are not as significant. Radiation patterns were also measured for 6- and 11-GHz operation. These measurements show the same qualitative effects as discussed above and are therefore omitted for brevity.

Wide-angle sidelobe suppression, like that noted above, is commonly attributed to reduced edge diffraction. If that were the case, a narrow strip of absorber adjacent to the side diffracting edges would accom-

plish the same function. This issue was explored in the second phase of the investigation.

2.2 Absorber-lined diffracting edges

In the second phase of our study, the multiple-edge blinders were removed, and a 3.5-inch strip of 2-inch-thick absorber was recessed and placed adjacent to each of the side diffracting edges, as illustrated by Fig. 3. Transverse polarization patterns were measured, with a typical result shown in Fig. 12 (near-in sidelobes were unaffected). We have noted that beyond approximately 40 degrees, the narrow absorber strip reduces sidelobes by 4 dB or more. This performance, while less

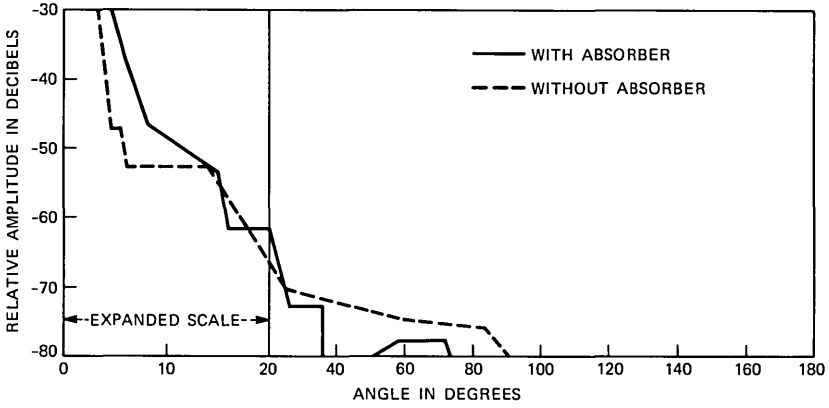

Fig. 11—Smoothed radiation pattern. Antenna equipped with blinders. Longitudinal polarization response to transverse polarization illumination, transverse measurement plane; 3.95 GHz.

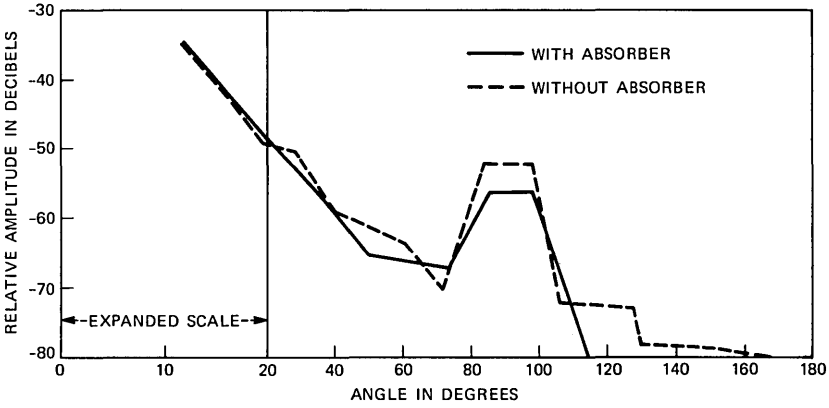

Fig. 12—Smoothed radiation pattern. Antenna not equipped with blinders. Transverse polarization, transverse measurement plane; 3.74 GHz.

impressive than the more consistent suppression exemplified by Fig. 8, shows the benefit of using absorber, and more clearly defines the diffraction-limited region of this antenna as lying beyond 40 degrees in the azimuthal plane.

After comparing the two absorber placement tests described above, we conclude: (1) within approximately 15 degrees of the main beam, lining the antenna sidewalls increases sidelobe levels, an effect probably due to the excitation of higher-order modes; (2) beyond approximately 40 degrees, the radiation pattern is dominantly affected by exterior aperture edge diffraction, and absorbent materials can significantly reduce that contribution to the far-field pattern; and (3) in the intermediate angular region of 15 to 40 degrees, absorber on the sidewalls affects the radiation pattern in unexpected ways. This last point is further developed in the next section.

III. ANALYTIC METHODS FOR DESCRIBING RADIATION FROM PYRAMIDAL HORN-REFLECTOR ANTENNAS

The Aperture Field Method (AFM) and Geometrical Theory of Diffraction (GTD) are the principal analytic methods used to describe radiation from large-aperture, reflector antennas. A number of different studies have shown the AFM to be quite accurate in predicting

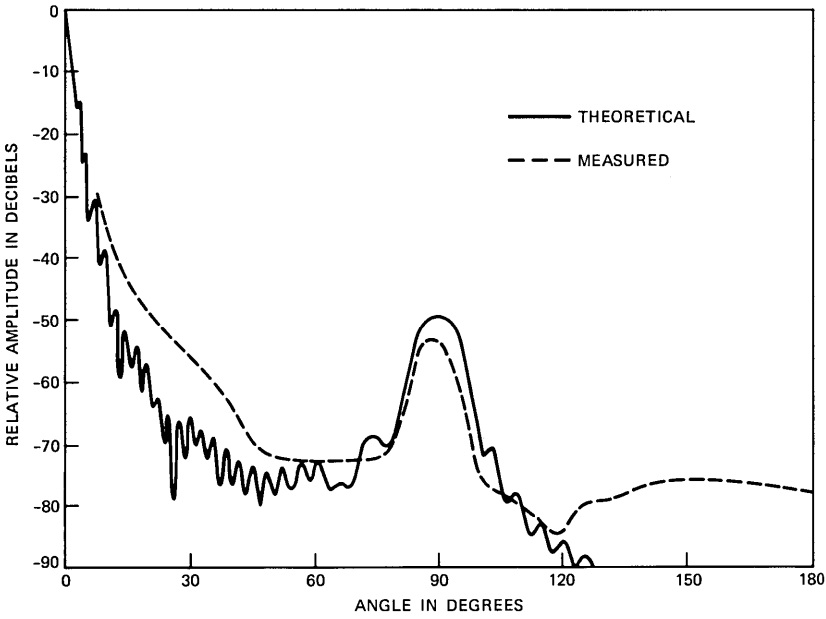

Fig. 13—Measured and theoretical patterns of a pyramidal horn-reflector antenna without multiple-edge blinders. Transverse polarization, transverse measurement plane; 4 GHz (adapted from Ref. 13).

sidelobe behavior down to -40 dB and within approximately 10 degrees of the main beam of a pyramidal horn-reflector antenna,[2,11,12] Theoretical limitations associated with this method for wide-angle radiation are well established.

Wide-angle radiation patterns are predicted using GTD. Transverse-plane analyses of the pyramidal horn-reflector by Thomas[4,5] and Siller[8] considered single diffraction from the exterior aperture edges with equivalent magnetic line sources. Their theoretical patterns showed good qualitative agreement with measured characteristics. Mentzer has used both the AFM and a more complete GTD model to analyze radiation from this antenna.[13] This latter analysis includes radiation from both the top and bottom aperture edges, using slope wave diffraction, as well as reradiative multiple diffraction. A result from Mentzer's study is presented in Fig. 13 for transverse polarization of the aforementioned standard horn-reflector antenna. Envelope discrepancies beyond 120 degrees, where the pattern is nearly 80 dB down, are not important and are probably due to radiation leakage during the measurements and/or small inadequacies in the analytic model. The pattern disparity between approximately 10 and 45 degrees is more prominent, however, and suggests radiating sources heretofore unconsidered.

Mentzer's analytic study did not include two sources of radiation that are intimately affected by absorber on the sidewalls of the visible antenna aperture. The first of these sources corresponds to wedge diffraction at the interface of the paraboloid and horn sidewalls. Radiation from these two wedges would be influenced by Semplak's absorber placement, as well as our own (see Fig. 2, appropriate to the first phase of this study). The second of the unconsidered sources corresponds to an infinite set of surface currents imaged into the walls of the visible aperture from the offset paraboloidal reflector. These imaged sources would also be influenced by our first absorber treatment. Simple ray optics and diffraction theory indicate that both of the aforementioned sources would radiate predominantly into the 0- to 45-degree region, though their relative contribution to the composite radiation pattern is presently unknown.

IV. CONCLUSIONS

An experimental investigation into the suppression of wide-angle radiation from pyramidal horn-reflector antennas is reported in this study. We first show that lining the sidewalls of the antenna dramatically affects sidelobe structure and energy, with sidelobe reduction occurring over a wide angular region for transverse polarization operation. Elevated near-in sidelobes are probably due to some aperture blockage, as well as the modification of radiation sources that have

not previously been considered in theoretical analyses of this antenna. Subsequent absorber placement on the antenna's side diffracting edges also leads to wide-angle sidelobe suppression and helps to identify the pattern region beyond approximately 40 degrees as predominantly diffraction limited.

These experimental results are related to a recent study by R. A. Semplak on selective near-in sidelobe reduction for a pyramidal horn-reflector antenna. Taken together, the investigations suggest that judicious microwave absorber placement could suppress sidelobe energy throughout major (i.e., near-in and far-out) regions of the azimuthal radiation plane.

V. ACKNOWLEDGMENT

The author is pleased to acknowledge J. E. Richard's assistance in making the radiation patterns reported in this study.

REFERENCES

1. R. A. Semplak, "Measurements of Selective Near-In Sidelobe Reduction of a Pyramidal, Horn-Reflector Antenna," B.S.T.J., *62,* No. 3 (March 1983), pp. 595–605.
2. A. B. Crawford et al., "A Horn-Reflector Antenna for Space Communications," B.S.T.J., *40,* No. 4 (July 1961), pp. 1095–116.
3. R. R. Grady, "Sidelobe Control in the Horn-Reflector Antenna," Proc. Nat. Elec. Conf., *26* (December 1970), pp. 360–3.
4. D. T. Thomas, "Analysis and Design of Elementary Blinders for Large Horn-Reflector Antennas," B.S.T.J., *50,* No. 9 (November 1971), pp. 2979–95.
5. D. T. Thomas, "Design of Multiple-Edge Blinders for Large Horn-Reflector Antennas," IEEE Trans. Ant. Propag., *AP-21* (March 1973), pp. 153–8.
6. C. A. Siller, Jr., "The Influence of Aperture Shape on the Radiation Patterns of Horn-Reflector Antennas," IEEE Trans. Ant. Propag., *AP-27* (May 1979), pp. 435–8.
7. C. A. Siller, Jr., "A Fiberglass Pyramidal Horn-Reflector Antenna for Point-to-Point Microwave Communications," 1974 IEEE-APS Int. Symp., Conf. Record, Session AP-S 9 (June 1974), pp. 239–41.
8. C. A. Siller, Jr., "Design of Multiple-Edge Blinders for Pyramidal Horn-Reflector Antennas," IEEE Trans. Ant. Propag., AP-23 (September 1975), pp. 695–8.
9. H. Jasik, "Fundamentals of Antennas," Chapter 2 in *Antenna Engineering Handbook,* H. Jasik, ed. New York: McGraw-Hill, 1961.
10. H. F. Lenzing, "Higher-Order Mode Excitation in Large-Aperture Receiving Antennas," The Microw. J., *12* (December 1969), pp. 61–5.
11. P. E. Butzien and C. A. Siller, Jr., "Spatial Radiation Characteristics of a Pyramidal Horn-Reflector Antenna," 1977 IEEE APS-URSI Symp., Conf. Record, Session AP-S 15 (June 1977), pp. 436–9.
12. P. E. Butzien, "Three-Dimensional Radiation Characteristics of a Pyramidal Horn-Reflector Antenna," B.S.T.J., *60,* No. 6 (July-August 1981), pp. 913–21.
13. C. A. Mentzer, "Analysis and Design of High Beam Efficiency Aperture Antennas," Dissertation, the Ohio State University, 1974.

AUTHOR

Curtis A. Siller, Jr., B.S.E.E., 1966, M.S., 1967 (Plasma Physics), Ph.D., 1969 (Electrical Engineering), University of Tennessee, Knoxville; AT&T Bell Laboratories, 1969–1978, 1979—. Mr. Siller's earliest experience at AT&T Bell Laboratories was in the analysis and design of large aperture antennas

for terrestrial line-of-sight microwave communications. Subsequently, he initiated an exploratory investigation of adaptive transversal equalization to mitigate the degradation of advanced digital radio systems during dispersive multipath fading. His most recent interests are in digital signal processing, particularly new techniques for digital filtering. Member, Phi Eta Sigma, Eta Kappa Nu, Tau Beta Pi, Phi Kappa Phi, Sigma Xi, American Association for the Advancement of Science, and the IEEE.

AT&T BELL LABORATORIES TECHNICAL JOURNAL
Vol. 63, No. 4, April 1984
Printed in U.S.A.

BER Degradations Caused by Switching in Digital Mobile Radio Systems Using Base Station Diversity

By B. S. GLANCE*

(Manuscript received August 3, 1983)

This paper presents a study of the Bit Error Rate (BER) degradation resulting from base station switching in digital mobile radio systems using base station diversity to combat shadow fading. The degradation is caused by the discontinuities of the signal received by the mobile unit when transmission is switched from one base station to another. To evaluate this effect, a simple statistical model has been devised for the spatial variations of shadow fading. It consists of a one-parameter spatial autocorrelation function for the (Gaussian) decibel value of the fading loss, which can be easily simulated. The single parameter is a correlation length, which can be varied to emulate different fading conditions in the urban environment. The shape of the autocorrelation function can similarly be varied. This model was used to evaluate the BER degradation of mobile radio systems using Phase-Shift-Keying (PSK) modulation. The results show that, in worst-case conditions, the BER is insignificantly affected by switching for BER values above 9×10^{-5} for two-PSK and 1.5×10^{-4} for four-PSK. Adding a threshold into the switching test can reduce or increase the switching degradation, depending on the threshold value.

I. INTRODUCTION

Shadow fading in mobile radio propagation is caused by large obstacles blocking the transmission path. This effect is combated in cellular systems by using base station diversity.[1] The arrangement consists of several base stations at different locations in the cell, which

*AT&T Bell Laboratories.

provide path diversity. Only one base station transmits to the mobile receiver. Switching tests are done at regularly spaced intervals, Δx, to compare the signals received by the base stations. As the mobile unit moves, the transmission is switched from one base station to another according to the base station receiving the strongest signal.

In mobile radio systems using digital modulation, the signal discontinuities caused by base station switching give rise to transient errors in the recovery of the digital information. The purpose of the present study is to evaluate the degradation of the Bit Error Rate (BER) due to switching in a cellular system using Phase-Shift-Keying (PSK) modulation and three-corner base station diversity.

Section II defines the mobile radio system used for this evaluation. A simple shadow model (including spatial variations) is proposed in Section III to emulate the shadow fading conditions in an urban environment. This model is used in Section IV to determine the statistics of the distance traveled by a mobile unit between consecutive switches. This is done for different mobile paths covering the surface of a cell and for different fading conditions. Section V evaluates the number of errors caused by switching, and Section VI evaluates the BER degradation caused by switching for two-PSK modulation. These calculations are done for different signaling rates, different distances between switching tests, and different fading conditions. The same evaluation is then replicated in Section VII for four-PSK modulation. Finally, Section VIII assesses the effect on the BER of a threshold condition in the switching test.

II. THE MOBILE RADIO SYSTEM

Consider a cellular, digital mobile radio system having a three-frequency reuse plan, and with three base stations per cell located at alternate corners (see Fig. 1). Shadow fading is combated by selecting the base station receiving the strongest mobile signal. This is achieved by periodically comparing the medium-term power of the mobile signals received by the three base stations; the power is measured over a time period adjusted so as to average out the Rayleigh fading.[2]

The power measured by a base station depends on the distance between the mobile receiver and the base station, and on the shadow attenuation affecting that transmission path. The measurement corresponding to the jth path, $j = 1, 2, or\ 3$, can be expressed by

$$\langle S_j \rangle = S_o \frac{L_j}{r_j^{\gamma}}, \tag{1}$$

where r_j is the distance in miles; S_o is the median power received at a distance of one mile; L_j is a random variable with a log-normal distribution, representing the shadow attenuation; and γ is the prop-

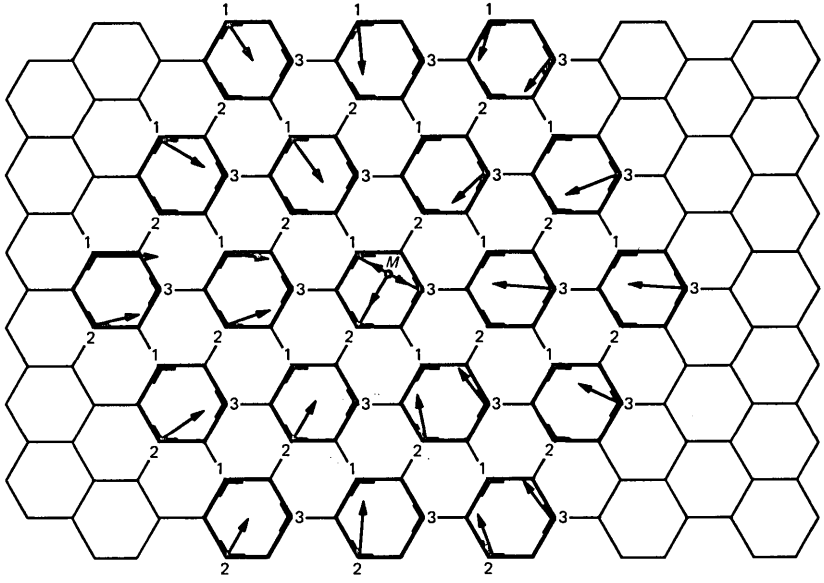

Fig. 1—Three-frequency reuse cellular configuration, with base stations that interfere with desired signal at mobile receiver.

agation law exponent. In our calculations, we assume that γ is 3.8 and that the standard deviation of the Gaussian variable 10 $\log_{10}\{L\}$ is 8 dB.[3,4]

The signal modulation is either two-PSK or four-PSK, with differential encoding. (Differential encoding is required because the mobile receiver cannot retrieve the absolute value of the carrier phase.) The signal at the receiver output of the mobile unit consists of several maximal-ratio-combined space diversity signals, where we assume three branches for two-PSK and four branches for four-PSK. The number of combining branches in each case represents the minimum number required to obtain a medium-term bit error rate $\langle BER \rangle$ below 10^{-3} with 90-percent probability. The combining can be done at both sides of the transmission path or at the base station only by using time-division retransmission;[5] the switching-induced degradation studied here is independent of which scheme is used.

The system performance is assumed to be primarily limited by the interference originating from transmitters using the same radio channel in other cells. Most of the interference comes from the nearest 18 cells[4] (see Fig. 1). The medium-term signal-to-interference ratio ($\langle SIR \rangle$) is given for the jth base station to mobile unit path by

$$\langle SIR_j \rangle = \left(\frac{L_j}{r_j^\gamma}\right) \Bigg/ \sum_{i=1}^{N} \frac{L_i}{r_j^\gamma} \qquad j = 1, 2, \text{ or } 3. \tag{2}$$

For the reception at the mobile unit, the quantity r_i represents the distance between the ith interfering base station and the mobile unit; L_i is the shadow attenuation of the same path; and N is the number of interfering base stations, a quantity varying between 0 and 18, depending on which base stations are transmitting in the 18 interfering cells. The quantity $\langle BER \rangle$ is a function of $\langle SIR \rangle$ for an uninterrupted base station–mobile radio link. When the base station is switched, additional errors caused by the signal discontinuity increase the $\langle BER \rangle$. The resulting value of $\langle BER \rangle$ thus depends on the switching frequency. For a given mobile unit path, the switching frequency varies according to the position of the mobile unit relative to the three base stations and with the values of the shadow attenuation of the three corresponding paths. A shadow fading model is proposed in the next section for use in calculating this effect.

III. THE SHADOW FADING MODEL

Measurements of the spatial variation of the shadow fading in an urban environment have been reported previously.[6] No statistical analysis has been made for results of this kind. It was therefore decided to represent shadow fading along a mobile unit path by a simple one-dimensional spatial autocorrelation function for the Gaussian random variable $10 \log_{10}\{L\}$, which can be easily simulated. The dependence of the autocorrelation function on the perpendicular direction to the mobile unit path is neglected by assuming a relatively large spacing between parallel paths. The autocorrelation function is characterized by a single parameter, defined as a correlation length, which can be varied to emulate different fading conditions in the urban environment. The same effect is also achieved by changing the shape of the autocorrelation function. This is done in the present study by using two different shapes. The first one, given by

$$\rho_1(x) = e^{-x/x_1}, \tag{3}$$

simulates fading conditions having a relatively fast decorrelation between fades. The second one, given by

$$\rho_2(x) = e^{-x/x_2}(1 + x/x_2), \tag{4}$$

represents fading conditions having a slower decorrelation for distances that are small relative to the decorrelation length. The two constants, x_1 and x_2, are adjusted so that the decorrelation length is the same for both functions, the correlation length being defined as the distance x, which makes both correlation functions decrease to 0.1.

The autocorrelation function $\rho_2(x)$ represents more realistically the spatial variation of shadow fading than does $\rho_1(x)$, which we believe

to be pessimistic because it decays faster near the origin. The shadow fading model is used in the next section to analyze the switching statistics, specifically, the statistics of the distance traveled by a mobile unit between consecutive base station switches.

IV. SWITCHING STATISTICS

The switching statistics are evaluated using a Monte Carlo computer program simulating a mobile receiver moving along a given path covering the entire cell. For simplicity, the simulation is assumed to be statistically stationary for the shadow fading process, including a fixed correlation length over the path. The same calculations are repeated for different values of the correlation length and for the two autocorrelation functions cited above. By assuming an artificial environment (e.g., statistically stationary, with fixed correlation length), but considering different shapes and parameter values, we aim to identify the critical features of the shadow fading process.

The signal received by the mobile unit originates from the base station that received the strongest medium-term power $\langle S_j \rangle$ [see eq. (1)] during the past measurement. A switching test is done after each mobile unit displacement, $\Delta\chi$, to compare the updated value of $\langle S_j \rangle$ to the similar quantities measured by the two other base stations. When $\langle S_j \rangle$ falls below one of the two other measurements, transmission is switched to the base station providing the strongest value. Otherwise, transmission is continued from the same base station until the next test.

The simulation is done for three different mobile unit paths to determine the influence of the path on the switching statistics. The diagonal of the hexagonal cell is taken to be 3000m. The first path is a meander made of parallel lines spaced every $(150\sqrt{3})/2$ meters, starting at base station 2 and directed towards the apex located between base stations 2 and 3 (see Fig. 2a). The second path is also a meander, perpendicular to the first one, starting from the apex located between base stations 1 and 2 and directed towards base station 1 (see Fig. 2b). The third path consists of concentric circles about the cell center, which is the origin of the mobile unit path (see Fig. 2c).

The distributions of the cumulative probability of the distance traveled by the mobile unit between consecutive switches is evaluated for fading conditions having decorrelation lengths of 50, 100, and 200m. This is done in each case for various values of the displacements, Δx. Two significant results emerge. First, the distributions corresponding to different decorrelation lengths can be fitted on the same curves when the distance, x, and the displacement, Δx, are both normalized by the decorrelation length, x_d. Second, the results are almost independent of the path followed by the mobile unit. Both these findings

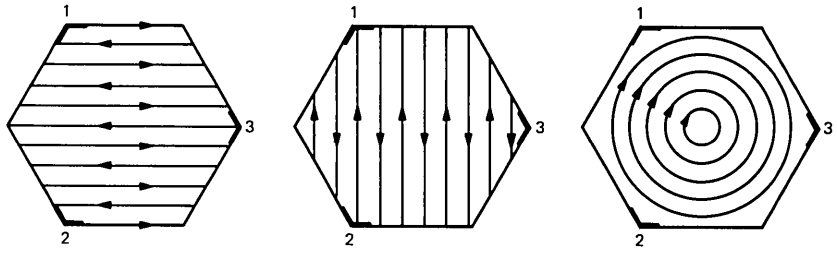

Fig. 2—Three different mobile unit paths used for calculations of switching statistics.

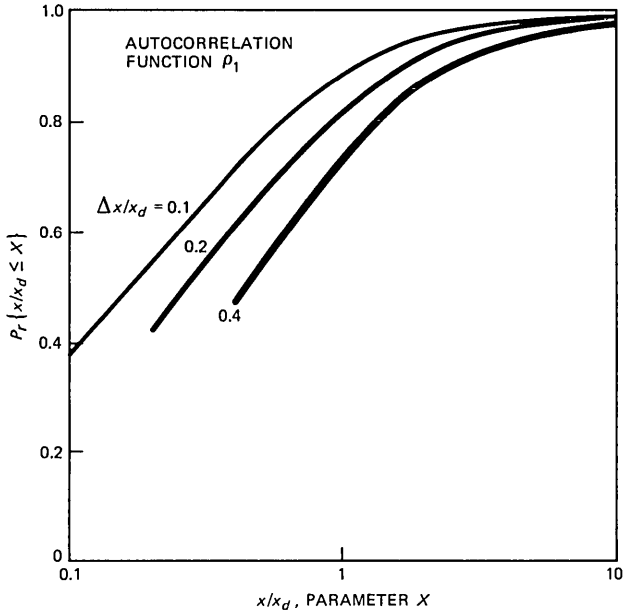

Fig. 3—Cumulative probability distribution of distance traveled by mobile unit between consecutive base station switches, calculated using autocorrelation function ρ_1.

are confirmed by the thickness of the curves in Fig. 3, which represent the spreads due to superimposing results for the three paths and the three decorrelation lengths. Note that the distributions are, however, dependent on the parameter Δx. These curves are all for the autocorrelation function ρ_1, [see (3)].

Similar results are obtained for the autocorrelation function ρ_2 [see (4)], as shown in Fig. 4. In this case, the spread due to the different paths is slightly larger, but the dependence on the parameter Δx is smaller and becomes almost nil for normalized values equal to or below 0.2. This effect is shown in Fig. 5, which compares the distribution

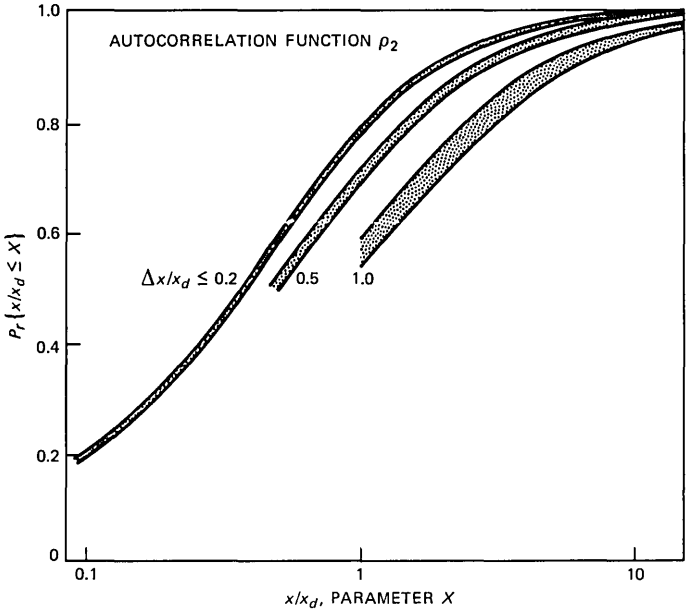

Fig. 4—Same results as in Fig. 3, for the autocorrelation function ρ_2.

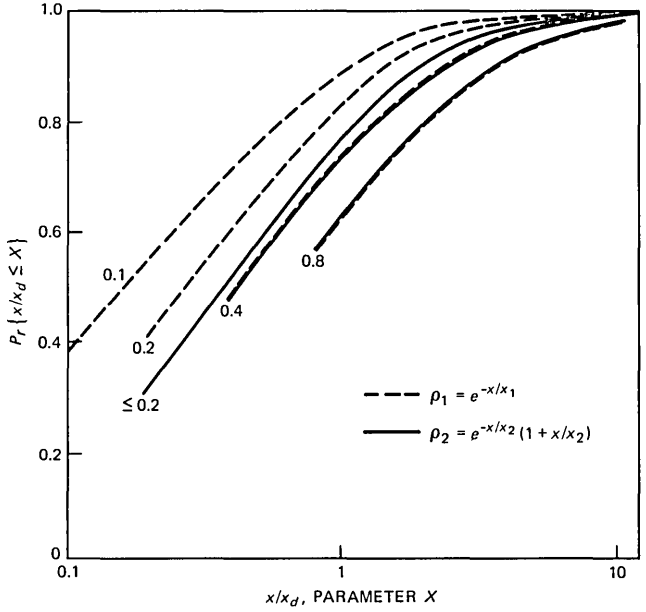

Fig. 5—Comparison between cumulative probabilities obtained with ρ_1 and ρ_2 for same normalized mobile unit displacement values of 0.1, 0.2, 0.4, and 0.8.

obtained for the two autocorrelation functions, calculated for a decorrelation length of 50m and displacements of 5, 10, 20, and 40m. As we expected, the divergence between the distributions is significant for Δx values below 10m, but becomes almost nil when Δx is increased to 20m—a value above which both autocorrelation functions are almost identical. Similar results are observed for the distributions calculated for the longer decorrelation lengths.

Another statistical result of interest is the average distance $\langle x \rangle$ traveled by the mobile unit between switches versus the mobile unit displacement, Δx. This quantity is averaged over all the distances given by the distribution for a given path, correlation function, and decorrelation length. These results corresponding to the autocorrelation functions ρ_1 and ρ_2 are shown, respectively, in Figs. 6 and 7, where

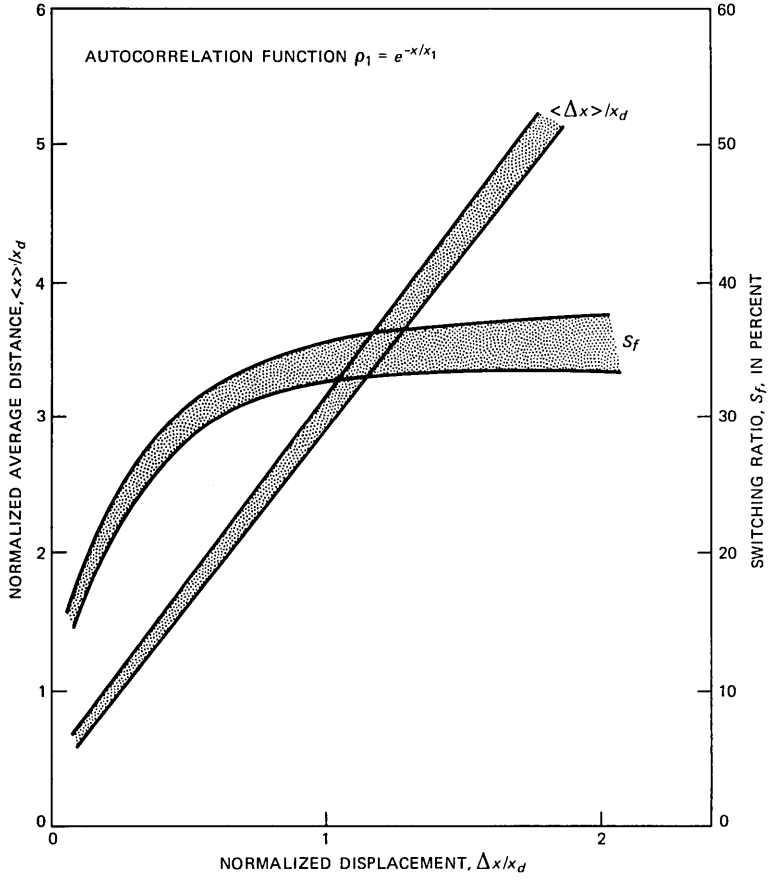

Fig. 6—Average distance and switching frequency versus mobile unit displacement calculated with ρ_1.

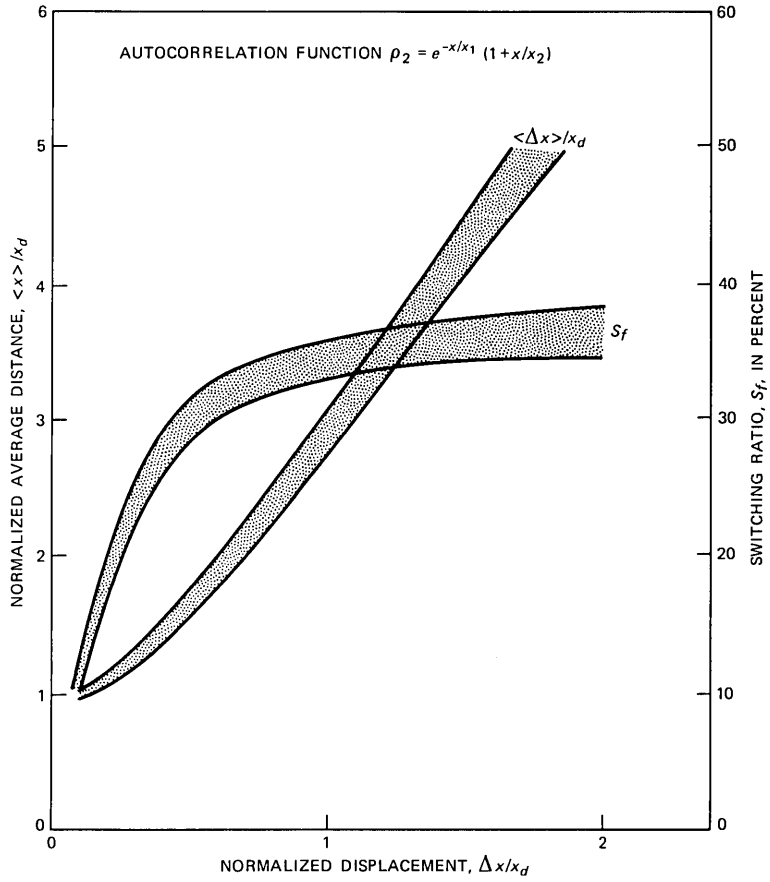

Fig. 7—Same results as for Fig. 6, calculated with ρ_2.

$\langle x \rangle$ and Δx are normalized by x_d. The spread shown by these curves is again due to superimposing the results for the paths and different decorrelation lengths. The other curves shown in these figures represent the switching frequency, measured as the ratio of the number of switches to the total number of tests along the path. Note that the frequency increases to about one third when the displacement is above one decorrelation length. This maximum frequency is equal to that given by random switching between the three base stations. Note also that the switching frequency is substantially reduced only when $\Delta x/x_d < 0.1$, a condition fulfilled for fading distribution having long decorrelation lengths.

V. ERRORS CAUSED BY SWITCHING

Switching between base stations causes phase and amplitude dis-

continuities in the signal received by the mobile unit. These effects generate errors in the demodulation process, in addition to those produced by the interference corrupting the desired signal. The number of switching errors depends on the type of demodulator used for recovering the data. Differential detection, which is only sensitive to phase discontinuities, gives rise, on average, to one-half error per switch because the phase discontinuities are random and uniformly distributed. The switching errors generated by a coherent demodulator lead to a more complex calculation, which depends on the phase and on the amplitude discontinuities.

The amplitude discontinuity is equal to the difference between the instantaneous signal levels received before and after the switch. In the radio mobile environment, these quantities vary randomly over very short distances. Note that the amplitude of the preswitch signal can be larger than that of the postswitch signal, even when the mean value of the latter signal is larger than that of the former. The two instantaneous amplitudes are described by independent random variables having a chi-square distribution of order three for two-PSK signals and order four for four-PSK signals, according to the diversity design defined in Section II.

The number of switching errors is evaluated for a demodulator using "modulation wipeoff" carrier recovery, according to a recently published technique.[7] This is done by assuming that the preswitch and postswitch signals have the same medium-term power and the same medium-term SIR. This approximation is valid when the interval between switching tests is relatively small compared to a decorrelation length. Under these assumptions, one finds that the average number of errors varies between one and two per switch for two-PSK differentially encoded signals, when the $\langle SIR \rangle$ increases from 0 dB to infinity. The same quantity for four-PSK differentially encoded signals varies between 1 and 2.6 errors per switch for the same range of $\langle SIR \rangle$ values (see Fig. 8).

Differential detection thus provides better protection against switching errors. For two-PSK, it also gives nearly the same performance as coherent detection in the absence of switching. For example, the values of $\langle BER \rangle$ given by the differential and coherent detection are, respectively, 4.8×10^{-4} and 3.1×10^{-4} for $\langle SIR \rangle = 9.6$ dB in the case of a three-branch combiner. (The value 9.6 corresponds to the 90-percentile $\langle SIR \rangle$ given by the cellular configuration described in Section II.) This result comes from relations[8]

$$\langle BER \rangle_{2\phi,\mathrm{Dif}} \approx \frac{1}{2} \frac{1}{[1 + \langle SIR \rangle]^3} \tag{5}$$

and

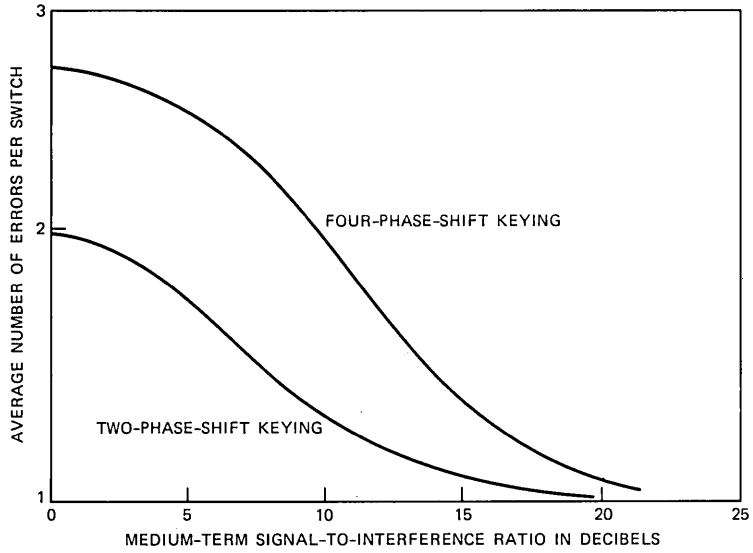

Fig. 8—Average number of switching errors versus $\langle SIR \rangle$, calculated for two-PSK and four-PSK coherently demodulated signals.

$$\langle \mathrm{BER} \rangle_{2\phi,\mathrm{Coh}} = 1 - \sqrt{\frac{\langle SIR \rangle}{1 + \langle SIR \rangle}} \left\{ 1 + \frac{1}{2[1 + \langle SIR \rangle]} + \frac{3}{8[1 + \langle SIR \rangle]^2} \right\}. \quad (6)$$

For four-PSK, on the other hand, differential detection is considerably less efficient than coherent detection. In this case, the $\langle BER \rangle$ expressions (5) and (6), applied to a four-branch combiner, become, respectively,[8]

$$\langle BER \rangle_{4\phi\mathrm{Dif}} \approx \frac{1}{\left[1 + \langle SIR \rangle \left(1 - \frac{1}{\sqrt{2}}\right)\right]^2} \quad (7)$$

and

$$\langle BER \rangle_{4\phi\mathrm{Coh}} = 1 - \sqrt{\frac{\langle SIR \rangle / 2}{1 + \langle SIR \rangle / 2}} \cdot \left\{ 1 + \frac{1}{2\left(1 + \frac{\langle SIR \rangle}{2}\right)} + \frac{3}{8\left(1 + \frac{\langle SIR \rangle}{2}\right)^2} + \frac{15}{48\left(1 + \frac{\langle SIR \rangle}{2}\right)^3} \right\}. \quad (8)$$

The $\langle BER \rangle$ calculated for the same $\langle SIR \rangle$ value is within the required value of 10^{-3} for coherent detection, but it increases to 5.5×10^{-3} for differential detection. In this case, the number of combiner branches would have to be increased by one to fulfill the $\langle BER \rangle$ requirement, a solution which may not be acceptable.

Consequently, the switching-induced degradation of $\langle BER \rangle$ will be computed assuming coherent demodulation for four-PSK signals, and differential detection for two-PSK signals.

VI. PERFORMANCE DEGRADATION DUE TO SWITCHING FOR TWO-PSK

6.1 Calculation of the $\langle BER \rangle$

The degradation is evaluated by comparing the cumulative distributions of $\langle BER \rangle$ obtained with and without switching errors. The distributions are calculated using Monte Carlo simulations, which assume a mobile unit moving along the path shown in Fig. 2a subjected to cochannel interference and shadow fading. (The results are essentially path independent, as noted in Section IV.)

The $\langle BER \rangle$ component due to the interference is calculated every 10m along the mobile unit path according to (5). Switching tests are simulated at regularly spaced intervals, the spacing being a parameter varying from 10m to several times this value. When a switch occurs, the $\langle BER \rangle$ is incremented by

$$\Delta(BER) = \frac{N_e}{S_r} \frac{v}{\delta x}, \tag{9}$$

where N_e represents the number of switching errors, one-half in the present case; S_r is the signaling rate; v is the mobile unit speed; and δx is the distance between $\langle SIR \rangle$ measurements. The calculations are made for the maximum mobile unit speed of 55 mph to obtain conservative estimates of degradation.

The results are first presented for the autocorrelation function ρ_2, which more realistically simulates shadow fading; and for a pessimistic correlation length of 50m, the approximate length of a city block. The results are given for different signaling rates and several values of Δx. The results are then compared to those obtained for longer decorrelation lengths, simulating less severe fading conditions. Finally, the results are also compared to those obtained with the autocorrelation function ρ_1.

6.2 Effect of signaling rate

The cumulative probability distribution was calculated for signaling rates of 16, 32, and 64 kb/s, using the autocorrelation function ρ_2, a correlation length of 50m, and a switching interval of 10m. Figure 9

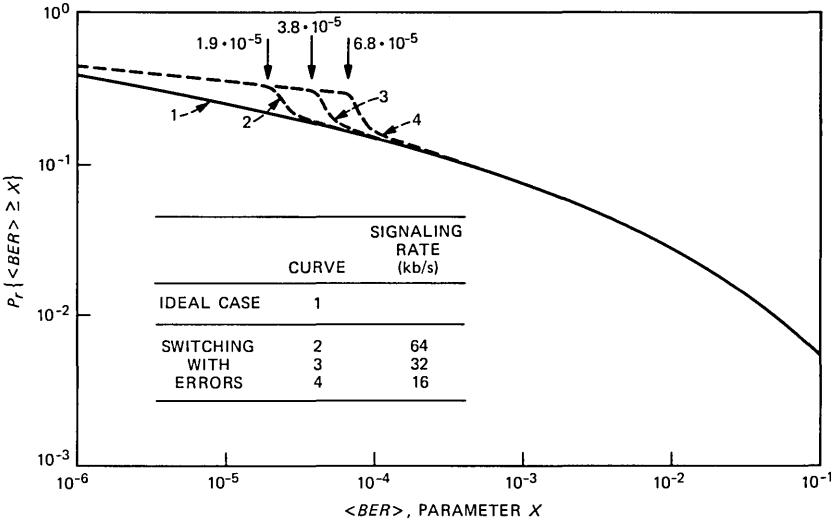

Fig. 9—Cumulative probability of $\langle BER \rangle$ for two-PSK signals, with signaling rate as a parameter.

shows the results and compares them to the ideal case, i.e., a receiver without switching errors. The results show very little switching degradation for $\langle BER \rangle$ values above 10^{-4}. Below this value there is a significant degradation that shifts to lower $\langle BER \rangle$ values when the signaling rate increases. For the above three signaling rates, the rapid change of the distribution begins, respectively, at the $\langle BER \rangle$ values of 6.8×10^{-5}, 3.8×10^{-5}, and 1.9×10^{-5}. These $\langle BER \rangle$ values are almost equal to those given by (9) for the same signaling rates: 7.65×10^{-5}, 3.82×10^{-5}, and 1.9×10^{-5}. At these points, the switching errors increase the cumulative probability by, respectively, 76, 58, and 45 percent.

6.3 Effect of switching interval

Figure 10 shows the cumulative probabilities calculated for the same autocorrelation function, ρ_2, and the same correlation length, 50m, but for different switching intervals, Δx, varying from 10 to 40m. In this case, the signaling rate is 16 kb/s. The results show that the amplitude of the "jump" occurring at the $\langle BER \rangle$ value given by (9) decreases as Δx increases. This effect is explained by noting that the frequency occurrence of the switching tests decreases in inverse proportion to Δx and the resulting degradation decreases accordingly. On the other hand, the use of a large Δx degrades the distribution for the large $\langle BER \rangle$ values because the switching tests are likely to miss the instant at which $\langle S_j \rangle$ [see eq. (1)] falls below that received by one of the two other base stations. This effect increases with the switching

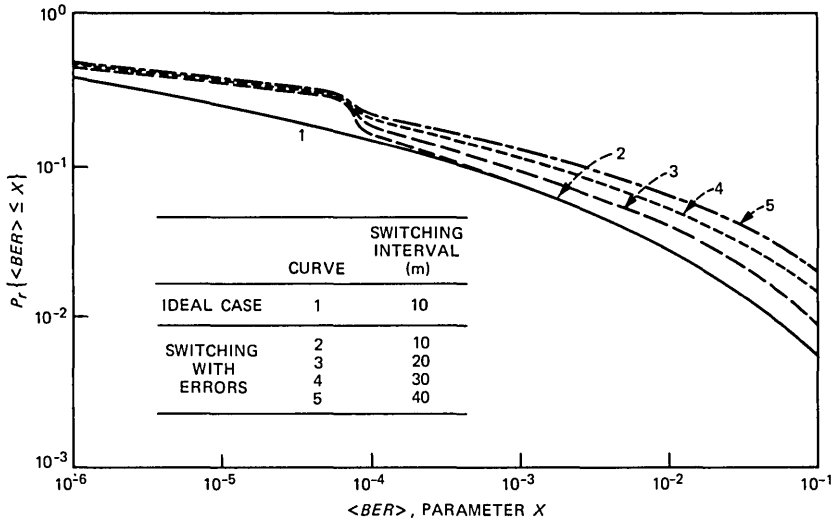

Fig. 10—Cumulative probability of $\langle BER \rangle$ for two-PSK signals, with switching interval as a parameter.

interval. For example, the 90-percentile value of the cumulative probability shifts from a $\langle BER \rangle$ value of 5×10^{-4} to the $\langle BER \rangle$ values of 8×10^{-4}, 1.6×10^{-3}, and 2.5×10^{-3} when the switching interval increases from 10m to, respectively, 20, 30, and 40m.

6.4 Effect of correlation length

Figure 11 illustrates the effect of the correlation length on the cumulative probability distribution of $\langle BER \rangle$. The results are calculated for the autocorrelation function ρ_2, a signaling rate of 16 kb/s, and the correlation lengths of 50, 100, and 200m. The same normalized switching intervals—0.2 and 0.6—are used for the three correlation lengths. As we found previously for the switching statistics, the $\langle BER \rangle$ statistics corresponding to these three correlation lengths fit nearly on the same curve for the same normalized switching interval, except for the section of the distribution on the left of the discontinuity; the amplitude of the discontinuity decreases when the correlation length increases. The explanation of this effect is the same as that given in the previous section.

6.5 Effect of autocorrelation function

The cumulative probabilities obtained with the autocorrelation functions ρ_1 and ρ_2 are compared in Fig. 12. The results correspond to a correlation length of 50m for both functions, a signaling rate of 16 kb/s and the three switching intervals of 10, 20, and 30m. The two

autocorrelation functions give nearly the same distribution for the lowest switching interval value. Above this value, the distributions corresponding to each autocorrelation function diverge increasingly with the length of the switching interval. For example, the 90-percentile point of the cumulative probability shifts from a $\langle BER \rangle$ value of

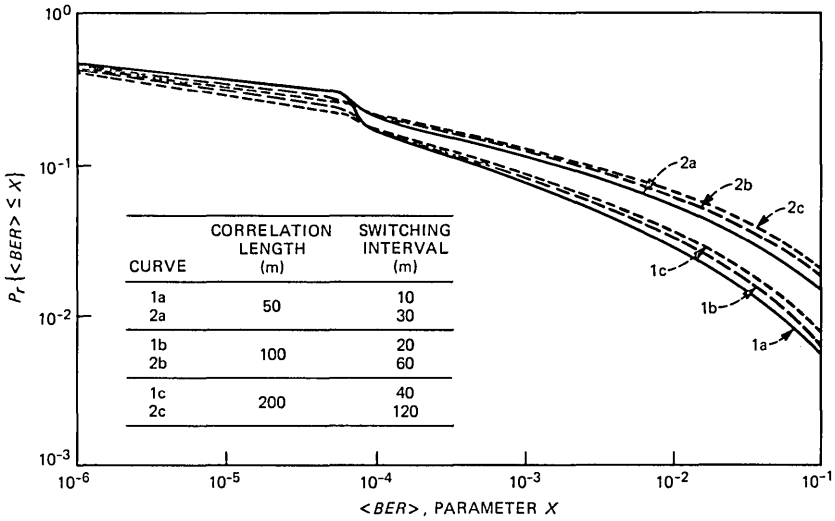

Fig. 11—Cumulative probability of $\langle BER \rangle$ for two-PSK signals, with correlation length as a parameter.

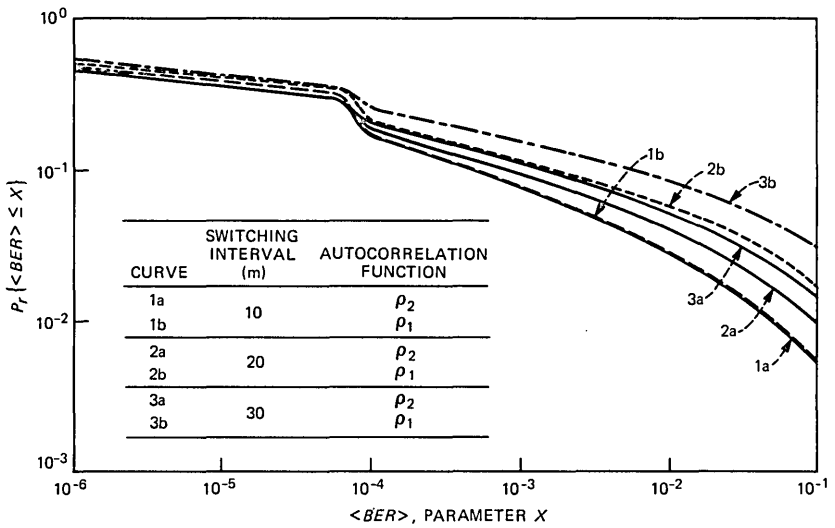

Fig. 12—Cumulative probability of $\langle BER \rangle$ for two-PSK signals, with autocorrelation shape function as a parameter.

8×10^{-4} to 1.8×10^{-3} for a switching interval of 20m, and from of 4.5×10^{-3} to 6×10^{-3} for a switching interval of 30m.

VII. PERFORMANCE DEGRADATION DUE TO SWITCHING FOR FOUR-PSK

The switching degradation for four-PSK is evaluated for coherently detected signals, using the same simulation as for two-PSK. In this case, however, the number of switching errors is given by the relation shown in Fig. 8, and the $\langle BER \rangle$ resulting from the interference is calculated according to (9). The results are presented as functions of the same parameters and for the same conditions as for two-PSK.

7.1 Effect of signaling rate

Cumulative probability distributions were calculated for signaling rates of 16, 32, and 64 kb/s, using the autocorrelation function ρ_2, a correlation length of 50m, and a switching interval of 10m. The results are shown in Fig. 13 and are compared to the ideal case without switching errors. The discontinuities of the distribution are now shifted to higher $\langle BER \rangle$ values, as expected from (9), since the number of switching errors is larger for four-PSK. They occur for the above signaling rates at, respectively, 1.3×10^{-4}, 7×10^{-5}, and 4×10^{-5}. These are about twice the values given for two-PSK.

7.2 Effect of switching interval

The effect of the switching interval is illustrated in Fig. 14, which

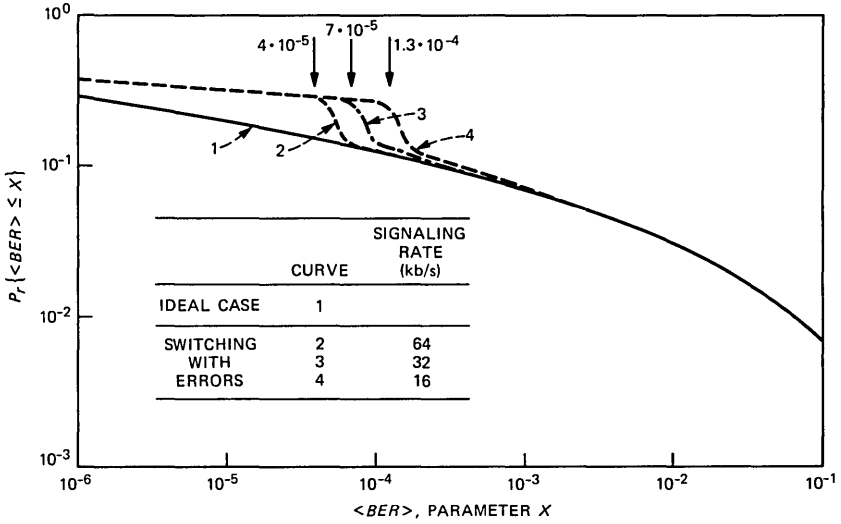

Fig. 13—Same results as in Fig. 9, for four-PSK signals.

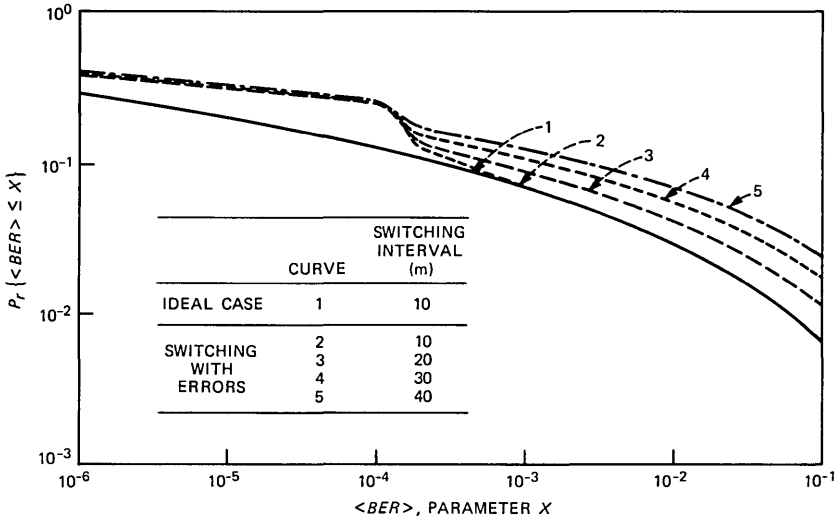

Fig. 14—Same results as in Fig. 10, for four-PSK signals.

gives the cumulative probabilities calculated for intervals varying from 10 to 40m. They are obtained using the autocorrelation function ρ_2, a decorrelation length of 50m, and a signaling rate of 16 kb/s. The effect of the switching interval is essentially the same as that found for two-PSK. The differences are that the discontinuities are shifted to higher $\langle BER \rangle$ values, as previously discussed, and the cumulative probability increases at this point by 100 percent (instead of 76 percent, as for two-PSK).

7.3 Effect of autocorrelation function

The effect of the autocorrelation function is illustrated in Fig. 15, which shows the cumulative probability for both autocorrelation functions calculated for a correlation length of 50m, a signaling rate of 16 kb/s, and the switching intervals of 10, 20, and 30m.

As in the two-PSK case, the two autocorrelation functions give nearly the same distribution for a switching interval of 10m. Above this value, the results are similar to those given by two-PSK, except for the positions of the discontinuities. Also, as before, the effect of the correlation length is small.

VIII. EFFECT OF A SWITCHING THRESHOLD

We conclude the study of the $\langle BER \rangle$ degradation by evaluating the effect of adding a threshold condition in the switching tests. The threshold consists of a reference to which the medium-term power $\langle S_j \rangle$ received by the transmitting base station is compared; switching

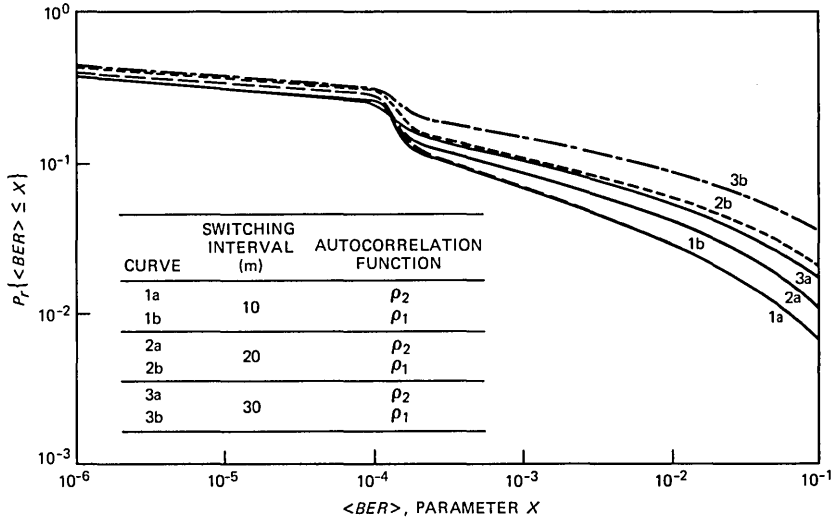

Fig. 15—Same results as in Fig. 12, for four-PSK signals.

is done only if $\langle S_j \rangle$ is smaller than the reference. This condition is added to reduce the switching frequency and thus to decrease the resulting $\langle BER \rangle$ degradation.

The threshold is adjusted relative to the median value of $\langle S_j \rangle$ (in dB) received by the base stations when the mobile unit is at the center of the cell. This quantity is the same for the three base stations.

The simulation was done for four-PSK, the autocorrelation function ρ_2, a decorrelation length of 50m, a switching interval of 10m, and a signaling rate of 16 kb/s. The results are shown in Fig. 16 for the threshold values of 0, −4, and −8 dB, and are compared to the cumulative probability obtained without a threshold for the same parameter values. The comparison shows a significant reduction of the discontinuity caused by switching, but at the cost of degrading the system performance for the $\langle BER \rangle$ values above $\Delta(BER)$. The best compromise is obtained for a threshold of 0 dB.

IX. CONCLUSION

A simple statistical model has been devised for the spatial variations of shadow fading, consisting of a one-parameter spatial autocorrelation function for the log-normal fading loss variable. The shape of the function and the value of the parameter can be varied to emulate different fading conditions in the urban environment. This model was used to simulate shadow fading for a mobile unit moving along a given path in a radio mobile cellular configuration using three-corner base station diversity.

Two significant geometric results emerge from this simulation study. First, the cumulative probability curves for the distance traveled by a mobile unit between consecutive switches, obtained for different fading conditions, can be fitted on the same curves when the distance between switches, and the length of the interval between switching tests are both normalized by the correlation length. Second, the above distribution, the average distance between switches, and the switching frequency are all nearly independent of the path followed by the mobile unit.

The above results were used to evaluate the $\langle BER \rangle$ degradations due to switching, for both two-PSK and four-PSK modulations. We found that, in the worst condition—a mobile unit moving at 55 mph, a decorrelation length equal to a city block, switching tests done every 10m, and a (low) signaling rate of 16 kb/s—the distributions are insignificantly affected by switching for $\langle BER \rangle$ values above 9×10^{-5} for two-PSK, and above 1.5×10^{-4} for four-PSK. These $\langle BER \rangle$ values are found to be about equal to the $\langle BER \rangle$ increment caused by switching for the respective modulation. The cumulative probability roughly doubles below these values. The amplitude of this effect is reduced by increasing the length of the switching test interval, but the improvement is more than canceled by an overall degradation of the cumulative probability distribution.

It was found, as expected, that the switching degradation is reduced when the correlation length increases. The same effect is obtained by

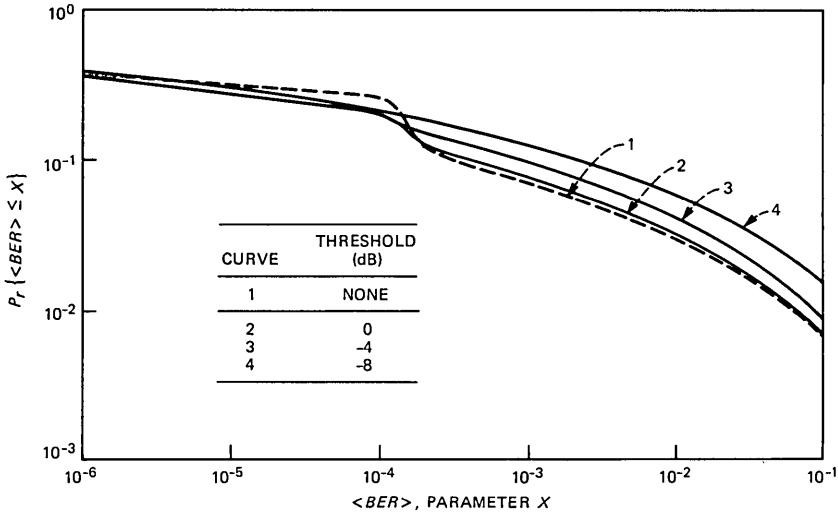

Fig. 16—Cumulative probability of $\langle BER \rangle$ for four-PSK signals, calculated with a threshold switching condition.

using a higher signaling rate or for a mobile unit moving at lower speed (if the switching tests are done at the same intervals).

The addition of a threshold condition in the switching test reduces the amplitude of the discontinuity of the cumulative probability functions. However, this is achieved at the cost of degrading the distribution for large $\langle BER \rangle$. An acceptable compromise between these two effects is obtained for a threshold of 0 dB.

Finally, the $\langle BER \rangle$ statistics are found to be nearly independent of the shape of the autocorrelation function if the switching tests are done at intervals smaller than or equal to 0.2 times the correlation length. Above this value, the results obtained for different shapes diverge increasingly with the length of the interval.

X. ACKNOWLEDGMENT

The author gratefully acknowledges L. J. Greenstein for his many helpful ideas and useful comments.

REFERENCES

1. W. C. Jakes, Jr., Ed., *Microwave Mobile Communication*, New York: Wiley, 1974, Chapters 2 and 5.
2. W. C. Y. Lee and Y. S. Yeh, "On the Estimation of the Second-Order Statistics of Log Normal Fading in Mobile Radio Environment," IEEE Trans. Commun., *COM-22*, No. 6 (June 1974), pp. 869–73.
3. G. D. Ott and A. Plitkins, "Urban Path-Loss Characteristics at 820 MHz," IEEE Trans Veh. Technol., *VT-27*, No. 4 (November 1978), pp. 129–97.
4. Y. S. Yeh and S. C. Schartz, "Outage Probability in Mobile Telephone Due to Multiple Log-Normal Interferers," Globecom '82, Miami, November 1982, pp. 71–98.
5. P. S. Henry and B. Glance, "A New Approach to High-Capacity Digital Mobile Radio," B.S.T.J., *60*, No. 8 (October 1981), pp. 1891–904.
6. D. M. Black and D. O. Reudink, unpublished work.
7. G. Vannucci, "A Digital Carrier Regenerator Applicable to TDMA Satellite Systems," Proc. Int. Symp. on Circuits and Systems, Rome, Italy, May 1982, pp. 1249–52.
8. R. W. Lucky, J. Salz, and E. J. Weldon, Jr., *Principles of Data Communication*, New York: McGraw-Hill, 1968, Chapter 9.

AUTHOR

Bernard S. Glance, Electronic Engineering, 1958, Ecole Speciale de Mechanique et Electricite, Paris, France; Electronic Engineering, 1960, Ecole Superieure d'Electricite, Paris, France; Ph.D. (Electronic Engineering), 1964, Paris University; Thompson, CSF, France, 1958–1966; Varian Associates, 1966–1968; AT&T Bell Laboratories, 1968—. At Thompson, CSF, Mr. Glance researched microwave and millimeter-wave tubes, and at Varian Associates he worked on microwave tube amplifiers. After joining AT&T Bell Laboratories, his initial field of interest was millimeter-wave integrated circuits and RF sources. He subsequently worked on microwave integrated components for use in communications satellites. More recently, he has been involved in analyses and simulations of digital mobile radio systems and point-to-point digital radio systems. Member, IEEE.

AT&T BELL LABORATORIES TECHNICAL JOURNAL
Vol. 63, No. 4, April 1984
Printed in U.S.A.

Processing Channel-Bank Spectrometer Data

By H. E. ROWE*

(Manuscript received June 29, 1983)

A channel-bank spectrometer produces weighted samples of its input spectrum, the weighting function being determined by the shape of the channel filters. We desire to compare two different input spectra, with similar shape but different widths, from their corresponding weighted samples. This problem arises in millimeter-wave astronomy. For example, a given astronomical source may contain two isotopes of the same molecule. If we know their rest frequencies, comparison of their observed spectra, with appropriate frequency shifts and scale changes, can determine whether the two isotopes have the same velocity distribution. Given the weighted samples for a particular input spectrum, we find the optimum way to calculate the samples for a narrower spectrum having the same shape. We determine the noise and distortion both for this optimum method and for an approximation to it. These results are compared for a particular example with those obtained from an ad-hoc algorithm called "Squish", currently used for this purpose; in this case Squish is almost as good as the approximation to the optimum method. The present results permit such comparisons in other cases that may be of interest, where the present method may offer significant improvement.

I. INTRODUCTION

Consider two well-separated spectral lines observed in a particular radio astronomical source. The intrinsic line widths are usually much smaller than the Doppler spread. If the lines correspond to two isotopes of the same molecule and have the same velocity distribution, these two lines will have the same normalized shape, the higher-frequency line being wider. Let their spectral densities be $P_{s_1}(f)$ and $P_{s_2}(f)$,

* AT&T Bell Laboratories.

centered on frequencies f_1 and f_2, respectively, with $f_2 > f_1$. Since Doppler frequency shift Δf and relative velocity v are related by $\Delta f/f = v/c$, where c is the velocity of light, the line widths are proportional to the ratio of center frequencies

$$\rho \equiv \frac{f_2}{f_1} > 1, \tag{1}$$

and the line shapes are related by

$$P_{s_2}(\rho f) = C \cdot P_{s_1}(f - f_2 + f_1) \tag{2}$$

if the two isotopes have the same velocity distribution, where the "shrink" parameter ρ is given by (1) and C is a line strength parameter. We call $P_{s_2}(\rho f)$ the "shrunk" version of $P_{s_2}(f)$.

The spectral density is not observed directly, but rather measured with a channel-bank spectrometer. This consists of a fixed bank of equally spaced filters of identical shape, each with its own detector. The input spectrum is first translated in frequency so that it lies at the center of the band covered by the filter bank. The detector outputs represent weighted, noisy samples of the input spectral density.

Let the translated spectra of the two isotopes be denoted $\hat{P}_{s_1}(f)$ and $\hat{P}_{s_2}(f)$; their centers now coincide. Then if

$$\hat{P}_{s_2}(\rho f) = C \cdot \hat{P}_{s_1}(f) \tag{3}$$

the two isotopes have the same velocity distribution. We must determine whether this is so by examining the spectral samples, corresponding to $\hat{P}_{s_2}(f)$ and $\hat{P}_{s_1}(f)$, produced by the spectrometer. To do so, we must compute the spectral samples of the shrunk spectrum $\hat{P}_{s_2}(\rho f)$ in terms of the measured spectral samples of the actual input spectrum $\hat{P}_{s_2}(f)$.

We therefore consider the following problem. A spectrometer with input spectral density $P_s(f)$ produces weighted spectral samples x_k, with sample noises n_k. Expressions for x_k and for the statistics of the n_k are given in the next section, and derived in the appendix. Denote the noiseless samples of the shrunk spectrum $P_s(\rho f)$ by $x_{\rho,k}$. Then we wish to estimate the set $\{x_{\rho,k}\}$ from the set $\{x_k + n_k\}$, and determine the mean-square estimation errors due to noise and distortion. This is accomplished by standard linear estimation techniques.

II. CHANNEL-BANK SPECTROMETER ANALYSIS

A typical section of a channel-bank spectrometer is illustrated in Fig. 5 in the appendix. The input signal plus noise are filtered, square-law rectified, and integrated to produce the output spectral sample. Equation (67) gives the spectral sample in terms of the input spectral

density and the common channel filter shape. For convenience, we consider an analogous time-domain model, in which approximate samples of a pulse $x(t)$ are obtained as follows:

$$x_k \equiv \int_{-\infty}^{\infty} x(t)a(t - kT)dt, \qquad -\infty < k < \infty. \tag{4}$$

The spectrum being measured is represented as $x(t)$, and hence is real, positive, and symmetric; the weight function $a(t)$ represents the square magnitude of the baseband equivalent channel-bank filter transfer function (64), and so it is real and positive, but not necessarily symmetric:

$$x(t) = x^*(t) = x(-t) \geqslant 0; \qquad a(t) = a^*(t) \geqslant 0. \tag{5}$$

Denote the Fourier transforms of $x(t)$ and $a(t)$ by $X(f)$ and $A(f)$, respectively. If $x(t)$ is passed through a filter with transfer function $A(-f)$, as in Fig. 1, the x_k are sample values of the filter output. $X(f)$ is real and symmetric (but not necessarily positive), while $A(f)$ is Hermetian. The weight function is normalized to unity at $t = 0$, its nominal center:

$$a(0) = \int_{-\infty}^{\infty} A(f)df = 1. \tag{6}$$

This corresponds to unit gain at midband of the channel-bank filters. A constant input will yield constant samples scaled by $A(0)$, the dc gain of the weighting filter:

$$x(t) = C, \qquad x_k = C \int_{-\infty}^{\infty} a(t)dt = C \cdot A(0). \tag{7}$$

The second-order sample noise statistics for a simultaneous channel-bank spectrometer are given in (76) and (86) when the integration time $\mathscr{T}$ for the integrator in Fig. 5 is large compared to the reciprocal channel-bank filter bandwidth (75). Thus, sample noises n_k are added to each of the samples x_k of (4); the resulting noisy samples are

$$x_k + n_k, \qquad -\infty < k < \infty. \tag{8}$$

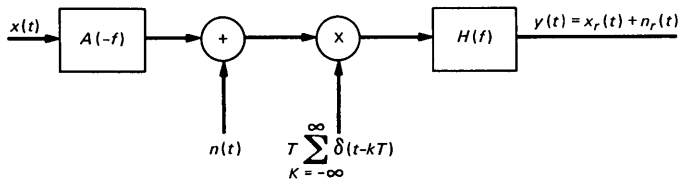

Fig. 1—Model of channel-bank spectrometer.

The n_k have the following statistics:

$$\langle n_k^2 \rangle = N \tag{9}$$

and

$$\langle n_{k+\kappa} n_k \rangle = N\phi_\kappa; \qquad \phi_\kappa = \frac{\int_{-\infty}^{\infty} a(t)a(t + \kappa T)dt}{\int_{-\infty}^{\infty} a^2(t)dt}. \tag{10}$$

The noise power N (77) is directly proportional to receiver noise temperature squared and inversely proportional to integration time. If different channel-bank filters overlap very little, i.e., if the weight functions $a(t - kT)$ for different k in (4) have little overlap, then different noise samples will have small correlation (10).

Finally, we recover an output $y(t)$ by a linear stationary operation on the infinite set of noisy samples (8),

$$y(t) = T \sum_{k=-\infty}^{\infty} (x_k + n_k)h(t - kT). \tag{11}$$

The weight function $h(t)$ chosen for reconstruction depends on what we desire as output.

The above set of operations may be represented by the block diagram of Fig. 1. The pulse $x(t)$ is passed through a filter with transfer function $A(-f)$, where $A(f)$ is the Fourier transform of $a(t)$ of (4):

$$A(f) = \int_{-\infty}^{\infty} a(t)e^{-j2\pi ft}dt. \tag{12}$$

Bandlimited Gaussian noise $n(t)$ is added, with spectral density

$$\begin{aligned} P_n(f) &= NT \sum_{m=-\infty}^{\infty} \phi_m e^{-j2\pi mfT}, \qquad |f| < \frac{1}{2T} \\ P_n(f) &= 0, \qquad |f| > \frac{1}{2T}. \end{aligned} \tag{13}$$

Here ϕ_m is the normalized discrete covariance of the noise samples, given in terms of the channel-bank filter characteristic a of (4) by (9) and (10). If the different filters overlap very little, the noise spectrum of (13) will be almost white. The noisy filtered output is sampled at interval T; finally, a reconstruction filter with transfer function

$$H(f) = \int_{-\infty}^{\infty} h(t)e^{-j2\pi ft}dt \tag{14}$$

yields an output $y(t)$ composed of a signal component $x_r(t)$ and noise

component $n_r(t)$ as shown. From (11) we get:

$$x_r(t) = T \sum_{k=-\infty}^{\infty} x_k h(t - kT)$$
$$n_r(t) = T \sum_{k=-\infty}^{\infty} n_k h(t - kT). \tag{15}$$

Returning to the problem in the introduction, from the noisy samples (8) we wish to estimate

$$x_{\rho,k} = \int_{-\infty}^{\infty} x(\rho t) a(t - kT) dt, \qquad -\infty < k < \infty, \tag{16}$$

with

$$\rho > 1, \tag{17}$$

i.e., the spectrometer response to the shrunk spectrum. In the noiseless case if we require that this be done without error, then we must be able to perfectly reconstruct $x(t)$ from x_k of (4); this requires that $x(t)$ be bandlimited:

$$X(f) = 0, \qquad f > W; \qquad WT < 0.5. \tag{18}$$

There is no aliasing as long as the bandwidth W of $x(t)$ is less than $1/(2T)$, where T is the sampling interval. Since only noise exists outside this band, $|f| > W$, we take the reconstruction filter transfer function to be zero there, whatever its purpose:

$$H(f) = 0, \qquad |f| > W. \tag{19}$$

The output noise $n_r(t)$ of Fig. 1 is stationary, as we see by (13) and (19).

We now determine $H(f)$, $|f| < W$, in order to recover the "shrunk" samples (16) from the noiseless samples (4).

III. DISTORTIONLESS ESTIMATE OF SHRUNK SPECTRUM

Assume that $x(t)$ is bandlimited (18) and that the added noise (9) is zero, $N = 0$. We wish to choose $h(t)$ in (11) such that the samples $x_r(\rho kT)$ of (15) and $x_{\rho,k}$ of (16) are equal:

$$x_r(\rho kT) = x_{\rho,k}. \tag{20}$$

From (18), (19), and Fig. 1 we see that

$$X_r(f) = A(-f)H(f)X(f). \tag{21}$$

For (20) we require

$$X_r\left(\frac{f}{\rho}\right) = A(-f)X\left(\frac{f}{\rho}\right). \tag{22}$$

Comparing (21) and (22) we get

$$H(f) = \begin{cases} \dfrac{A(-\rho f)}{A(-f)}, & |f| < W; \\ 0, & |f| > W; \end{cases} \qquad 0 < WT < 0.5. \tag{23}$$

Equation (23) gives the transfer function for the ideal reconstruction filter for the bandlimited case (18), in the absence of noise. The bandlimited case in our time-domain model corresponds in the appendix to an input spectral density $P_s(f)$ that varies sufficiently slowly compared to the channel-bank filter spacing, F. We will use the filter (23) throughout, and calculate the resulting errors due to noise, and to linear distortion and aliasing when (18) is not satisfied.

The noise $n_r(t)$ in Fig. 1 is stationary; consequently, the noise associated with the samples (20) is

$$\langle n_r^2 \rangle = \int_{-W}^{W} P_n(f) \left| \frac{A(\rho f)}{A(f)} \right|^2 df, \qquad WT < 0.5, \tag{24}$$

where $P_n(f)$ is given by (13). If the noise is almost white, we may set $P_n(f) = NT$.

The reconstruction filter characteristic (23) depends on the shrink factor, ρ. If for a given ρ we desire a fixed filter for all spectra that can be handled by the spectrometer, we take $WT = 0.5$. However, if we know that a given spectrum varies more slowly, we can improve the signal-to-noise ratio by taking a smaller value for W. The minimum value for W, for bandlimited $x(t)$ (18), is determined by our present requirement that the aliasing be zero.

IV. DISTORTION IN ESTIMATE OF SHRUNK SPECTRUM

Suppose now that $x(t)$ is not strictly bandlimited as in (18), but merely that $X(f)$ falls off rapidly for $|f| > 1/(2T)$. Suppose further that we estimate the shrunk spectrum by the reconstruction filter of (23) with $W = 1/(2T)$ (recall that W is no longer the bandwidth of $x(t)$). There will now be linear distortion and aliasing in the estimate. The principal aliasing will come from the first-order modulation products at the sampler output in Fig. 1. Assume that the added noise (9) is zero, $N = 0$. Then (20), (21), and (22) become, respectively:

$$x_r(\rho kT) = x_{\rho,k} + d(\rho kT), \tag{25}$$

$$X_r(f) = X(f)A(-\rho f) + \left[X\left(f - \frac{1}{T}\right) A\left(-f + \frac{1}{T}\right) + X\left(f + \frac{1}{T}\right) A\left(-f - \frac{1}{T}\right)\right] \frac{A(-\rho f)}{A(-f)}, \qquad |f| < \frac{1}{2T}$$

$$X_r(f) = 0, \qquad |f| > \frac{1}{2T}. \tag{26}$$

$$X_r\left(\frac{f}{\rho}\right) = A(-f)X\left(\frac{f}{\rho}\right) + D\left(\frac{f}{\rho}\right). \tag{27}$$

If we compare (26) and (27), the distortion $D(f)$ is given by

$$D(f) = \left[X\left(f - \frac{1}{T}\right) A\left(-f + \frac{1}{T}\right) + X\left(f + \frac{1}{T}\right) A\left(-f - \frac{1}{T}\right)\right] \frac{A(-\rho f)}{A(-f)}, \qquad |f| < \frac{1}{2T}, \tag{28}$$

$$D(f) = -A(-\rho f)X(f), \qquad |f| > \frac{1}{2T}.$$

The inverse transform of (28), $d(t)$, determines the distortion in the reconstructed samples of the shrunk spectrum (25). The noise remains as given by (24).

If $X(f)$ is strictly bandlimited (18) to $|f| < 1/(2T)$, $d(t) = 0$, and we have perfect reconstruction of the shrunk spectrum (Section III) in the absence of noise.

V. SUMMARY OF RESULTS

An input spectrum $x(t)$ is analyzed by a channel-bank spectrometer, producing spectral samples x_k (4) with additive noise samples n_k (8) through (10).

A shrunk spectrum $x(\rho t)$, $1 < \rho$, will similarly produce spectral samples $x_{\rho,k}$, with the same noise samples n_k.

We estimate $x_{\rho,k}$ by $y(\rho kT)$, with $y(t)$ given by (11) with $h(t)$ the inverse transform of (23). Then:

$$y(\rho kT) = x_{\rho,k} + n_r + d(\rho kT). \tag{29}$$

In the absence of noise and distortion, the second and third terms of (29) are zero, and $y(\rho kT)$ gives perfect results for the spectral samples $x_{\rho,k}$ of the shrunk spectrum $x(\rho t)$. Zero distortion requires that $X(f)$ be bandlimited (18), i.e., $X(f) = 0, f > 1/(2T)$.

The noise power $\langle n_r^2 \rangle$ is given by (24).

The distortion $d(t)$ is approximately the inverse Fourier transform of (28). This may be evaluated if we know the input spectrum $x(t)$. However, normally this is what we are trying to measure; it is of course obvious that $d(t)$ cannot be determined merely from the spectral samples x_k, even in the absence of noise. Consequently, (28) is of value only for calculating the distortion in representative cases, not for removing its effects in a given set of measurements.

VI. SINGLE-POLE FILTER

Assume the channel-bank filters are single pole. For this characteristic the above results are readily written out in closed form. Then $a(t)$ of (4) and its Fourier transform $A(f)$ are:

$$a(t) = \frac{1}{1 + \left(\frac{t}{t_o}\right)^2} \tag{30}$$

and

$$A(f) = \pi t_o e^{-2\pi t_o |f|}. \tag{31}$$

The 3-db half-width of the filter is t_o. Assume the spacing between adjacent filters is such that their transfer functions coincide at the 3-db points:

$$T = 2t_o. \tag{32}$$

The noise sample correlation is

$$\phi_m = \frac{1}{1 + m^2}. \tag{33}$$

The power spectrum of the added noise (Fig. 1) is

$$\begin{aligned} P_n(f) &= NT \sum_{m=-\infty}^{\infty} \frac{1}{1 + m^2} e^{-j2\pi mTf}, \qquad |f| < \frac{1}{2T} \\ P_n(f) &= 0, \qquad |f| > \frac{1}{2T}. \end{aligned} \tag{34}$$

The transfer function of the reconstruction filter is (23)

$$\begin{aligned} H(f) &= e^{-\pi T(\rho-1)|f|}, \qquad |f| < \frac{1}{2T} \\ H(f) &= 0, \qquad |f| > \frac{1}{2T}. \end{aligned} \tag{35}$$

The impulse response of the reconstruction filter is

$$h(t) = 2\,\frac{\pi T(\rho - 1)\left[1 - e^{-\frac{\pi}{2}(\rho-1)} \cos \pi \frac{t}{T}\right] + 2\pi t e^{-\frac{\pi}{2}(\rho-1)} \sin \pi \frac{t}{T}}{[\pi T(\rho - 1)]^2 + (2\pi t)^2}. \tag{36}$$

Observe that as $\rho \to 1$, $h(t) \to [\sin \pi(t/T)]/(\pi t)$.

The Fourier transform of the distortion $d(t)$ is (28):

$$D(f) = \frac{\pi T}{2} e^{-\pi} e^{\pi\rho Tf} \left[X\left(f - \frac{1}{T}\right) + X\left(f + \frac{1}{T}\right) e^{-2\pi Tf} \right], \qquad -\frac{1}{2T} < f < 0$$

$$D(f) = \frac{\pi T}{2} e^{-\pi} e^{-\pi\rho Tf} \left[X\left(f - \frac{1}{T}\right) e^{2\pi Tf} + X\left(f + \frac{1}{T}\right) \right], \qquad 0 < f < \frac{1}{2T} \tag{37}$$

$$D(f) = -\frac{\pi T}{2} e^{-\pi\rho T|f|} X(f), \qquad |f| > \frac{1}{2T}.$$

For $x(t)$ essentially bandlimited, $X(f)$ will fall off rapidly for $|f| > 1/(2T)$, and most of the contribution to $D(f)$ occurs for $|f|$ near $1/(2T)$. In this region we may approximate $D(f)$ by exponentials.

Finally, the output sample noise is

$$\langle n_r^2 \rangle = \frac{N(\rho - 1)}{\pi} \sum_{m=-\infty}^{\infty} \frac{1}{1 + m^2} \frac{1 - (-1)^m e^{-\pi(\rho-1)}}{(\rho - 1)^2 + m^2}$$

$$= \frac{N}{\rho} \left[1 + 2 \frac{\rho - 1}{2 - \rho} \frac{e^{-\pi\rho} - e^{-2\pi}}{1 - e^{-2\pi}} \right]. \tag{38}$$

Suppose we approximate $P_n(f)$ of (34) by its $m = 0$ term, i.e., regard $P_n(f)$ as white or equivalently neglect correlation between different noise samples (10). This corresponds to keeping only the $m = 0$ term in the output sample noise, in the first line of (38):

$$\langle n_r^2 \rangle \approx \frac{N}{\pi(\rho - 1)} [1 - e^{-\pi(\rho-1)}], \qquad P_n(f) \text{ white.} \tag{39}$$

As $\rho \to 1$ (39) and (38) both yield $\langle n_r^2 \rangle \to N$. This suggests that for expansion factors only a little larger than unity, the correlation between noise samples may be neglected.

The single-pole filter is special in that most of the general results may be written out explicitly. In contrast, approximations are used in the treatment of more general filters, such as the double-pole filter treated in the following section.

VII. DOUBLE-POLE FILTER

We now consider maximally flat double-pole channel-bank filters. $a(t)$ of (4) and its Fourier transform $A(f)$ are:

$$a(t) = \frac{1}{1 + \left(\frac{t}{t_o}\right)^4} . \tag{40}$$

$$A(f) = \frac{\pi t_o}{\sqrt{2}} e^{-\sqrt{2}\pi t_o |f|} \left[\cos\sqrt{2}\pi t_o f + \sin\sqrt{2}\pi t_o |f|\right] . \tag{41}$$

t_o is the 3-db half-width of the filter. We again assume that the spacing between adjacent filters is such that their transfer functions coincide at the 3-db points:

$$T = 2t_o. \tag{42}$$

The calculation of ϕ_m of (10) is straightforward but messy. Rather than perform it here, we rely on the example of the single-pole filter, treated in the preceding section, which suggests that correlation between noise samples is unimportant. Consequently, we take $\phi_m \approx 0$, $m \neq 0$, thus approximating the noise of (13) and Fig. 1 as white; note that $\phi_0 = 1$.

The transfer function $H(f)$ of the reconstruction filter is determined by substituting (41) into (23). Unlike the single-pole filter of the preceding section, in the present case the inverse transform, yielding the reconstruction filter impulse response $h(t)$, is not readily calculated exactly. Consequently, we must either invert $H(f)$ numerically for each value of ρ, or use an approximation valid for ρ in the range of interest, here a little larger than one.

First, we note that since $|f| < 1/(2T)$, the maximum value of the argument (in exponential and trigonometric functions) that can occur in (41) and (42) is $\pi/(2\sqrt{2}) \approx 1.111$. Next, the first zero of (41) and (42) occurs when the argument is $3\pi/4 \approx 2.356$. Consequently, a zero of (41) and (42) never occurs in the range of interest, and consequently $H(f)$ of (23) will never have a pole.

$H(f)$ decreases monotonically as f varies from 0 to $1/(2T)$, and remains positive for $0 < \rho < 2$. This suggests a parabolic approximation:

$$H(f) \begin{cases} \approx 1 - K_\rho(2Tf)^2, & |f| < \dfrac{1}{2T} \\ = 0, & |f| > \dfrac{1}{2T} . \end{cases} \tag{43}$$

For Taylor series approximation $K_\rho = (\pi^2/8)(\rho^2 - 1)$. Alternatively, we may approximate $H(f)$ by a parabola that agrees exactly at $f = 0$

and $f = \pm 1/(2T)$. For $\rho = 1.05$ the agreement is better than 0.3 percent, while for $\rho = 1.1$ the agreement is better than 0.75 percent. For this approximation

$$K_\rho = 1 - \frac{e^{-\frac{\pi}{2\sqrt{2}}\rho}\left(\cos\frac{\pi}{2\sqrt{2}}\rho + \sin\frac{\pi}{2\sqrt{2}}\rho\right)}{e^{-\frac{\pi}{2\sqrt{2}}}\left(\cos\frac{\pi}{2\sqrt{2}} + \sin\frac{\pi}{2\sqrt{2}}\right)}. \tag{44}$$

The corresponding filter impulse response is in either case

$$h(t) = \frac{1}{T}\frac{\sin\frac{\pi t}{T}}{\frac{\pi t}{T}} + \frac{K_\rho}{T}\frac{2\frac{\pi t}{T}\sin\frac{\pi t}{T} - \left(\frac{\pi t}{T}\right)^3\sin\frac{\pi t}{T} - 2\left(\frac{\pi t}{T}\right)^2\cos\frac{\pi t}{T}}{\left(\frac{\pi t}{T}\right)^4}. \tag{45}$$

The distortion transform $D(f)$ for the ideal case is again given by substituting (41) and (42) into (28). A similar expression is readily written out for the approximate transfer function (43), which yields additional distortion.

The output sample noise, neglecting correlation between noise samples as discussed in the paragraph following (42), with the approximate transfer function of (43), is

$$\langle n_r^2 \rangle \approx N(1 - K_\rho). \tag{46}$$

VIII. EXAMPLE: DOUBLE-POLE FILTER, LORENTZ SPECTRUM

Assume a Lorentz spectrum as input:

$$x(t) = \frac{1}{1 + \left(\frac{t}{t_{\mathscr{L}}}\right)^2}. \tag{47}$$

Assume the channel-bank filter characteristic is given by (40), with separation given by (42). The samples x_k (4) are

$$x_k = \frac{\pi T}{2\sqrt{2}}\frac{\left(\frac{T}{t_{\mathscr{L}}}k\right)^2 + \left(1 + \frac{T}{\sqrt{2}t_{\mathscr{L}}}\right)\left[1 + \frac{T}{\sqrt{2}t_{\mathscr{L}}} + \left(\frac{T}{2t_{\mathscr{L}}}\right)^2\right]}{\left(\frac{T}{t_{\mathscr{L}}}k\right)^4 + 2\left(1 + \frac{T}{\sqrt{2}t_{\mathscr{L}}}\right)\left(\frac{T}{t_{\mathscr{L}}}k\right)^2 + \left[1 + \frac{T}{\sqrt{2}t_{\mathscr{L}}} + \left(\frac{T}{2t_{\mathscr{L}}}\right)^2\right]^2}. \tag{48}$$

For line width large compared to the filter spacing, $t_{\mathscr{L}} \gg T$,

$$\frac{T}{t_{\mathscr{L}}} \xrightarrow{\lim} 0 \; x_k = \frac{\pi T}{2\sqrt{2}} \frac{1}{1 + \left(\frac{T}{t_{\mathscr{L}}} k\right)^2}. \tag{49}$$

The samples $x_{\rho,k}$ (16) are found by substituting $t_{\mathscr{L}} \rightarrow t_{\mathscr{L}}/\rho$ in (48).

The transform $D(f)$ of the distortion $d(t)$ of (25) is given as follows:

$$\begin{aligned} D(f) &= A(-\rho f)X(f)\left[\frac{A(-f)}{A(-\rho f)} H(f) - 1\right] \\ &\quad + \left[X\left(f - \frac{1}{T}\right) A\left(-f + \frac{1}{T}\right)\right. \\ &\quad \left. + X\left(f + \frac{1}{T}\right) A\left(-f - \frac{1}{T}\right)\right] \cdot H(f), \qquad |f| < \frac{1}{2T}. \\ D(f) &= -A(-\rho f)X(f), \qquad |f| > \frac{1}{2T}. \end{aligned} \tag{50}$$

Here $A(f)$ is given by (41) and (42), and $X(f)$ is the transform of (47):

$$X(f) = \pi t_{\mathscr{L}} e^{-2\pi t_{\mathscr{L}} |f|}. \tag{51}$$

For $H(f)$ the ideal reconstruction filter of (23), (41) and (42), and (50) yields (28). The approximate $H(f)$ of (43) yields additional distortion. Various approximations are necessary in different cases to evaluate $d(t)$ as the inverse transform of (50).

As a single illustration, assume a Lorentz spectrum with half-width equal to five times the filter spacing:

$$\frac{t_{\mathscr{L}}}{T} = 5. \tag{52}$$

Assume a shrink factor

$$\rho = 1.1. \tag{53}$$

Figure 2 shows the transform of the desired output; Fig. 3 shows the transform of the distortion with the ideal reconstruction filter (23), (41), and (42); and Fig. 4 shows the transform of the distortion with the Taylor series approximate filter of (43) with $K_\pi = \pi^2/8\ (\rho^2 - 1)$. Note that the transforms in Figs. 2, 3, and 4 are normalized to $1/(\pi T)^2$.

For the ideal reconstruction filter, the principal contribution to distortion occurs near $|f| = 1/(2T)$. The form of $D(f)$ in Fig. 3 in this region suggests that we approximate $D(f)$ by exponentials; this yields

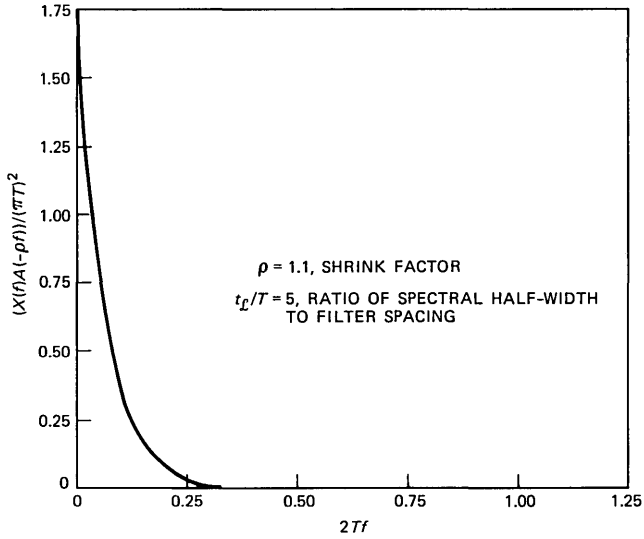

Fig. 2—Desired output for the Lorentz spectrum.

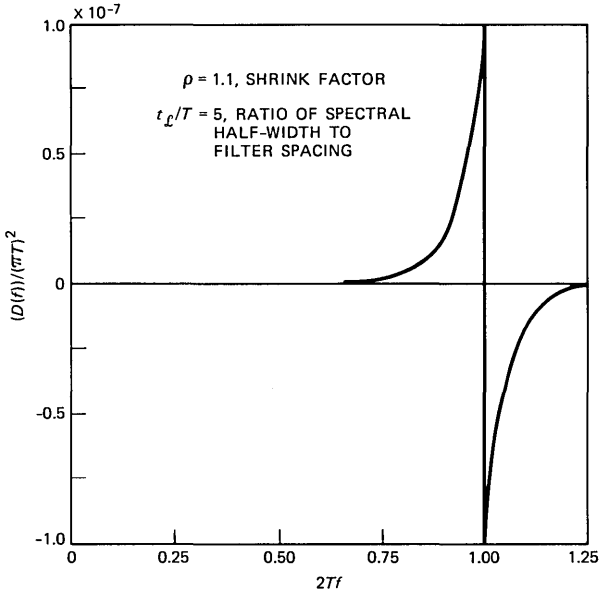

Fig. 3—Distortion with ideal filter for the Lorentz spectrum.

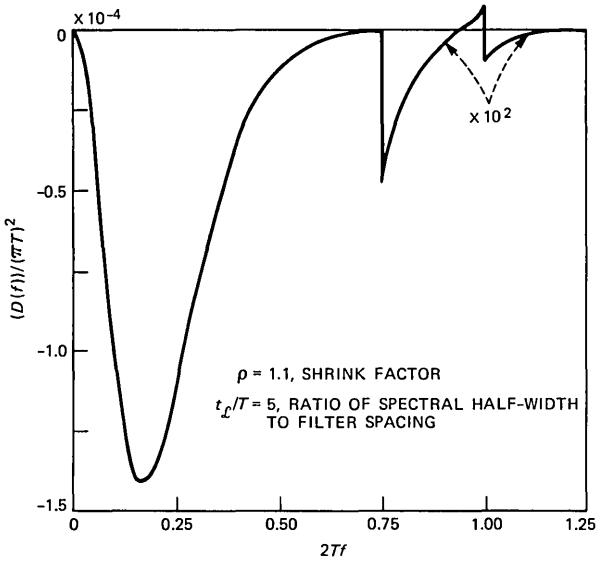

Fig. 4—Distortion with Taylor series filter for the Lorentz spectrum.

a closed-form approximation for $d(t)$, and thence for the error $d(\rho kT)$ in the reconstructed samples (29). Similarly, for the Taylor series approximate filter the form of $D(f)$ in Fig. 4 suggests a Gaussian approximation for $D(f)$, similar to that used in LaPlace's method, to obtain an approximation for $d(t)$.

We shall not carry out either of these approximations here; rather, we will content ourselves with simple upper bounds on the maximum distortion. Clearly,

$$d_{\max} \equiv d(t)\,|_{\max} \leqslant \int_{-\infty}^{\infty} |D(f)|\,df. \tag{54}$$

For the ideal filter, we estimate from Fig. 3 that

$$d_{\max} < \approx 5 \times 10^{-8}\,(\pi^2/2)T \approx 2.5 \times 10^{-7}\,T.$$

This estimate will be too large; $|d(t)|_{\max}$ will occur for t away from the origin, and consequently the maximum error will occur at the edge of the spectrum in (29).

For the Taylor series approximate filter, we estimate from Fig. 4 that $d_{\max} < \approx 1.5 \times 10^{-4}\,(\pi^2/2)\,T \approx 7.5 \times 10^{-4}\,T$. This estimate will be fairly accurate; $d(t)|_{\max}$ occurs for $t = 0$, and consequently the maximum error occurs at the center of the spectrum, $k = 0$ in (29).

Finally, the noise in the reconstructed samples is given approxi-

mately for the Taylor series filter by (46) as

$$\langle n_r^2 \rangle \approx N\left[1 - \frac{\pi^2}{8}(\rho^2 - 1)\right] = 0.741N. \tag{55}$$

The noise for the ideal filter will be a little larger.

IX. "SQUISH"

We compute the distortion and noise in the current algorithm "Squish", for comparison with the results of the preceding section. Squish may be described as follows. Associate with the samples x_k of (4) the function

$$s(t) \equiv \sum_{k=-\infty}^{\infty} x_k \operatorname{rect}\left(\frac{t}{T} - k\right), \tag{56}$$

where we recall that

$$\operatorname{rect}(t) \equiv \begin{cases} 1, & |t| < 1/2 \\ 0, & |t| > 1/2. \end{cases} \tag{57}$$

Similarly, define

$$s_q(t) \equiv \sum_{k=-\infty}^{\infty} q_k \operatorname{rect}\left(\frac{t}{\rho T} - k\right). \tag{58}$$

Choose the $\{q_k\}$ such that

$$\int_{t - k\rho T - \frac{\rho T}{2}}^{t - k\rho T + \frac{\rho T}{2}} [s_q(t) - s(t)]dt = 0; \tag{59}$$

equivalently,

$$q_k = \frac{1}{\rho T} \int_{t - k\rho T - \frac{\rho T}{2}}^{t - k\rho T + \frac{\rho T}{2}} s(t)dt. \tag{60}$$

The q_k are assumed to approximate the samples $x_{\rho,k}$ of (16):

$$q_k = x_{\rho,k} + d_k + n_k, \tag{61}$$

where d_k and n_k represent the distortion and noise from the desired output.

The following results correspond to the parameters of (52) and (53).

k	d_k	$\langle n_k^2 \rangle$
0	$-1.85 \times 10^{-3}\ T$	$0.83\ N$
1	$-4.87 \times 10^{-3}\ T$	$0.76\ N$
2	$-4.47 \times 10^{-3}\ T$	$0.65\ N$
3	$-1.59 \times 10^{-3}\ T$	$0.57\ N$
4	$0.91 \times 10^{-3}\ T$	$0.52\ N$
5	$2.18 \times 10^{-3}\ T$	$0.5\ N$
6	$2.51 \times 10^{-3}\ T$	$0.52\ N$
7	$2.36 \times 10^{-3}\ T$	$0.57\ N$
8	$2.02 \times 10^{-3}\ T$	$0.65\ N$
9	$1.65 \times 10^{-3}\ T$	$0.76\ N$
10	$0.12 \times 10^{-3}\ T$	$0.83\ N$

(62)

The peak distortion $d_{\max} \equiv |d_k|_{\max} = 4.87 \times 10^{-3}\ T$ occurs at $k = 1$. The peak noise $\langle n_k^2 \rangle_{\max} = 0.83\ N$ occurs at $k = 0, 10, \cdots$, i.e., when $\rho k =$ integer; the variation of noise with k makes evident the nonstationary nature of "Squish".

X. DISCUSSION

We have shown how to relate the measurements obtained with a channel-bank spectrometer on two spectra, $P_s(f)$ and $P_s(\rho f)$, having similar shape but different scales along the frequency axis. This problem arises in radio astronomy, in determining whether two isotopes have the same velocity distribution.

As a single numerical example, we have considered a Lorentz line 10 samples wide between its half-power points, analyzed by a channel-bank spectrometer with double-pole filters spaced so that their 3-db points coincide. We have determined the noise and distortion in computing the corresponding samples for a Lorentz spectrum 90.9 percent as wide, by the present methods and with the current algorithm "Squish". We summarize these results of Sections VIII and IX in Table I.

Table I—Comparison between present and proposed processing methods

	Ideal Filter	Taylor Series Filter	Squish
Maximum distortion	$<2.5 \times 10^{-7}$ T	7.5×10^{-4} T	4.87×10^{-3} T
Maximum noise power	>0.741 N	0.741 N	0.83 N

These values are to be compared with the maximum sample value, $x_0 = 1.10\ T$, obtained from (48) with $k = 0$.

In the present example Squish has a little more distortion and noise

than the Taylor series approximation to the ideal reconstruction filter; the ideal filter, of course, has much less distortion. For a narrower input spectrum, i.e., larger ρ, Squish will be relatively worse.

Such comparisons may vary widely, depending on the spectrum under study and the channel-bank filter characteristic. The behavior in the main part of the spectrum may be quite different from that far out on the tails.

XI. ACKNOWLEDGMENT

I would like to thank R. W. Wilson for suggesting this problem, and the unknown reviewer for a number of helpful suggestions.

APPENDIX

Output Statistics of Channel-Bank Spectrometer

Figure 5 shows a typical section of a channel-bank spectrometer, consisting of a filter, square-law detector, and integrator. The input $s(t)$ represents the noise whose spectral density $P_s(f)$ we wish to determine; $P_s(f)$ is real and symmetric, i.e., $P_s(f) = P_s^*(f) = P_s(-f)$. $\nu(t)$ represents the receiver input noise, assumed white, with spectral density $\mathcal{N}$. Assume throughout this appendix that the measurement starts at $t = 0$ and that the integration time is $\mathcal{T}$; then the integrator output $w_k(\mathcal{T})$ is the noisy sample of (8).

We assume the receiver input noise is much larger than the noise whose spectrum is being measured:

$$P_s(f) \ll \mathcal{N}. \tag{63}$$

The random "signal" $s(t)$ and noise $\nu(t)$ each produce a dc and a random component at the outputs $w_k(t)$. The dc component of $w_k(\mathcal{T})$ due to $s(t)$ is the desired spectral sample. The dc component due to receiver front-end noise $\nu(t)$ is uninteresting here. The random component due to $s(t)$ is much smaller than the random component due to $\nu(t)$; we ignore the former, and consider the latter as the "noise" in the sample. In summary, the dc component of $w_k(\mathcal{T})$ due to $s(t)$ (the

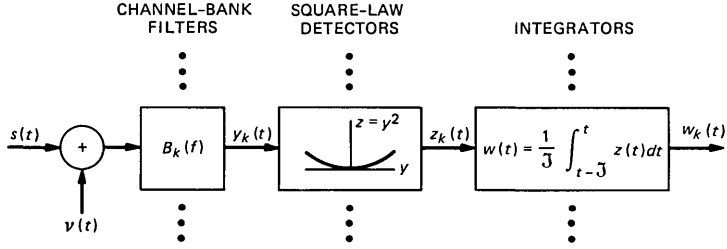

Fig. 5—Typical section of a channel-bank spectrometer.

noise being measured) corresponds to x_k of (4) and (8); the random component due to receiver noise $\nu(t)$ corresponds to n_k of (8) and (9).

Assume the channel-bank filters are equally spaced with the same shape; let $B(f)$ be their common baseband equivalent filter. Then the kth channel-bank filter has transfer function

$$B_k(f) = B(f - kF) + B^*(-f - kF), \tag{64}$$

where F represents the filter spacing. We assume that $B(f)$, and hence $B_k(f)$, are causal; thus their respective Fourier transforms satisfy $b(t) = 0$ and $b_k(t) = 0$ for $t < 0$. $b_k(t)$ is real, but $b(t)$ is not necessarily real; while $B_k(f)$ is Hermetian, $B(f)$ need not be. We also assume that the spectra of interest are narrowband, so that the $\{k\}$ of interest in (64) are large enough such that

$$B(f) \approx 0, \qquad |f| > |k|F, \tag{65}$$

and the two terms in (64) are essentially nonoverlapping.

Assume that $\nu(t) = 0$ in Fig. 5. Then

$$\langle w_k(t)\rangle = \langle z_k(t)\rangle = \langle y_k^2(t)\rangle = \int_{-\infty}^{\infty} |B_k(f)|^2 P_s(f)df. \tag{66}$$

From (64) and (65), we have in terms of the equivalent baseband filter transfer function

$$\langle w_k(\mathscr{T})\rangle = \int_{-\infty}^{\infty} 2|B(f - kF)|^2 P_s(f)df \tag{67}$$

for the desired sample output. Since k and F are positive, by (65) the main contribution to the integral in (67) occurs close to $f \sim kF$, and there is no significant contribution to this integral for $f < 0$. Setting $f \to t$, $F \to T$, $P_s(\,) \to x(\,)$, $2|B(\,)|^2 \to a(\,)$, and $\langle w_k(\mathscr{T})\rangle \to x_k$, we obtain (4).

Assume now that $s(t) = 0$ in Fig. 5. Then

$$\begin{aligned}\langle w_k(t)\rangle = \langle z_k(t)\rangle = \langle y_k^2(t)\rangle &= \mathscr{N}\int_{-\infty}^{\infty} |B_k(f)|^2 df \\ &= \mathscr{N}\int_{-\infty}^{\infty} 2|B(f)|^2 df,\end{aligned} \tag{68}$$

the last step following from (64) and (65). Define

$$\begin{aligned} w_{kac}(t) &\equiv w_k(t) - \langle w_k(t)\rangle \\ z_{kac}(t) &\equiv z_k(t) - \langle z_k(t)\rangle. \end{aligned} \tag{69}$$

Then the spectral density of the second quantity in (69) is

$$P_{z_{kac}}(f) = 2\mathscr{N}^2 |B_k(f)|^2 \oplus |B_k(f)|^2, \tag{70}$$

where $\circledast$ represents convolution. Now the integrator has impulse response

$$i(t) = \begin{cases} \dfrac{1}{\mathcal{T}}, & 0 < t < \mathcal{T} \\ 0, & \text{otherwise.} \end{cases} \tag{71}$$

The integrator transfer function, the Fourier transform of (71), is

$$I(f) = e^{-j\pi f \mathcal{T}} \frac{\sin \pi f \mathcal{T}}{\pi f \mathcal{T}} . \tag{72}$$

Then

$$\langle w_{kac}^2(t) \rangle = \int_{-\infty}^{\infty} |I(f)|^2 P_{z_{kac}}(f) df. \tag{73}$$

Now by (64), $P_{z_{kac}}(f)$ of (70) consists of a low-frequency part centered around $f = 0$,

$$P_{z_{kac}}^{\text{low}}(f) = 4\mathcal{N}^2 |B(f)|^2 \circledast |B(-f)|^2, \tag{74}$$

and a high-frequency part centered around $f = \pm 2kF$. By (65) these two parts are essentially nonoverlapping. Since $|I(f)|^2$ becomes small for $|f| \gg 1/\mathcal{T}$, only the portion (74) will be significant in (73) if $1/\mathcal{T} \ll |k|F$, i.e., if the integration time is large compared to the reciprocal frequency being measured. This is always true, and hence we may replace $P_{z_{kac}}(f)$ in (73) by (74). Moreover, we assume

$$\frac{1}{\mathcal{T}} \ll \text{width of } B(f). \tag{75}$$

Then (73) and (74) yield

$$\langle w_{kac}^2(t) \rangle = \frac{\mathcal{N}^2}{\mathcal{T}} \int_{-\infty}^{\infty} [2|B(f)|^2]^2 df. \tag{76}$$

Setting $f \to t$, $2|B(\,)|^2 \to a(\,)$, and $\langle w_{kac}^2(\mathcal{T}) \rangle \to N$, (76) becomes

$$N = \frac{\mathcal{N}^2}{\mathcal{T}} \int_{-\infty}^{\infty} a^2(t) dt \tag{77}$$

to be substituted in (9) and (10).

Finally, we find the correlation between different noise samples (10); i.e., in the notation of the present appendix we seek

$$\langle w_{kac}(\mathcal{T}).\ w_{k'ac}(\mathcal{T}) \rangle.$$

We set $s(t) = 0$, and have the following relations between cross-spectra:

$$P_{y_k y_{k'}}(f) = \mathcal{N} B_k(f) B_{k'}^*(f). \tag{78}$$

$$P_{w_{kac} w_{k'ac}}(f) = P_{z_{kac} z_{k'ac}}(f) \cdot \left(\frac{\sin \pi f \mathcal{T}}{\pi f \mathcal{T}}\right)^2. \tag{79}$$

We relate $P_{z_{kac} z_{k'ac}}(f)$ to $P_{y_k y_{k'}}(f)$ as follows:

$$\phi_{z_{kac} z_{k'ac}}(\tau) \equiv \langle z_{kac}(t + \tau) z_{k'ac}(t) \rangle$$
$$\equiv \langle y_{kac}^2(t + \tau) y_{k'ac}^2(t) \rangle - \langle z(t) \rangle^2, \tag{80}$$

where we omit the subscript from the final term because the expected detector outputs are the same for all channels by (68). Assuming the receiver input noise $\nu(t)$ is Gaussian, the $y_k(t)$ are jointly Gaussian, and using (68)

$$\phi_{z_{kac} z_{k'ac}}(\tau) = 2\phi_{y_k y_{k'}}^2(\tau). \tag{81}$$

The Fourier transform of (81) yields the following relationship between the cross-spectra of different y and the ac components of corresponding z:

$$P_{z_{kac} z_{k'ac}}(f) = 2 P_{y_k y_{k'}}(f) \circledast P_{y_k y_{k'}}(f). \tag{82}$$

Combining (78), (79), and (82) we get:

$$P_{w_{kac} w_{k'ac}}(f) = 2\mathcal{N}^2 \left[\frac{\sin \pi f \mathcal{T}}{\pi f \mathcal{T}}\right]^2 \cdot [B_k(f) B_{k'}^*(f)] \circledast [B_k(f) B_{k'}^*(f)]. \tag{83}$$

Then

$$\langle w_{kac}(t) w_{k'ac}(t) \rangle = \int_{-\infty}^{\infty} P_{w_{kac} w_{k'ac}}(f) df. \tag{84}$$

By (75) we may approximate $P_{w_{kac} w_{k'ac}}(f)$ of (83) by its value for $f = 0$ in (84), yielding

$$\langle w_{kac}(t) w_{k'ac}(t) \rangle = \frac{2\mathcal{N}^2}{\mathcal{T}} \int_{-\infty}^{\infty} |B_k(f)|^2 |B_{k'}(f)|^2 df. \tag{85}$$

From (64) and (65) we express (85) in terms of the baseband equivalent filter as

$$\langle w_{kac}(t) w_{k'ac}(t) \rangle = \frac{\mathcal{N}^2}{\mathcal{T}} \int_{-\infty}^{\infty} 2|B(f)|^2 \cdot 2|B(f - (k - k')F)|^2 df. \tag{86}$$

Setting $f \to t$, $F \to T$, $2|B(\,)|^2 \to a(\,)$, $\langle w_{kac}(\,\mathcal{T}) w_{k'ac}(\,\mathcal{T}) \rangle \to \langle n_k n_{k'} \rangle$, and $k' - k = \kappa$ in (86), and using (77), we obtain (10).

AUTHOR

Harrison E. Rowe, B.S., M.S., Sc.D. (Electrical Engineering), Massachusetts Institute of Technology, 1948, 1950, and 1952; U. S. Navy, 1945–1946, AT&T

Bell Laboratories, 1952—. Mr. Rowe joined AT&T Bell Laboratories as a Member of Technical Staff in the Radio Research Laboratory. Presently, he is in the Radio Physics Research Department. His publications include numerous papers and one textbook, spanning a variety of fields including parametric amplifiers, noise, and communication theory; propagation in random media; and related problems in waveguide, radio, and optical communication systems. His is the joint author of five patents. Fellow, IEEE; corecipient, 1977 David Sarnoff Award and 1972 Microwave Prize; member, Commission C of URSI, Sigma Xi, Tau Beta Pi, and Eta Kappa Nu.

AT&T BELL LABORATORIES TECHNICAL JOURNAL
Vol. 63, No. 4, April 1983
Printed in U.S.A.

Weighting Strategies for Companded PCM Transmitted Over Rayleigh Fading and Gaussian Channels

By C.-E. SUNDBERG,* W. C. WONG,† and R. STEELE‡

(Manuscript received July 29, 1983)

We present three methods of weighting N-bit μ-law Pulse Code Modulation (PCM) with binary modulation, and evaluate their performances theoretically for transmission over Rayleigh fading and Gaussian channels. The digital modulation methods considered are noncoherent frequency shift keying and coherent phase shift keying. Ideal selection combining and ideal maximal ratio combining diversity techniques are employed when the transmission is over fading channels. Weighting System 1 is the conventional weighted pulse code modulated system, where the bits in every PCM word have the same weighting profile. Weighting System 2 has 2^N unique weighting profiles, while System 3 has an addendum to System 2, where every bit in a particular word is further weighted by a unique multiplicative factor. For Rayleigh fading channels and the encoder operating at an input level that provided maximum signal-to-quantization noise-ratio, we obtained gains in overall signal-to-noise ratio (s/n) over unweighted μ-law PCM of 3, 4.5, and 6 dB for Systems 1, 2, and 3, respectively. When the systems were used in conjunction with Gaussian channels, the corresponding gains were 10, 12, and 17 dB, for a channel s/n of 10 dB. In addition to the theoretical results, we conducted computer simulations using four concatenated speech sentences transmitted via our weighted μ-law PCM systems over mobile radio channels. The simulation performances were in good agreement with our theoretical results, which were based on input signals having an exponential distribution.

* University of Lund, Sweden. † AT&T Bell Laboratories. ‡ University of Southampton, England.

I. INTRODUCTION

When analog signals are PCM-encoded into binary words, the bits in any word represent different contributions to the decoded analog sample.[1-3] For example, in 8-bit piecewise μ-law Pulse Code Modulation (PCM),[2] the first bit in each PCM word represents the polarity of the speech sample, the next three bits identify the segment number, and the final four bits locate the value of the sample within the segment. Clearly, there is a hierarchical structure, with the most significant magnitude bit being the most influential in determining the accuracy of the recovered speech sample, and the importance of the subsequent bits declining rapidly until the least significant bit (LSB) is reached.

Binary errors inevitably will occur to some extent in the regeneration process at the receiver, and therefore it seems reasonable to mitigate the effect of these errors by matching the energy of each bit prior to transmission in a manner dependent on their contribution to the accuracy of the recovered decoded sample. If this approach is adopted, the average energy used in the transmission of each binary word is arranged to be identical to that in conventional PCM, where all bits have the same energy. Thus the energies allocated to the most significant magnitude bits are enhanced at the expense of the least significant bits whose energies are curtailed.

This concept, due to Bedrosian,[1] has an instant appeal as a technique for reducing the noise due to binary transmission errors in the recovered speech signal. A PCM system that weights the binary levels by differing amounts, i.e., the binary amplitudes may be different for each bit in the PCM word, is known as weighted PCM. Sundberg[2] generalized the analysis of Bedrosian to include companded PCM, making use of the A factors, which he and Rydbeck conceived.[3,4]

For transmission of unweighted PCM by means of a binary modulation scheme, the bit error probability is the same for all bits, independent of their position in the word. This is clearly not so for weighted PCM, where the weighting of the bit energies reduces the error probabilities of the more significant bits. As the average energy (or power) per transmitted bit is constant, irrespective of whether weighting is applied, it follows that the error probabilities of the less significant bits must increase. However, the effect of weighting is to improve the overall signal-to-noise ratio (s/n) for a given channel s/n.

Our intention in this discourse is to describe new weighting strategies for μ-law PCM transmitted over Rayleigh fading and Gaussian channels by means of either binary Noncoherent Frequency Shift Keying (NCFSK) or binary Coherent Phase Shift Keying (CPSK) modulation. For each weighting profile and channel we will present

formulae for the noise power in the recovered signal due to the effect of transmission errors. The theoretical overall s/n is then presented as a function of channel s/n and compared to simulated results using speech signals. However, before we introduce our new weighting methods we will briefly review the basic concepts of how transmission errors in companded PCM manifest as noise in the recovered analog signal.

II. DIGITAL NOISE IN CONVENTIONAL COMPANDED PCM

In companded PCM the input sample x may be initially compressed to

$$y = f(x), \tag{1}$$

where a common choice of $f(x)$ is the μ- or A-law.[3] These laws are defined as follows. For μ-law PCM,

$$f(x) = \begin{cases} \dfrac{\log(1 + \mu x)}{\log(1 + \mu)}; & 0 \leqslant x \leqslant 1 \\ -f(-x); & -1 \leqslant x < 0, \end{cases} \tag{2}$$

and for A-law,

$$f(x) = \begin{cases} \dfrac{Ax}{1 + \log A}; & 0 \leqslant x \leqslant \dfrac{1}{A} \\ \dfrac{1 + \log(Ax)}{1 + \log A}; & \dfrac{1}{A} < x \leqslant 1 \\ -f(-x); & -1 \leqslant x < 0. \end{cases} \tag{3}$$

In stating $f(x)$ we have followed the practice[2,5] of normalizing the range of both x and y to the interval -1 to $+1$. The compressed sample y is quantized to y_i, which can have one of 2^N possible values. Encoding of y_i into an N-bit binary word L_i ensues, and the words are generated at a rate in excess of the Nyquist rate. The stream of binary words is suitably filtered and modulates a carrier for transmission. Figure 1 is a block diagram of a companded PCM system, although the input filter and sampler, and the final interpolating filter are not displayed.

The receiver demodulates the incoming signal and regenerates the binary words. For the transmitted word L_i, the regenerated word is $L_{i,l}$, where the subscript l signifies that one or more bits may be erroneously produced. We may represent $L_{i,l}$ as the exclusive-OR operation on the binary vectors L_i and e_l, where e_l is an N-bit sequence whose subscript l identifies the error sequence. Thus, we may express $L_{i,l}$ as

$$L_{i,l} = L_i \oplus e_l. \tag{4}$$

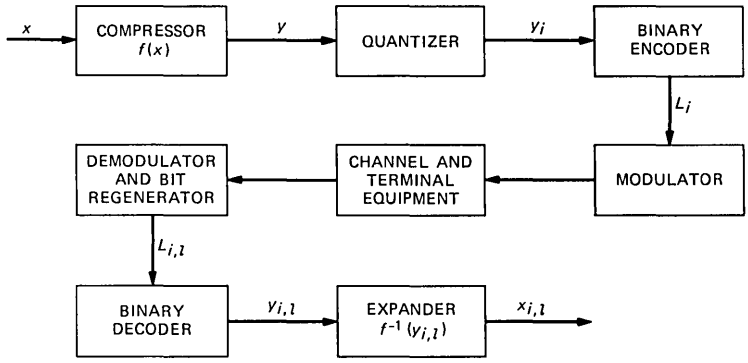

Fig. 1—Block diagram of a conventional PCM system (filters and sampler not shown).

For example, the error sequence 00110000 means that the bits in the third and fourth bit positions are erroneously regenerated. Observe that there are $2^N - 1$ possible e_l sequences. We do not consider the all-zero e_l sequence, as it implies no bit errors are present in the regenerated word. The word $L_{i,l}$ is binary decoded to $y_{i,l}$ and the recovered sample is

$$x_{i,l} = f^{-1}(y_{i,l}). \tag{5}$$

If no transmission binary errors occur, the recovered sample is

$$x_{i,l} = f^{-1}(y_i) = x_i \tag{6}$$

and the overall noise power reduces to the encoder noise power

$$\epsilon_e^2 = E\{(x - x_i)^2\}, \tag{7}$$

where the expected value is formed over the source statistics. However, we are not concerned here with the noise power generated in the encoder, but with the noise power in the recovered samples due to transmission errors, which we call digital noise power. This power is

$$\epsilon_a^2 = E_{i,l}\{(x_i - x_{i,l})^2\}, \tag{8}$$

where the expectation is performed over all 2^N levels of x_i, and over all $2^N - 1$ possible error sequences e_l. The set of $2^N - 1$ error sequences e_l may be subdivided into groups containing single, double, $\cdots$, N-bit errors per PCM word. These groups are described by the Hamming weight, w, so that $w = 1, 2, \cdots, N$. The input signal and PCM encoder are independent of the channel imperfections enabling us to express ϵ_a^2 as

$$\epsilon_a^2 = \sum_{l=1}^{2^{N-1}} \rho_l E_i\{(x_i - x_{i,l})^2\}$$
$$= \sum_{l=1}^{2^{N-1}} \rho_l A_l, \tag{9}$$

where

$$A_l \triangleq E_i\{(x_i - x_{i,l})^2\} \tag{10}$$

are the A-factors, and ρ_l is the probability of occurrence of the lth error sequence e_l, corresponding to the A-factor A_l. Observe that A_l is the average noise power in the output sequence due to the existence of the specific error sequence e_l, the expectation being made over all the values i, namely over the 2^N quantized levels.

When independent errors occur with average bit error probability P, then the probability of w errors in an N-bit word is

$$P_w = P^w(1 - P)^{N-w}.$$

Thus, when the error sequence e_l has w bit errors in the N-bit word, $P_l = P_w$. A case of particular interest is when no more than one error occurs in any PCM word and $P \ll 1$, whence $P_w \simeq P$, and the digital noise power becomes

$$\epsilon_a^2 = P \sum_{l=1}^{N} A_l,$$

where $A_1, A_2, \cdots, A_N$, are the single-error A-factors for errors in bits 1 to N.

III. WEIGHTED PCM

The digital noise power ϵ_a^2 in a PCM system is determined using eq. (9), and we now seek to weight all the bits in the transmitted signal in order to reduce ϵ_a^2. We consider the case when single bit errors occur in any PCM word, knowing that for more severe error conditions the overall s/n is, in general, unacceptably low. Thus, for this case we approximate eq. (9) as

$$\epsilon_a^2 = \sum_{l=1}^{N} \rho_l \mathrm{A}_l. \tag{11}$$

We emphasize that consideration will be given only to binary modulation schemes. From eq. (10),

$$A_l = \sum_{i=0}^{2^{N-1}} p_X(x_i)\Delta_i(x_i - x_{i,l})^2, \tag{12}$$

where $x_{i,l}$ and x_i are given by eqs. (5) and (6), respectively,

$$\Delta_i = \frac{2^{1-N}}{f'(x_i)} \tag{13}$$

is the quantization interval associated with x_i, $p_X(x_i)$ is the PDF of the input sequence, assumed constant over the interval Δ_i, and $f'(x_i)$ is the derivative of $f(x)$ at $x = x_i$.

The validity for this assumption is that there are many quantization levels, as indeed there are for our 8-bit μ-law PCM encoding considered in this paper. In addition to our 256 quantization levels, we have normalized the ranges of x and y to -1, $+1$, and the compressed signal y is uniformly quantized.[3] Writing

$$a_l(x_i) = (x_i - x_{i,l})^2, \tag{14}$$

and observing that the probability of x being located in the quantization interval Δ_i is

$$p_i = p_X(x_i)\Delta_i \tag{15}$$

allows us[5] to express the A-factors as

$$A_l = \sum_{i=0}^{2^N-1} p_i a_l(x_i). \tag{16}$$

Thus, the digital noise power is from eqs. (11) and (16):

$$\epsilon_a^2 = \sum_{l=1}^{N} \sum_{i=0}^{2^N-1} \rho_l p_i a_l(x_i). \tag{17}$$

The probability ρ_l of the error sequence e_l occurring depends upon the modulation scheme employed, e.g., CPSK, NCFSK, whether diversity reception is used, the channel type, the channel s/n, and the method of weighting the bits in the PCM words. We will describe three weighting schemes, which for brevity we will designate Systems 1, 2, and 3.

3.1 Weighted PCM System 1

As a means of introducing weighted PCM we will consider binary amplitude modulation. For this situation each unweighted bit b_l in every PCM word has its magnitude multiplied by $\sqrt{\phi_l}$, where $l = 1, 2, \cdots, N$ refers to the first, second, $\cdots$, LSB, respectively, and $\{\phi_l\}_{l=1}^N$ is the weighting profile for the PCM word, generated as l is varied from 1 to N. For a particular bit, the lth, say, ϕ_l is also referred to as its weight. Observe that in this weighting scheme, each of the 2^N words has identical weighting profiles. The N weighting samples $\sqrt{\phi_l}$, $l = 1, 2, \cdots, N$, are stored in a circulating shift register. As each PCM bit

b_l, $l = 1, 2, \cdots, N$ is generated, the appropriate value of $\sqrt{\phi_l}$ is removed from the shift register and is multiplied by b_l. Thus the weighted bit applied to the transmission terminal equipment is

$$B_{1,l} = \sqrt{\phi_l} b_l; \qquad b_l = \pm 1, \tag{18}$$

where the subscript 1 in $B_{1,l}$ signifies System 1. The receiver is identical to that of unweighted PCM, and the received bits are regenerated by observing at a sampling instant if

$$\begin{aligned} \hat{B}_{1,l} &\geqslant 0; \qquad \text{bit of logical 1} \\ \hat{B}_{1,l} &< 0; \qquad \text{bit of logical 0,} \end{aligned} \tag{19}$$

where $\hat{B}_{1,l}$ is the received value of $B_{1,l}$.

For the general modulation case, let the energy of the lth bit be

$$E_l = \phi_l E, \tag{20}$$

where E is the average energy per bit of the PCM signal,

$$E = \frac{1}{N} \sum_{l=1}^{N} E_l, \tag{21}$$

and by definition ϕ_l is the energy weight assigned to the lth bit. The constraint on the weights in System 1 is, with the aid of eqs. (20) and (21),

$$N = \sum_{l=1}^{N} \phi_l. \tag{22}$$

Thus, from eq. (20), the channel s/n for the lth bit is

$$\Gamma_l = \phi_l \Gamma; \qquad \text{System 1,} \tag{23}$$

where Γ is the average channel s/n, viz:

$$\Gamma = \frac{E}{N_o} \tag{24}$$

and N_o is the one-sided spectral density function of the additive white Gaussian noise.

3.2 Weighted PCM System 2

System 1 deploys fixed weighting profiles, where the same profile is used for every PCM word. This is a suboptimum weighting strategy. Observing that as the digital noise power depends on the value of the quantized sample x_i, it appears desirable to have 2^N different weighting profiles, one for each value of i. By this means we are able to select the unique weighting profile that best suits the particular PCM word to be transmitted. Thus, having generated a μ-law PCM word we use

the index i to address a Read-Only Memory (ROM) that provides us with the optimum weighting profile $\{\phi_l(x_i)\}_{l=1}^{N}$ for that particular word. Weighting then ensues and the weighted lth bit has an amplitude

$$B_{2,l} = \sqrt{\phi_l(x_i)}\, b_l; \qquad b_l = \pm 1 \tag{25}$$

for binary amplitude modulation, where the input sample x is quantized to x_i. The PCM decoder for this system, as with the other two weighted PCM systems, is the same as that employed in conventional PCM.

Because the weighting depends upon the value of the quantized level x_i, we amend eq. (23) to

$$\Gamma_l(x_i) = \phi_l(x_i)\Gamma; \qquad \text{System 2.} \tag{26}$$

3.3 Weighted PCM System 3

In System 2 each profile $\{\phi_l(x_i)\}_{l=1}^{N}$ is optimum for the particular word associated with the quantized level x_i, with the imposed constraint that the word energy for every PCM word is the same. However, the digital noise power varies from word to word, and this leads us to the notion of a subsequent modification to the weighted bit $B_{2,l}$. Specifically, the amplitudes of the weighted bits in the word associated with quantization level x_i are

$$B_{3,l} = \sqrt{W_i} B_{2,l}; \qquad l = 1, 2, \cdots, N, \tag{27}$$

where W_i is a multiplicative factor to the determined. Adopting this approach we arrange for the overall average word energy (and thus the overall average bit energy), rather than the individual word energy, to be constant. We will show that by combining the individual word weighting $\phi_l(x_i)$ of System 2 with the multiplicative factor W_i, a significant enhancement in overall s/n is achieved. In Section 4.3 the constraints on the factor W_i are specified.

The weighting strategy employed in System 3 results in a channel s/n for the lth bit and the ith quantization level of

$$\Gamma_l(x_i) = \phi_l(x_i) W_i \Gamma; \qquad \text{System 3.} \tag{28}$$

3.4 Determining the digital noise power

In order to formulate the digital noise power of eq. (17) we commence with an expression for probability ρ_l that applies for a particular modulation scheme. This probability is dependent upon the long-term channel s/n, Γ, and we replace Γ by one of our values of Γ_l given by either eq. (23), (26), or (28). Thus we obtain an equation of ϵ_a^2 as a function of our weighting factor, namely, ϕ_l, $\phi_l(x_i)$, or $\phi_l(x_i)W_i$. The optimum weighting factor is then found that minimizes the digital noise power, and thereby maximizes the overall s/n. This is the essence

of our approach, and in Section IV we present the derivation of the digital noise power in detail.

3.5 *Objective system performance criterion*

The probability of bit error is a poor measure of system performance, as we discussed in Section 4.1. Instead we opt for overall s/n, given by

$$s\hat{/}n = \frac{E\{x^2\}}{\epsilon_q^2 + \epsilon_c^2 + \epsilon_a^2} = \frac{\sigma_x^2}{\epsilon^2}, \tag{29}$$

where $E\{x^2\}$ or σ_x^2 is the mean signal power, and ϵ_q^2, ϵ_c^2, and ϵ_a^2 are the quantization, clipping, and transmission error noise power components of ϵ^2, respectively. The derivation of eq. (29) is given in Ref. 3. By assuming that N is large, e.g., $N = 8$, the noise power generated in the μ-law PCM encoder is $\epsilon_q^2 + \epsilon_c^2$. The quantization noise power ϵ_q^2 is produced in the quantization process when the input variable x is within the range of the quantizer, namely, -1, $+1$. Clipping noise ϵ_c^2 is produced when x exceeds the range of the quantizer as the recovered signal amplitudes are truncated. The channel noise power ϵ_a^2 is added to the encoder noise power to yield the total noise power.

IV. WEIGHTED PCM FOR FADING CHANNELS

The weighting profiles for PCM when the transmission is over channels subjected to Rayleigh fading will now be determined. Unless otherwise stated, it will be assumed that NCFSK modulation is employed.

4.1 *Weighted PCM System 1*

Let us weight the bits in each word using the same profile for a given channel s/n. The bits are scrambled prior to transmission and on descrambling at the receiver the burst errors on the channel manifest as independent random errors. For NCFSK modulation the average bit error probability for M-fold diversity with Ideal Maximal Ratio Combining (IMRC) is[6]

$$P = \frac{2^{M-1}}{(2 + \Gamma)^M}, \tag{30}$$

where Γ is the average per branch channel s/n. From eqs. (23) and (30) we identify ρ_l of eq. (11) as

$$\rho_l = \frac{2^{M-1}}{(2 + \phi_l\Gamma)^M}, \tag{31}$$

and hence from eqs. (16) and (17) the digital noise power becomes

$$\epsilon_a^2 = \sum_{l=1}^{N} \sum_{i=1}^{2^N-1} \frac{2^{M-1}}{(2 + \phi_l \Gamma)^M} p_i a_l(x_i) = \sum_{l=1}^{N} \frac{2^{M-1} A_l}{(2 + \phi_l \Gamma)^M}, \tag{32}$$

where the constraint of eq. (22) is applicable. In Appendix A, ϵ_a^2 is minimized if the weights

$$\phi_l = \frac{(A_l)^{\frac{1}{M+1}}}{\frac{1}{N} \sum_{k=1}^{N} (A_k)^{\frac{1}{M+1}}} + \frac{2}{\Gamma} \left(\frac{(A_l)^{\frac{1}{M+1}}}{\frac{1}{N} \sum_{k=1}^{N} (A_k)^{\frac{1}{M+1}}} - 1 \right) \tag{33}$$

are employed. Observe that when no diversity is used M is unity, and for this case the average bit error probability $P = 1/(2 + \Gamma)$ is upper bounded by $P \leq 1/\Gamma$. This bound is tight for channel s/n values of interest, and calculating the weight profile ϕ_l using the upper bound yields the first term in eq. (33), which is independent of Γ. The approximate weighting profile that assumes the upper bound of P for $M = 1$ is also the optimum weights when Γ approaches infinity.

Substituting ϕ_l of eq. (33) into eq. (32) yields the digital noise power

$$\epsilon_a^2 = \frac{2^{M-1}}{(2 + \Gamma)^M} \left(\frac{1}{N} \right)^M \left[\sum_{l=1}^{N} (A_l)^{\frac{1}{M+1}} \right]^{M+1}. \tag{34}$$

For weights other than those of eq. (33), the above expression is a lower bound on the digital noise power. The average bit error probability from eq. (31) is

$$P_{av} = \frac{1}{N} \sum_{l=1}^{N} \rho_l = \frac{1}{N} \sum_{l=1}^{N} \frac{2^{M-1}}{(2 + \Gamma \phi_l)^M}. \tag{35}$$

The large contributions to P_{av} derive from the least significant bits because their energy is less than in the unweighted case. The average bit error probability P_{av} for the weighted system does not equal P, and in general it is not a useful design parameter, since the effect of different bit errors on the recovered signal $x_{i,l}$ is radically different. Therefore, we avoid comparing the various weighted PCM systems on the basis of average bit error probabilities. Rather we make our system comparisons at the same average channel s/n, and use as our performance measure the overall s/n given by eq. (29). The $\hat{s/n}$ is a good measure of this quality, and although for a given channel s/n the weighting may increase P_{av}, it nearly always reduces ϵ_a^2, and hence increases $\hat{s/n}$.

We point out that it is not essential to have N different bit weights to obtain significant reductions in ϵ_a^2 compared to unweighted PCM. Suboptimum weighting schemes with fewer weights than N are dis-

cussed in Ref. 2, but we will confine ourselves here to the optimum weighting profile condition.

On rare occasions the weighting profile may include negative weights, for example, when the channel s/n, Γ, is low in eq. (33). The occurrence of negative weights is primarily due to the oversimplified optimization procedures we adopted. Ideally the optimization should always include the constraint $\phi_l \geq 0$, $l = 1, 2, \cdots, N$, even when we choose to ignore the effect of double errors, which become more probable for low Γ's and small weights. However, for high-channel signal-to-noise ratios the simplified optimization procedure employed here is quite sufficient. Negative weights can be avoided without this constraint if we elect to discard the second term in eq. (33), i.e., we employ the optimum weights appropriate for high-channel s/n. Of course, the low-channel s/n's that result in a weight becoming negative are of no practical value, as the overall s/n, $\hat{s/n}$, is then unacceptably low. However, the unrestricted optimization we have performed always provides upper bounds on the gains in $\hat{s/n}$ that apply to the different weighting schemes; bounds that are reasonable estimates of the gains in $\hat{s/n}$ that can be practically expected. Thus, in our simulations we employed the asymptotic weight, i.e., the first term in eq. (33), namely,

$$\phi_l = \frac{(A_l)^{\frac{1}{M+1}}}{\frac{1}{N}\sum_{k=1}^{N}(A_k)^{\frac{1}{M+1}}}. \tag{36}$$

This weight was also employed in our simulations using CPSK modulation.

4.2 *Weighted PCM System 2*

The individual word weighting profiles are dependent upon the $a_l(x_i)$ terms in the A-factors [see eqs. (14) and (16)]. These $a_l(x_i)$ functions enable us to know how the effect of an error in the lth bit varies with the input level x_i. The reader is referred to Ref. 7 for a detailed account of the variation of $a_l(x_i)$ as a function of x_i for $l = 1, 2, \cdots, 8$, for 8-bit μ-law PCM, $\mu = 255$.

We now consider the digital noise power that occurs in this weighting scheme. First, the value of $\Gamma_l(x_i)$ given by eq. (26) replaces Γ in eq. (30). The expression for ρ_l so formulated is then substituted into eq. (17) to give the digital noise power of

$$\epsilon_a^2 = \sum_{i=0}^{2^N-1} p_i \sum_{l=1}^{N} \frac{2^{M-1}a_l(x_i)}{(2 + \phi_l(x_i)\Gamma)^M}. \tag{37}$$

Minimizing ϵ_a^2 with respect to $\phi_l(x_i)$ yields the optimum weights

$$\phi_l(x_i) = \frac{[a_l(x_i)]^{\frac{1}{M+1}}}{\frac{1}{N}\sum_{k=1}^{N}[a_k(x_i)]^{\frac{1}{M+1}}} + \frac{2}{\Gamma}\left[\frac{[a_l(x_i)]^{\frac{1}{M+1}}}{\frac{1}{N}\sum_{k=1}^{N}[a_k(x_i)]^{\frac{1}{M+1}}} - 1\right] . \quad (38)$$

If we use the optimum weights specified by eq. (38), the digital noise power is given by

$$\epsilon_a^2 = \frac{2^{M-1}}{(2+\Gamma)^M}\left(\frac{1}{N}\right)^M \sum_{i=0}^{2^N-1} p_i \left[\sum_{l=1}^{N}[a_l(x_i)]^{\frac{1}{M+1}}\right]^{M+1} . \quad (39)$$

For high-channel s/n only the first term in eq. (38) need be considered. The variation of $\phi_l(x_i)$ as a function of quantized level x_i for 8-bit μ-law PCM, $\mu = 255$, is displayed in Fig. 2 for each bit in the PCM word. The discontinuities in $\phi_l(x_i)$ derive from the discontinuities in $\{a_k(x_i)\}_{k=1}^{N}$. In the case of $\phi_1(x_i)$, where $a_1(x_i)$ is a monotonic function, the summation of $a_k(x_i)$ in the denominator of $\phi_l(x_i)$ is responsible for the jumps observed in $\phi_1(x_i)$ in Fig. 2a. When diversity is applied, $M = 2$, the word weighting profiles $\phi_l(x_i)$ for System 2 are altered, although they have similar shapes to those shown in Fig. 2.

The average bit error probability is

$$P_{av} = \sum_{i=0}^{2^N-1} p_i \frac{1}{N}\sum_{l=1}^{N}\frac{2^{M-1}}{[2+\phi_l(x_i)\Gamma]^M} . \quad (40)$$

4.3 Weighted PCM System 3

Let us commence our investigation into this form of weighting by introducing the constraint

$$\sum_{i=0}^{2^N-1} p_i \frac{E_i}{N_o} = \frac{E}{N_o} , \quad (41)$$

where p_i is given by eq. (15). We introduce the word weighting factor W_i by ensuring that the channel s/n for x_i is

$$\frac{E_i}{N_o} = W_i \frac{E}{N_o} ; \qquad i = 0, 1, 2, \cdots, 2^N - 1. \quad (42)$$

From eqs. (41) and (42) we formulate our imposed constraint on the word weighting factor W_i, viz:

$$\sum_{i=0}^{2^N-1} p_i W_i = 1. \quad (43)$$

The individual bit weights in the PCM words are given by eq. (38), and the previous constraint of eq. (22) with $\phi_l = \phi_l(x_i)$ still applies. We observe that although the word energy is no longer constant, the

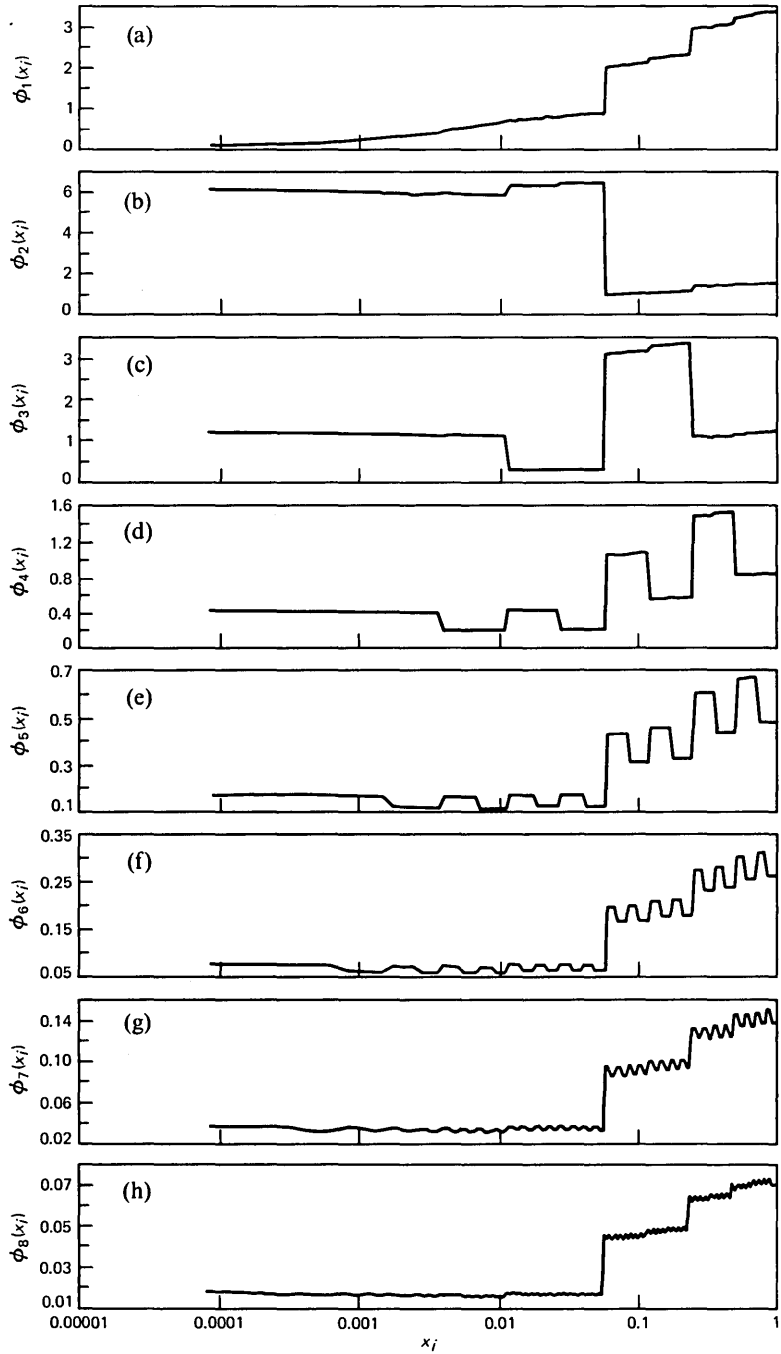

Fig. 2—The variation of the word weighting profiles $\phi_l(x_i)$ as a function of x_i for 8-bit μ-law Rayleigh fading channel PCM, $\mu = 255$, input signal level of -17 dB. The subfigures (a), (b), $\cdots$, (h), relate to $l = 1, 2, \cdots, 8$, respectively.

average PCM word energy E is unchanged by this subsequent word weighting of W_i.

The minimization of the digital noise power is divided into two steps. The optimum bit weight profiles, $\phi_l(x_i)$, are basically the same as in the previous section, with the exception that the word weights are now varied with the "word s/n", i.e., E_i/N_o. The average digital noise power when the weighting set $\{W_i\}$ is included is, from eqs. (17), (28), and (30),

$$\epsilon_a^2 = \sum_{i=0}^{2^N-1} p_i \sum_{l=1}^{N} \frac{2^{M-1} a_l(x_i)}{[2 + W_i \phi_l(x_i)\Gamma]^M} . \tag{44}$$

The optimum weights $\phi_l(x_i)$ given by eq. (38) enable ϵ_a^2 of eq. (44) to be expressed as

$$\epsilon_a^2 = \sum_{i=0}^{2^N-1} p_i \left\{ \frac{2^{M-1}}{(2 + W_i\Gamma)^M} \right\} \beta(x_i), \tag{45}$$

where

$$\beta(x_i) = \left(\frac{1}{N}\right)^M \left[\sum_{l=1}^{N} [a_l(x_i)]^{\frac{1}{M+1}} \right]^{M+1} . \tag{46}$$

The function $\beta(x_i)$ depends upon the magnitude of the quantized level and upon $a_l(x_i)$, whose discontinuties cause $\beta(x_i)$ to have sharp jumps as x_i changes segments.

The optimum word weights W_i are determined by minimizing ϵ_a^2 with respect to W_i, employing the constraint of eq. (43). By this method the optimum word weights are

$$W_i = \frac{[\beta(x_i)]^{\frac{1}{M+1}}}{\sum_{k=0}^{2^N-1} p_k [\beta(x_k)]^{\frac{1}{M+1}}} + \frac{2}{\Gamma} \left[\frac{[\beta(x_i)]^{\frac{1}{M+1}}}{\sum_{k=0}^{2^N-1} p_k [\beta(x_k)]^{\frac{1}{M+1}}} - 1 \right] . \tag{47}$$

Substituting W_i into eq. (45) yields the digital noise power

$$\epsilon_a^2 = \frac{2^{M-1}}{(2 + \Gamma)^M} \left[\sum_{i=0}^{2^N-1} p_i [\beta(x_i)]^{\frac{1}{M+1}} \right]^{M+1} . \tag{48}$$

The average bit error probability is

$$P_{av} = \sum_{i=0}^{2^N-1} p_i \sum_{l=1}^{N} \frac{1}{N} \frac{2^{M-1}}{(1 + \phi_l(x_i) W_i \Gamma)^M} . \tag{49}$$

4.4 Weighting for ideal selection combining diversity and NCFSK

When Ideal Selection Combining (ISC) diversity is employed, the average bit error probability of an unweighted PCM system can be shown to be[6-8]

$$P = \frac{M}{2\Gamma} \sum_{k=0}^{M-1} \binom{M-1}{k} (-1)^k \frac{1}{\left(\frac{1}{\Gamma} + \frac{k}{\Gamma}\right) + \frac{1}{2}}, \tag{50}$$

where M is the order of the diversity. The channel s/n Γ is changed according to the method of weighting, as described in Sections 3.1 through 3.3. For Systems 1, 2, and 3, Γ is replaced by $\phi_l\Gamma$, $\phi_l(x_i)\Gamma$, and $\phi_l(x_i)W_i\Gamma$, respectively. Satisfactory values of the weights are the asymptotic weights derived for the different weighting procedures for ideal maximal ratio combining diversity. Thus, the weights given by eq. (36) are used for System 1; $\phi_l(x_i)$ of eq. (38) is used when Γ tends to infinity [i.e., the asymptotic values of $\phi_l(x_i)$, for System 2], while the same $\phi_l(x_i)$ used for System 2 is also used for System 3, together with the asymptotic value of W_i [see eq. (47)]. As before, the values of ρ_l so determined are substituted into eq. (17) to give the digital noise power for the three systems.

4.5 Weighting for CPSK modulation

When Ideal Maximal Ratio Combining (IMRC) diversity is employed with CPSK, the average bit error probability is[6-8]

$$P = \frac{1}{2}\left[1 - \frac{1}{\sqrt{1 + \frac{1}{\Gamma}}} \sum_{k=1}^{M} \binom{2k-2}{k-1} \left(\frac{1 - \frac{1}{1 + \frac{1}{\Gamma}}}{4}\right)^{k-1}\right]. \tag{51}$$

The value of Γ in the above equation is changed according to eq. (23), (26), or (28), depending on whether System 1, 2, or 3 is employed. We employed the asymptotic weights derived for NCFSK and IMRC diversity for this case of CPSK modulation. The probability ρ_l computed by this means is substituted into eq. (17) to yield the digital noise power.

For the case of ISC diversity and CPSK modulation the average bit error probability is[6-8]

$$P = \frac{1}{2} \sum_{k=0}^{M} (-1)^k \binom{M}{k} \frac{1}{\sqrt{1 + \frac{k}{\Gamma}}}. \tag{52}$$

We convert P into ρ_l as before by replacing Γ with the appropriate value given by eq. (23), (26), or (28), and then use the asymptotic weights derived for the case of NCFSK and IMRC diversity.

4.6 Unweighted PCM

For conventional PCM, i.e., where weighting is not employed, and bit scrambling is provided prior to transmission, the modulation being NCFSK, then the digital noise power can be shown to be[7]

$$\epsilon_a^2 = \sum_{w=1}^{N} T_w \left(\frac{2^{M-1}}{(2 + \Gamma)^M} \right)^w \tag{53}$$

for IMRC diversity, where

$$T_w = \sum_{j=1}^{w} S_w \binom{N-j}{w-j} (-1)^{w-j}; \qquad w = 1, 2, \cdots, N, \tag{54}$$

and S_w is the sum of the A-factors associated with error sequences containing w ones. When ISC diversity is employed, the digital noise power is[7]

$$\epsilon_a^2 = \sum_{w=1}^{N} T_w \left[\frac{M}{2\Gamma} \sum_{j=0}^{M-1} (-1)^j \binom{M-j}{j} \frac{1}{\left(\frac{1}{\Gamma} + \frac{j}{\Gamma} + \frac{1}{2} \right)} \right]^w. \tag{55}$$

Equations (53) and (55) are included as bench marks against which the digital noise power of weighted PCM can be measured.

V. WEIGHTED PCM FOR THE GAUSSIAN CHANNEL

For this channel there is no need for diversity, nor bit scrambling prior to transmission, as the bit errors are independent in nature.

5.1 Weighted PCM System 1

For NCFSK modulation and unweighted PCM the average bit error probability is

$$P = \frac{1}{2} e^{-\frac{E}{2N_o}}, \tag{56}$$

and when bit weighting is applied such that the lth bit, $l = 1, 2, \cdots, N$, has its amplitude individually adjusted, the expression for P is modified to eq. (23), viz:

$$\rho_l = \frac{1}{2} e^{-\phi_l \frac{E}{2N_o}}. \tag{57}$$

Substituting ρ_l into eq. (17) gives the digital noise power ϵ_a^2. In Appendix B we show that the optimum weights that minimize this digital noise power are

$$\phi_l = 1 + \frac{\ln\left(\frac{A_l}{A_o}\right)}{\frac{E}{2N_o}}; \qquad l = 1, 2, \cdots, N, \tag{58}$$

where

$$A_o = \left(\prod_{l=1}^{N} A_l\right)^{1/N}. \tag{59}$$

The optimum weights ϕ_l are thus dependent on the channel s/n, namely E/N_o. Substituting the optimum weights ϕ_l into eq. (17) yields

$$\epsilon_a^2 = NA_oP, \tag{60}$$

where P is the average bit error probability given by eq. (56).

The average bit error probability for the unweighted scheme is, from eq. (57),

$$P_{av} = \frac{1}{N}\sum_{l=1}^{N}\frac{1}{2}e^{-\phi_l\frac{E}{2N_o}}. \tag{61}$$

When weighting is applied, and the weighting is optimum at each channel s/n, the average bit error probability is determined by substituting ϕ_l from eq. (58) into eq. (61), viz:

$$P_{av} = \frac{P}{N}\sum_{l=1}^{N}\left(\frac{A_o}{A_l}\right), \tag{62}$$

where P is the average bit error probability for NCFSK when no weighting is used [see eq. (56)].

5.2 Weighted PCM System 2

As the individual word weighting profile ϕ_l depends in this weighting scheme on the value of x_i, we express ϕ_l as $\phi_l(x_i)$, $l = 1, 2, \cdots, N$, for each of the 2^N values of x_i. In Appendix C the weighting profile is shown to be

$$\phi_l(x_i) = 1 + \frac{\ln\left(\frac{a_l(x_i)}{a_o(x_i)}\right)}{\frac{E}{2N_o}}$$

$$l = 1, 2, \cdots, N,$$

$$i = 0, 1, 2, \cdots, 2^N - 1, \tag{63}$$

where

$$a_o(x_i) = \left(\prod_{l=1}^{N} a_l(x_i) \right)^{1/N}. \tag{64}$$

Thus we have the most significant bit (MSB), next MSB, $\cdots$, LSB, weighted by $\phi_1(x_i)$, $\phi_2(x_i)$, $\cdots$, $\phi_N(x_i)$, respectively, for quantized level x_i, and these word weighting profiles are available for the 2^N values of i, i.e., the 2^N different PCM words. When these optimum weights $\phi_l(x_i)$ are employed, the average digital noise power is, from eqs. (17) and (63),

$$\epsilon_a^2 = P \sum_{i=0}^{2^N-1} p_i N a_o(x_i). \tag{65}$$

The average bit error probability for the optimum individual weighting profiles is, with the aid of eqs. (61) and (63),

$$P_{av} = P \sum_{i=0}^{2^N-1} \frac{p_i}{N} \sum_{l=1}^{N} \frac{a_o(x_i)}{a_l(x_i)}, \tag{66}$$

where P is the bit error probability for NCFSK.

5.3 Weighted PCM System 3

The average digital noise power for System 3 is from eqs. (17), (28), and (56):

$$\epsilon_a^2 = \sum_{i=0}^{2^N-1} p_i N a_o(x_i) \frac{1}{2} e^{-\frac{W_i E}{2N_o}}. \tag{67}$$

The word weighting factors are optimized such that ϵ_a^2 is minimized. This minimization is performed in Appendix D, from which

$$W_i = 1 + \frac{2N_o}{E} \left\{ \ln[N a_o(x_i)] - \sum_{k=0}^{2^N-1} p_k \ln[N a_o(x_k)] \right\}$$

$$i = 0, 1, 2, \cdots, 2^N - 1. \tag{68}$$

The final optimum bit weight is found by multiplying W_i with $\phi_l(x_i)$ of eq. (63), where E is replaced by E_i/W_i. When this is performed the minimum digital noise power becomes

$$\epsilon_a^2 = P e^{\sum_{i=0}^{2^N-1} p_i \ln[N a_o(x_i)]}. \tag{69}$$

The average bit error probability for this combined individual and word-by-word weighting is

$$P_{av} = \sum_{i=0}^{2^N-1} p_i \left\{ \frac{1}{N} \sum_{l=1}^{N} \frac{a_o(x_i)}{a_l(x_i)} \right\} e^{-\frac{W_i E}{2N_o}}. \tag{70}$$

Substituting W_i from eq. (68) into eq. (70) yields

$$P_{av} = P \sum_{i=0}^{2^N-1} \frac{p_i \prod_{k=0}^{2^N-1} [Na_o(x_k)]^{p_k}}{Na_o(x_i)} \cdot \frac{1}{N} \sum_{l=1}^{N} \frac{a_o(x_i)}{a_l(x_i)} . \tag{71}$$

5.4 Unweighted PCM

The digital noise power can be shown to be[7]

$$\epsilon_a^2 = \sum_{w=1}^{N} P^w (1 - P)^{N-w} S_w = \sum_{w=1}^{N} T_w P^w \tag{72}$$

and the value of P depends upon the modulation used. For NCFSK

$$P = \frac{1}{2} e^{-\Gamma/2}, \tag{73}$$

and for CPSK

$$P = Q(\sqrt{2\Gamma}), \tag{74}$$

where $Q(x)$ is the error function

$$Q(x) = \frac{1}{\sqrt{2\pi}} \int_x^\infty e^{-t^2/2} dt. \tag{75}$$

5.5 Peak power constraint

The formulae for the previous weighting schemes have been derived without imposing a limit on the peak power. When such limitations are applied the optimization problem changes, and the digital noise power may increase. Thus our formulae provide upper bounds for the gains in overall s/n, or, alternatively, reductions in digital noise power, compared to unweighted PCM at the same channel s/n.

VI. RESULTS

In this section we present numerical and graphical interpretations of the formulae derived in Section IV. We also provide computer simulation results for speech signals that were subjected to our different weighting strategies and conveyed over simulated Rayleigh fading and Gaussian channels. The encoder was 8-bit μ-law PCM, $\mu = 255$, where the quantized levels were binary encoded using a folded binary code.

6.1 Results for the Rayleigh fading channel

The constant word weighting profile ϕ_l of eq. (36) for $M = 1$, computed using A_l of eq. (10), where $l = 1$ to 8, is presented in Table I for input powers of -17 and -40 dB. The individual word weighting

Table I—Constant word weighting profile $\{\phi_l\}_{l=1}^{N}$ for the Rayleigh fading channel (asymptotic weights)

Input Power	Bit Number l							
	1	2	3	4	5	6	7	8
−17 dB	1.9432	2.5643	2.0376	0.7974	0.3553	0.1732	0.0860	0.0429
−40 dB	0.6156	6.0135	0.7787	0.3250	0.1445	0.0704	0.0349	0.0174

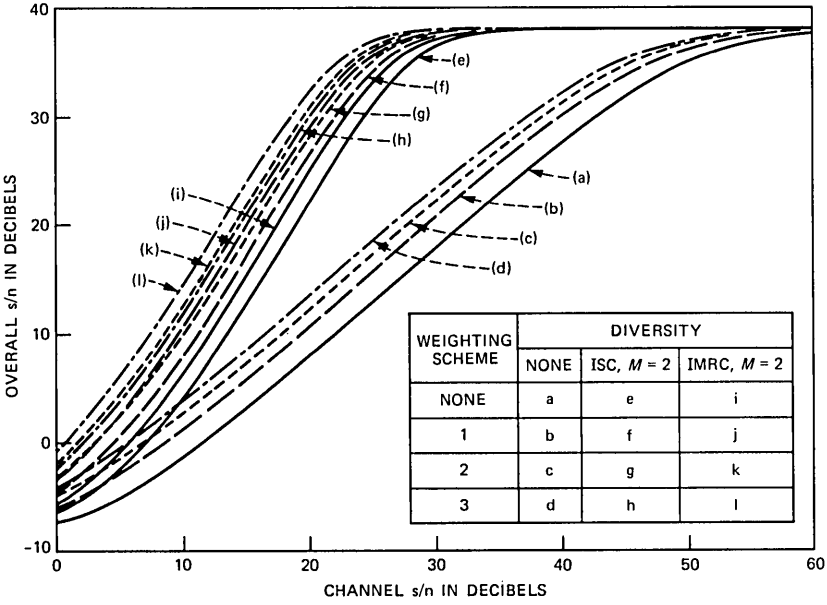

Fig. 3—Rayleigh fading channel. Theoretical curves of overall s/n as a function of channel s/n for NCFSK and an input power level of −17 dB.

profiles $\phi_l(x_i)$ of eq. (38) are displayed in Fig. 2 for $M = 1$. The word weighting factors W_i of eq. (47) are presented in Table II for input powers of −17 and −40 dB, and $M = 1$.

The $\hat{s/n}$ given by eq. (29) is used as our objective performance measure. In the absence of transmission errors ϵ_a^2 is zero, and the $\hat{s/n}$ becomes $\sigma_x^2/(\epsilon_q^2 + \epsilon_c^2)$. For an 8-bit μ-law PCM codec, $\mu = 255$, the variation of $\sigma_x^2/(\epsilon_q^2 + \epsilon_c^2)$ as a function of input power σ_x^2 is determined using well-established results.[2] Two input power levels of −17 and −40 dB relative to the clipping level (±1) are considered, having a correspondence to voiced and unvoiced signal levels, respectively. Knowing σ_x^2 and $\sigma_x^2/(\epsilon_q^2 + \epsilon_c^2)$ enables $(\epsilon_q^2 + \epsilon_c^2)$ to be found. The next task is to compute the digital noise power ϵ_a^2 given by eq. (17). We consider the PDF of the source to be exponential

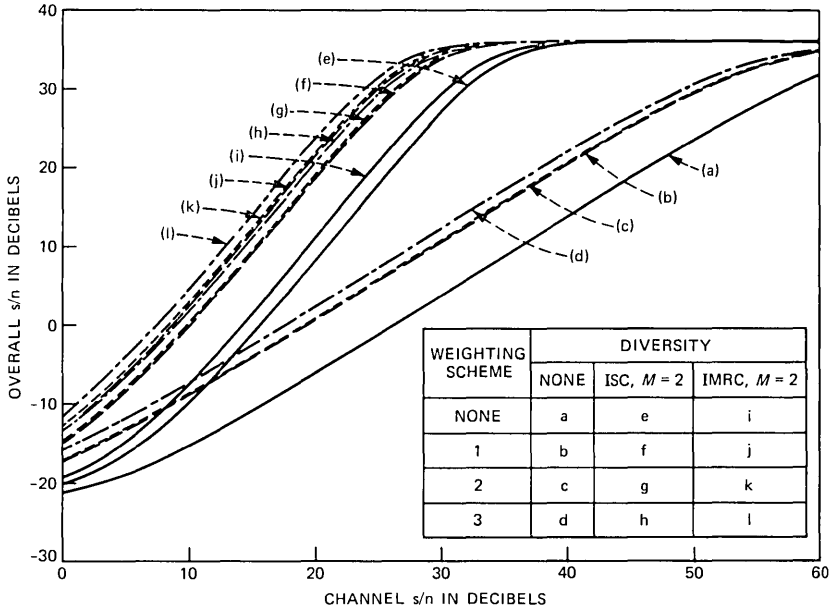

Fig. 4—Rayleigh fading channel. Theoretical curves of overall s/n as a function of channel s/n for NCFSK and an input power level of −40 dB.

$$p_X(x_i) = \frac{1}{\sigma_x\sqrt{2}} \exp\left(-\frac{\sqrt{2}x_i}{\sigma_x}\right), \tag{76}$$

from which the 2^N values of p_i are determined using the 2^N values of x_i. The values of p_i and the $a_l(x_i)$ factors are substituted in eq. (16) to yield the set of A-factors A_l.

The digital noise power ϵ_a^2 of unweighted N-bit μ-law PCM, $N = 8$, $\mu = 255$, is found using either eq. (53) or (55). The variation of ϵ_a^2 as a function of channel s/n is next determined. For a given input power σ_x^2 the $\hat{s/n}$ depends only on ϵ_a^2, and hence Γ. Consequently, we are able to obtain the graphs of theoretical $\hat{s/n}$ as a function of channel s/n for unweighted PCM, as shown by curves a in Figs. 3, 4, 5, and 6, where the curves in Figs. 3 and 5 and those in Figs. 4 and 6 apply for input levels of −17 and −40 dB, respectively. These unweighted PCM curves are included as references to which our weighted PCM curves can be compared.

The optimum weights for high-channel s/n values for Systems 1, 2, and 3, i.e., asymptotic weights, are the first term in eqs. (33), (38), and (47), respectively. The digital noise power for the various schemes and conditions applicable to Figs. 3 to 6 is formulated with the aid of eqs. (32), (37), and (44), where the asymptotic weights are used.

Figure 3 shows the curves of theoretical $\hat{s/n}$ as a function of channel

Table II—Word weight factors W_i for the Rayleigh fading channel (asymptotic weights)

Input Power = −17 dB								
0.1204	0.1258	0.1313	0.1372	0.1432	0.1496	0.1562	0.1632	0.1704
0.1780	0.1859	0.1941	0.2028	0.2118	0.2212	0.2310	0.2410	0.2517
0.2629	0.2746	0.2868	0.2995	0.3128	0.3268	0.3412	0.3564	0.3722
0.3888	0.4060	0.4241	0.4429	0.4626	0.4753	0.4964	0.5185	0.5415
0.5655	0.5907	0.6169	0.6443	0.6727	0.7026	0.7338	0.7664	0.8003
0.8359	0.8729	0.9117	0.9507	0.9929	1.0370	1.0829	1.1310	1.1811
1.2335	1.2882	1.3451	1.4047	1.4670	1.5320	1.5999	1.6708	1.7448
1.8222	0.4804	0.5020	0.5245	0.5481	0.5725	0.5982	0.6250	0.6530
0.6805	0.7110	0.7428	0.7760	0.8104	0.8467	0.8844	0.9239	0.9436
0.9857	1.0297	1.0756	1.1232	1.1733	1.2256	1.2802	1.3337	1.3931
1.4551	1.5199	1.5870	1.6576	1.7313	1.8083	1.2848	1.3422	1.4020
1.4646	1.5289	1.5971	1.6682	1.7426	1.8100	1.8906	1.9747	2.0626
2.1530	2.2488	2.3487	2.4532	2.4303	2.5385	2.6511	2.7690	2.8900
3.0184	3.1523	3.2924	3.4170	3.5688	3.7270	3.8925	4.0622	4.2426
4.4305	4.6272							
Input Power = −40 dB								
0.3664	0.3827	0.3996	0.4174	0.4359	0.4552	0.4754	0.4966	
0.5185	0.5416	0.5657	0.5908	0.6171	0.6445	0.6731	0.7031	
0.7333	0.7659	0.8000	0.8356	0.8727	0.9115	0.9520	0.9943	
1.0384	1.0845	1.1327	1.1830	1.2356	1.2905	1.3478	1.4077	
1.4464	1.5107	1.5778	1.6478	1.7210	1.7974	1.8772	1.9605	
2.0472	2.1381	2.2329	2.3320	2.4355	2.5435	2.6564	2.7742	
2.8932	3.0215	3.1555	3.2954	3.4415	3.5941	3.7535	3.9199	
4.0931	4.2745	4.4640	4.6619	4.8685	5.0843	5.3096	5.5449	
1.4618	1.5275	1.5961	1.6678	1.7421	1.8202	1.9018	1.9870	
2.0708	2.1635	2.2603	2.3613	2.4662	2.5764	2.6914	2.8116	
2.8715	2.9996	3.1334	3.2732	3.4181	3.5705	3.7295	3.8956	
4.0586	4.2393	4.4279	4.6250	4.8293	5.0442	5.2683	5.5026	
3.9097	4.0844	4.2664	4.4568	4.6526	4.8601	5.0764	5.3027	
5.5078	5.7532	6.0090	6.2766	6.5515	6.8431	7.1471	7.4560	
7.3956	7.7246	8.0675	8.4263	8.7943	9.1852	9.5926	10.0189	
10.3980	10.8599	11.3413	11.8449	12.3614	12.9102	13.4822	14.0806	

s/n for NCFSK; an input power level of −17 dB; no diversity, and two-branch diversity, when IMRC and ISC techniques are used; and the effect of employing the three weighting schemes. Curves b, c, and d apply to weighting PCM Systems 1, 2, and 3, respectively, when diversity reception is not used. Comparing these curves to the unweighted PCM curve a, we observe that over the range of channel s/n where these are parallel, the gain in $\hat{s/n}$ is 2.8, 4.5, and 6 dB, respectively. When second-order diversity is employed, curves e to l apply. Curves e, f, g, and h relate to unweighted PCM and weighted PCM Systems 1, 2, and 3, respectively; the diversity is ISC. We observe that the gains in $\hat{s/n}$ for Systems 1, 2, and 3 compared to unweighted PCM are significantly larger than those for the case of $M = 1$. Further, the systems are able to operate at a much lower channel s/n, Γ, for the same $\hat{s/n}$. When we use IMRC diversity the gains in $\hat{s/n}$ are similar to those achieved with ISC, but for a given Γ, the values of $\hat{s/n}$ are increased by approximately 2 dB.

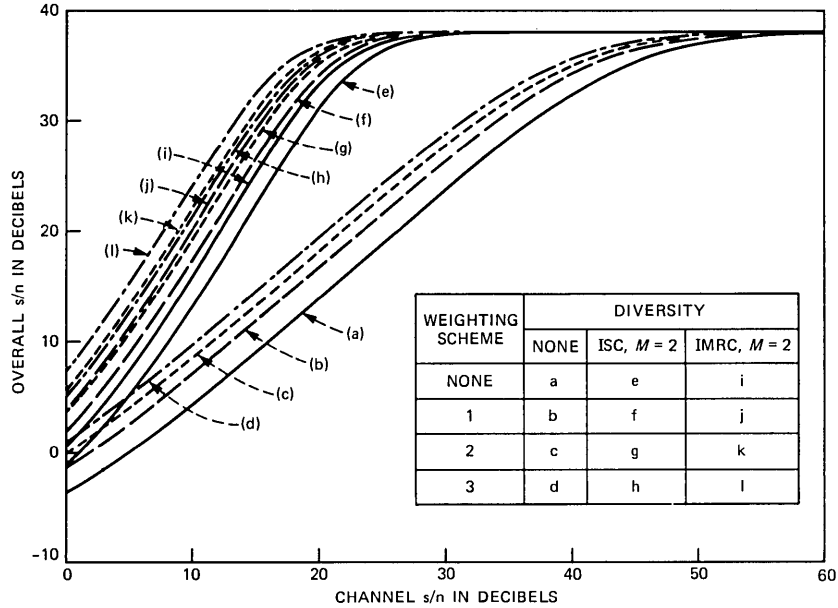

Fig. 5—Rayleigh fading channel. Theoretical curves of overall s/n as a function of channel s/n for CPSK and an input power level of −17 dB.

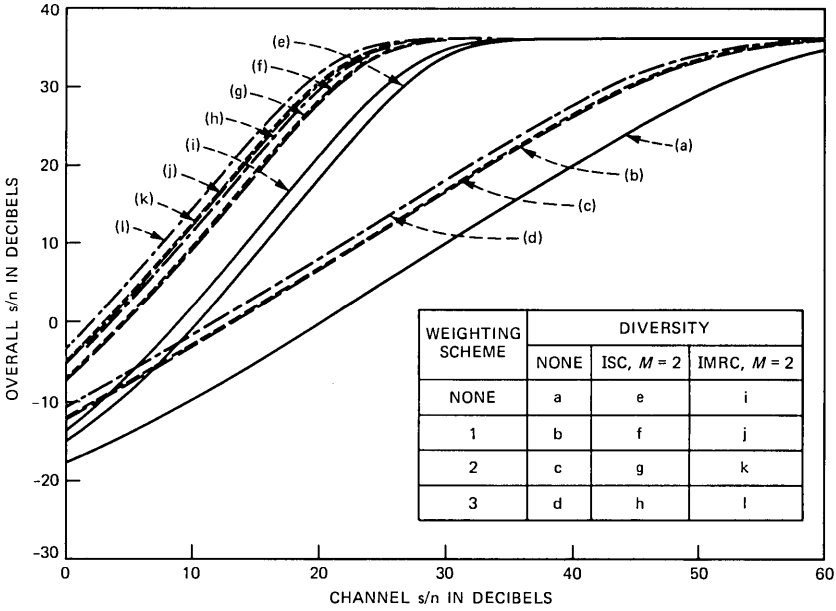

Fig. 6—Rayleigh fading channel. Theoretical curves of overall s/n as a function of channel s/n for CPSK and an input power level of −40 dB.

When the level of the input signal is reduced to −40 dB the curves in Fig. 4 are obtained. Curves a to l relate to the same system parameters as those in Fig. 3. As we expected the peak $\hat{s}/n$ (at high values of Γ) are reduced by 2 dB due to coarse quantization at low signal levels. The slopes of the curves in Fig. 4 are lower than those in Fig. 3. However, the curves of $\hat{s}/n$ for Systems 2 and 3 are approximately the same when no diversity is applied. Marginally greater gains in $\hat{s}/n$ occur at this lower power level of −40 dB when second-order diversity reception is employed.

The theoretical curves for CPSK are shown in Figs. 5 and 6. The curves a to l in Figs. 5 and 6 correspond to those in Figs. 3 and 4, respectively. The essential difference between the curves is that for the same $\hat{s}/n$, the Γ is 6 dB lower when CPSK is employed compared to when NCFSK modulation is used.

6.1.1 Speech input signals

Speech composed of four concatenated sentences, "Glue the sheet to the dark blue background," "Rice is often served in round bowls," "Four hours of steady work faced us," and "The box was thrown beside the parked truck," were used as our speech input signal. The former two sentences were spoken by females, the latter two sentences by males. The speech signal was bandlimited between 200 to 3200 Hz, sampled at 8 kHz, and stored in the computer. Eight-bit μ-law PCM encoding ensued, the bit stream suitably weighted, and two-level CPSK modulation of a Radio Frequency (RF) carrier performed. From a hardware simulator of frequency-selective Rayleigh-fading mobile radio paths[9] samples of the envelope function $C(t)$ were taken at a rate of 32 kHz and stored in the computer to provide the fading envelope of a mobile unit traveling at 15 mph. By resampling $C(t)$ different vehicle speeds could be simulated. The regenerated lth bit at the kth instant was[10]

$$\hat{B}_{(\cdot),l}(k) = C(k)B_{(\cdot),l}(k) + I(k) \geq 0; \qquad \text{logical 1 generated}$$

$$\hat{B}_{(\cdot),l}(k) = C(k)B_{(\cdot),l}(k) + I(k) < 0; \qquad \text{logical 0 generated}$$

$$l = 1, 2, \cdots, N, \tag{77}$$

where $(\cdot)$ is 0, 1, 2, or 3, depending on whether the PCM was unweighted or System 1, 2, or 3 was used, respectively. The amplitude of the Rayleigh envelope, the transmitted bit, and the additive interference level are represented in eq. (77) by $C(k)$, $B_{(\cdot),l}(k)$ and $I(k)$, respectively. After bit regeneration the μ-law PCM words were formulated and subsequently decoded. This decoded speech sequence was subtracted from its counterpart in the input speech sequence to yield the noise sequence. The $\hat{s}/n$ was computed as the ratio of the input

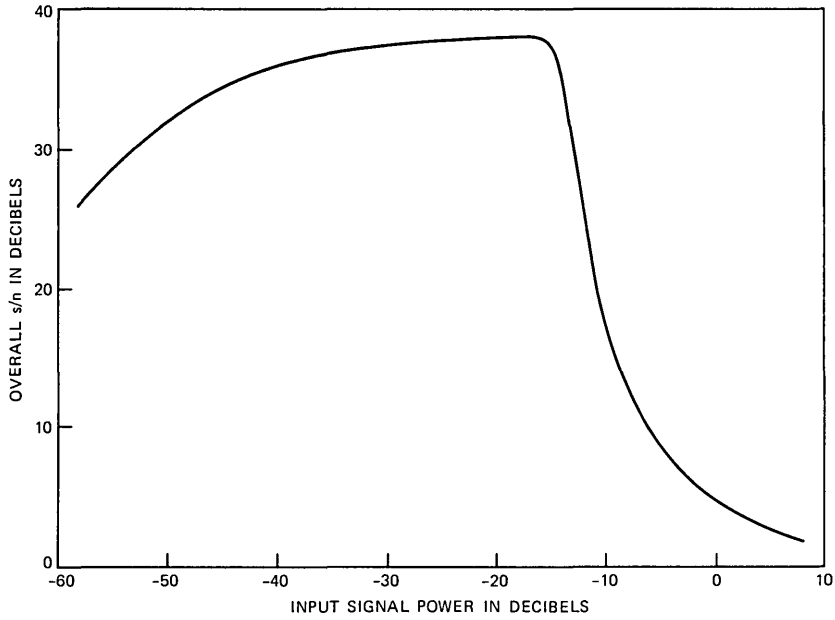

Fig. 7—Overall s/n as a function of input speech power for zero bit error rate.

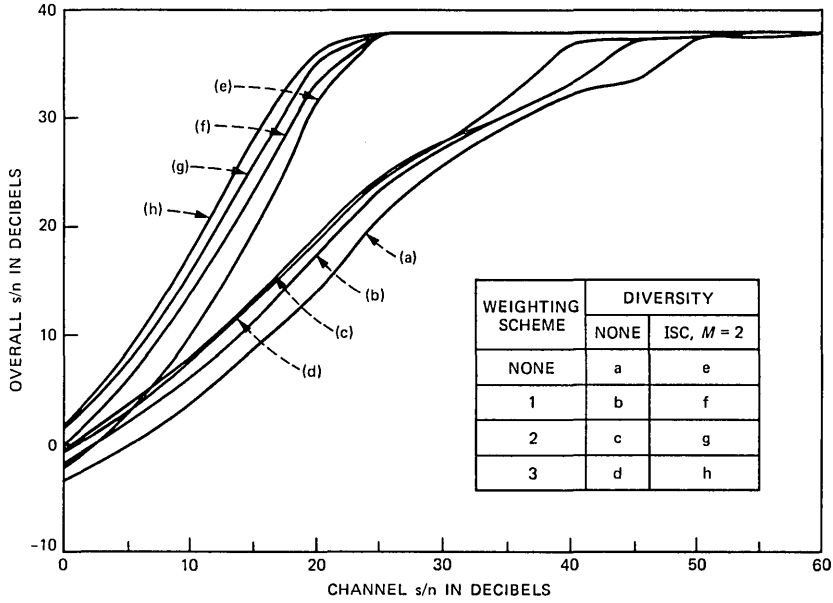

Fig. 8—Mobile radio channel. Overall s/n versus channel s/n for CPSK and speech input signals. The input power level is −17 dB and the vehicular speed is 30 mph.

speech power to the noise sequence power. The curve of $\hat{s/n}$ as a function of input speech power is displayed in Fig. 7 for zero BER.

Figure 8 shows the performance of our three weighting systems and unweighted PCM in the absence of diversity and when second-order ISC diversity was employed for an input level of −17 dB. The corresponding performance when the vehicular speech was 60 mph is displayed in Fig. 9. The effects of the nonstationary speech statistics and the duration of the speech and Rayleigh envelope data conspire to cause the curves in Figs. 8 and 9 to lose the parallelism of those in Fig. 5. However, the $\hat{s/n}$ advantage due to using diversity and our weighting systems when speech input signals are employed has a close correspondence with the gains predicted from our theoretical results. We note that the performance of the system as the vehicular speed doubles is, in general, very similar, although there are some large local variations.

Figure 10a shows a segment of speech, while Fig. 10b, c, d, and e were the recovered speech waveforms for unweighted PCM, weighted PCM Systems 1, 2, and 3, respectively, when the vehicular speech was 30 mph, an input level of −17 dB, CPSK modulation, no diversity, $\Gamma = 16$ dB. When ISC, $M = 2$ was employed and the other conditions remained unchanged, the results were the corresponding recovered speech waveforms in Fig. 10 f, g, h, and i. We observe that the effect

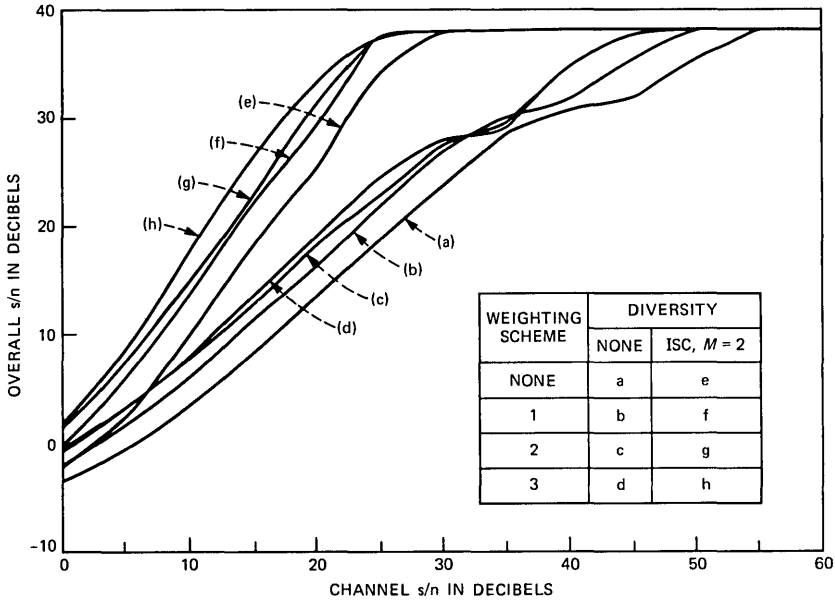

Fig. 9—Mobile radio channel. Overall s/n versus channel s/n for CPSK and speech input signals. The input power level is −17 dB and the vehicular speed is 60 mph.

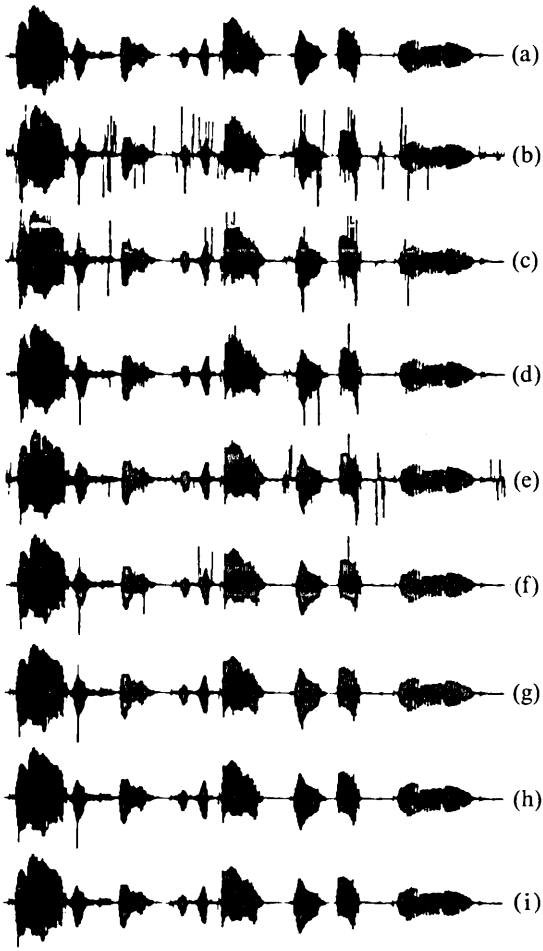

WEIGHTING SCHEME	DIVERSITY	
	NONE	ISC, $M = 2$
NONE	a	e
1	b	f
2	c	g
3	d	h

Fig. 10—Segment of the speech signal. Overall s/n versus channel s/n for CPSK and speech input signals. The input power level is −17 dB and the vehicular speed is 30 mph. The channel s/n is 16 dB and the original speech segment is waveform i.

of employing Systems 3 and 2 results in a considerable reduction in digital noise power compared to the conventional unweighted PCM.

6.1.2 Average error probability

We assert in Section 4.1 that for weighted PCM systems the average bit error probability P_{av} is not a suitable performance parameter. To lend credence to this statement we display in Fig. 11 the curves of error probability for the MSB, next MSB, $\cdots$, LSB, namely ρ_1, ρ_2, $\cdots$, ρ_8, respectively, as a function of channel s/n, for Weighted PCM System 1. Also shown is the variation of the probability of bit error P for a conventional, unweighted PCM system. The results are for a

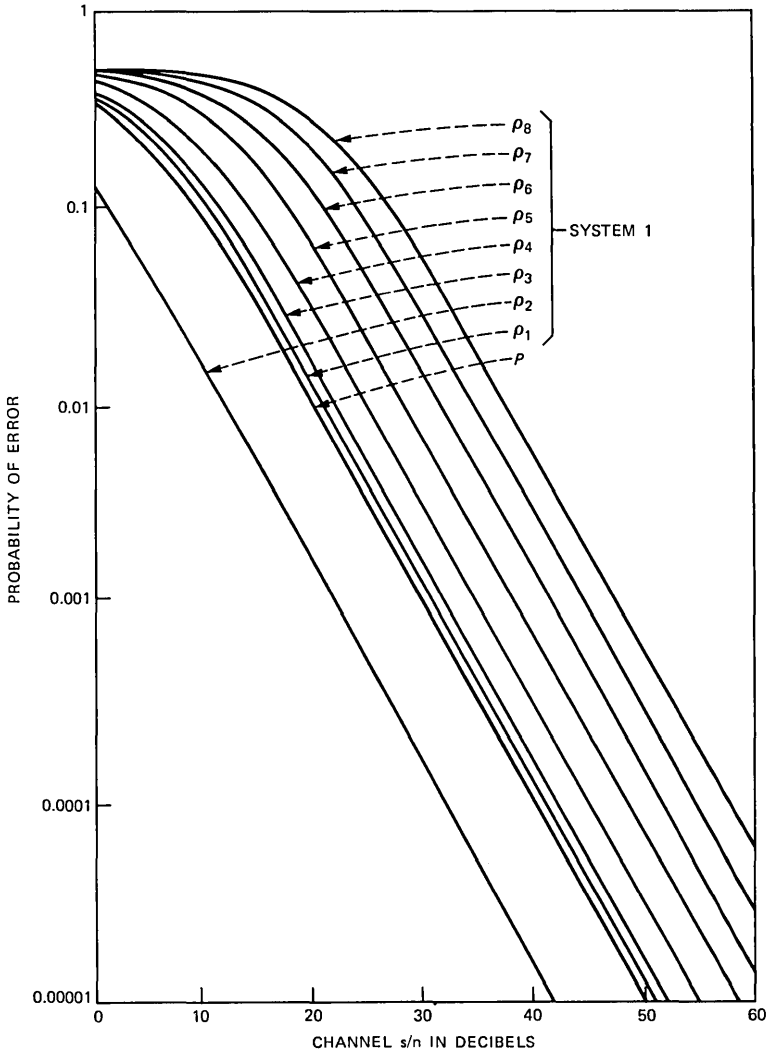

Fig. 11—Curves of probability of error as a functin of channel s/n for the individual probability of bit errors $\rho_1, \rho_2, \cdots, \rho_8$ for System 1. It is a Rayleigh fading channel with no diversity, and in input level of −40 dB. Also displayed is the probability of error P for the unweighted PCM system as a function of channel s/n.

Rayleigh fading channel, no diversity, and an input level of −40 dB. The weighting strategy for System 1 arranges for the LSB to have a lower transmitted energy than the other bits, and, consequently, a greater probability of error. However, an error in the LSB causes the smallest contribution to the digital noise power compared to the contributions from the other bits. We observe that $\rho_8 > \rho_7 > \rho_6 > \rho_5$

$> \rho_4 > \rho_3 > \rho_2$, i.e., the larger the contribution to the digital noise power caused by the regeneration of an erroneous bit, the lower is its probability of being in error. Probability ρ_2 is associated with the most significant magnitude bit of the quantized sample, and we see that $\rho_2 < \rho_1$. This inequality originates in the optimization process, indicating that an error in the most significant magnitude bit will, in general, generate more digital noise than an error in the polarity bit of the reconstituted sample. The probability of error P for the unweighted PCM is seen to be marginally smaller than ρ_1, but significantly greater than ρ_2.

When the average probability P_{av} is computed according to eq. (35), we have the curve displayed in Fig. 12. As we expected from the curves in Fig. 11, P_{av} for Weighted PCM System 1 is considerably in excess of the probability P for unweighted PCM. Also shown in Fig. 12 are P_{av} for Weighted PCM Systems 2 and 3. From our previous figures displaying $\hat{s/n}$, and those depicting P_{av} in Figs. 11 and 12, we conclude that systems that provide superior $\hat{s/n}$ also have inferior P_{av}. Hence we reject P_{av} as a meaningful performance parameter. However, knowledge of P_{av} does contribute to our insight into weighted PCM systems.

6.2 Results for the Gaussian channel

When the fixed weighting profile described in Section 5.1 is used, the digital noise power is given by eq. (60). The optimum weights ϕ_l of eq. (58), having the same A_l factors as used in the unweighted case, are tabulated in Table III. However, we observe that ϕ_l is a function of the channel s/n. Applying the same procedure as for the theoretical results in Section 6.1, we change the weighting ϕ_l with channel s/n to ensure that ϵ_a^2 is minimized. The curves in Figs. 13 and 14 are therefore optimum for every channel s/n. The improvement attained in $\hat{s/n}$ for Weighted PCM Systems 1, 2, and 3 compared to unweighted PCM are 10, 12, and 17 dB, respectively, for an input signal level of −17 dB, respectively, when the channel s/n is 10 dB. The optimum fixed word weighting profile of System 1 enables the channel s/n to deteriorate by 1.5 and 2 dB for input signal levels of −17 and −40 dB, respectively, compared to unweighted PCM, while $\hat{s/n}$ is maintained at 30 dB. Observe that at low values of channel s/n where the BER is high, the application of fixed word weighting can increase $\hat{s/n}$ by 10 to 20 dB. These large gains can transform unintelligible speech into distorted but partially intelligible speech. We note that the gain in $\hat{s/n}$ when the individual word weighting profile is used instead of the fixed weighting profile is only 1 to 2 dB.

The digital noise power ϵ_a^2 for the individual word weighting profiles of System 2 is given by eq. (65), where the $a_l(x_i)$ factors are given in Ref. 7. The individual word weighting profiles of eq. (63) are presented

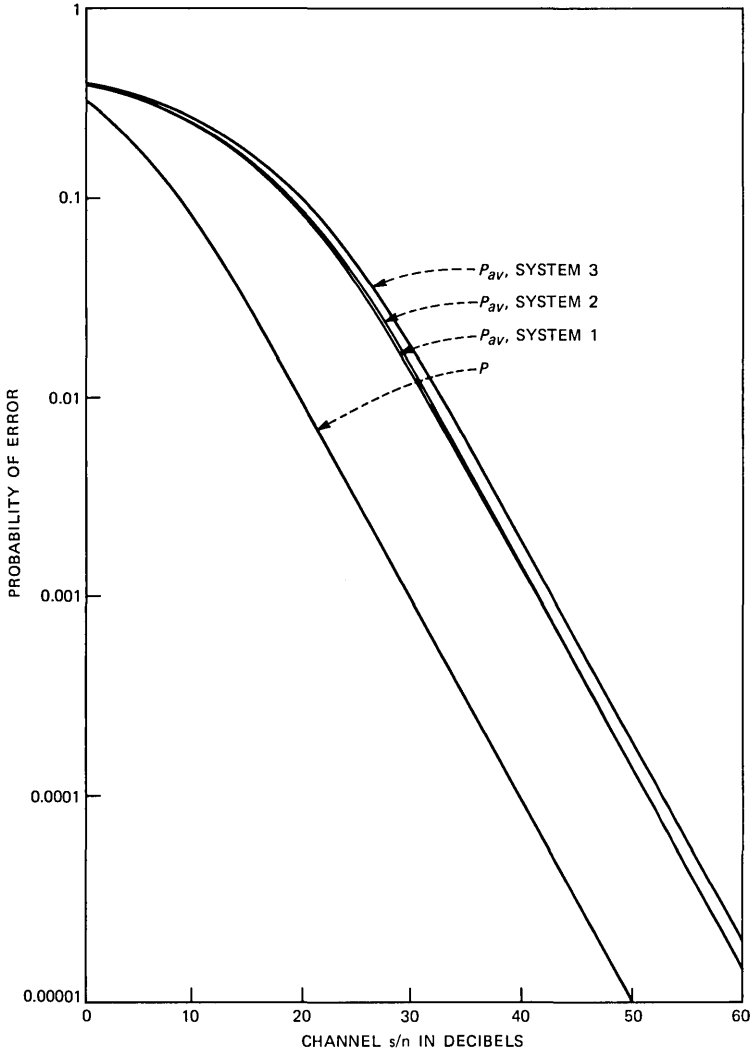

Fig. 12—Curves of average probability for Systems 1, 2, and 3, and the probability of error P for unweighted PCM, as a function of channel s/n.

Table III—The constant word weighting profile $\{\phi_l\}_{l=1}^{N}$ for the Gaussian channel (optimized for a channel s/n of 11 dB)

Input Power	Bit Number l							
	1	2	3	4	5	6	7	8
−17dB	1.4612	1.5493	1.4763	1.1782	0.9213	0.6930	0.4707	0.2500
−40 dB	1.3247	2.0489	1.3994	1.1217	0.8643	0.6355	0.4131	0.1924

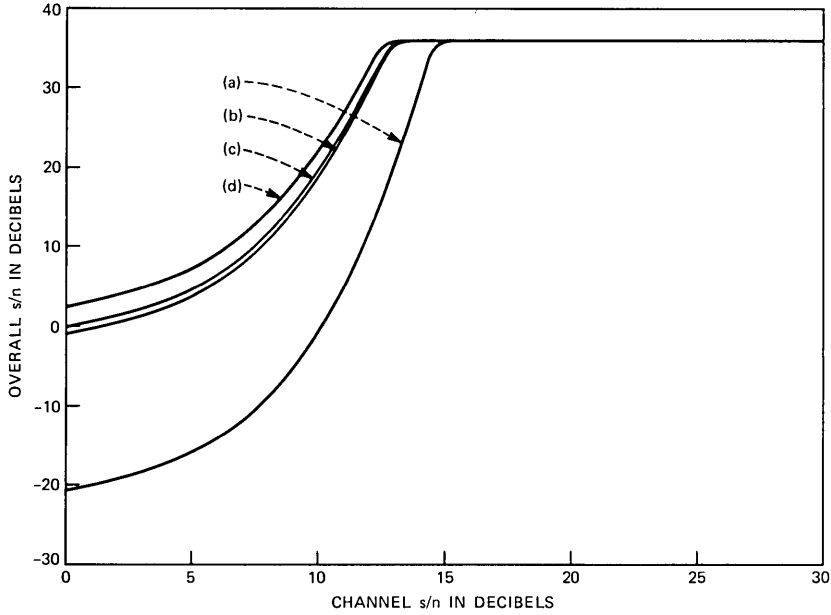

Fig. 13—Gaussian channel. Theoretical curves of overall s/n versus channel s/n for an input level of −17 dB. Curves a, b, c, and d relate to no weighting, weighting scheme 1, 2, and 3, respectively. No diversity was employed.

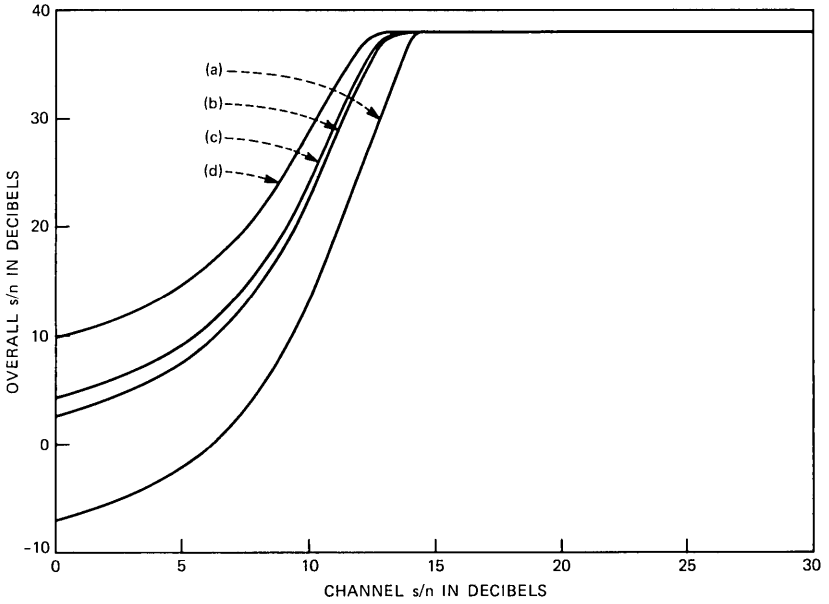

Fig. 14—Gaussian channel. Theoretical curves of overall s/n versus channel s/n for an input level of −40 dB. Curves a, b, c, and d relate to no weighting, weighting scheme 1, 2, and 3, respectively. No diversity was employed.

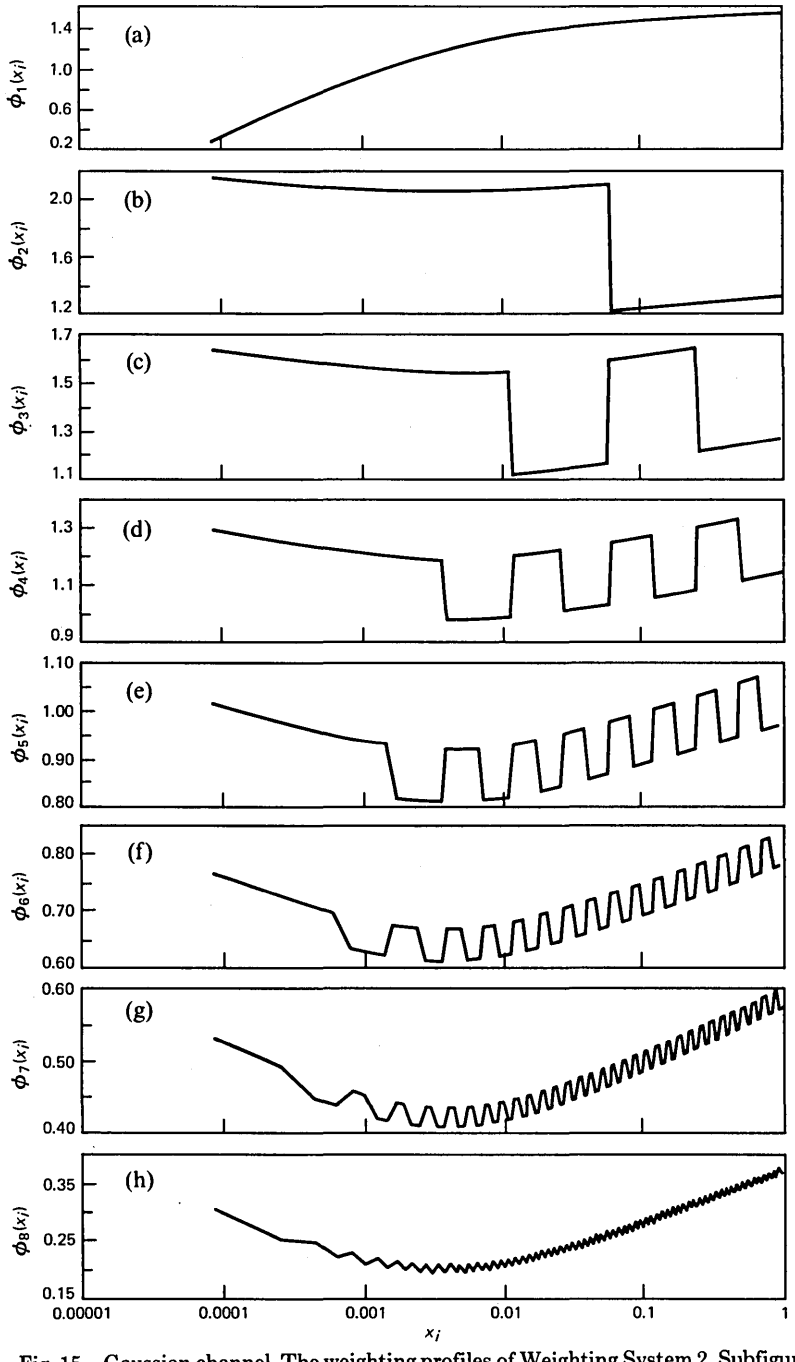

Fig. 15—Gaussian channel. The weighting profiles of Weighting System 2. Subfigures a, b, · · · , h, corresponding to a single bit error in the polarity bit, the most significant magnitude bit, · · · , the least significant magnitude bit, respectively.

Table IV—The word weighting factors W_i for the Gaussian channel (optimized for channel s/n of 11 dB)

Input Power = −17 dB								
0.0785	0.1333	0.1648	0.1893	0.2105	0.2297	0.2476	0.2645	0.2807
0.2963	0.3116	0.3264	0.3410	0.3553	0.3694	0.3833	0.3971	0.4107
0.4242	0.4376	0.4509	0.4641	0.4772	0.4903	0.5033	0.5162	0.5291
0.5419	0.5547	0.5674	0.5801	0.5927	0.6054	0.6179	0.6305	0.6430
0.6555	0.6680	0.6805	0.6929	0.7053	0.7177	0.7301	0.7424	0.7548
0.7671	0.7794	0.7917	0.8040	0.8163	0.8286	0.8408	0.8531	0.8653
0.8775	0.8898	0.9020	0.9142	0.9264	0.9385	0.9507	0.9629	0.9751
0.9872	0.9994	1.0116	1.0237	1.0358	1.0480	1.0601	1.0723	1.0844
1.0965	1.1086	1.1207	1.1329	1.1450	1.1571	1.1692	1.1813	1.1934
1.2055	1.2176	1.2297	1.2418	1.2538	1.2659	1.2780	1.2901	1.3022
1.3143	1.3263	1.3384	1.3505	1.3626	1.3746	1.3867	1.3988	1.4108
1.4229	1.3450	1.4470	1.4591	1.4712	1.4832	1.4953	1.5074	1.5194
1.5315	1.5435	1.5556	1.5677	1.5797	1.5918	1.6038	1.6159	1.6279
1.6400	1.6521	1.6641	1.6762	1.6882	1.7003	1.7123	1.7244	1.7364
1.7485	1.7605							
Input Power = −40 dB								
0.6457	0.7005	0.7320	0.7566	0.7778	0.7970	0.8148	0.8317	0.8479
0.8636	0.8788	0.8937	0.9082	0.9226	0.9367	0.9506	0.9644	0.9870
0.9915	1.0049	1.0182	1.0314	1.0445	1.0576	1.0705	1.0835	1.0963
1.1092	1.1219	1.1347	1.1473	1.1600	1.1726	1.1852	1.1978	1.2103
1.2228	1.2353	1.2477	1.2602	1.2726	1.2850	1.2973	1.3097	1.3220
1.3344	1.3467	1.3590	1.3713	1.3836	1.3958	1.4081	1.4203	1.4326
1.4448	1.4570	1.4692	1.4814	1.4936	1.5058	1.5180	1.5302	1.5423
1.5545	1.5667	1.5788	1.5910	1.6031	1.6152	1.6274	1.6395	1.6516
1.6638	1.6759	1.6880	1.7001	1.7122	1.7243	1.7364	1.7485	1.7606
1.7727	1.7848	1.7969	1.8090	1.8211	1.8332	1.8453	1.8574	1.8694
1.8815	1.8936	1.9057	1.9178	1.9298	1.9419	1.9540	1.9660	1.9781
1.9902	2.0022	2.0143	2.0264	2.0384	2.0505	2.0626	2.0746	2.0867
2.0987	2.1108	2.1229	2.1349	2.1470	2.1590	2.1711	2.1832	2.1952
2.2073	2.2193	2.2314	2.2434	2.2555	2.2675	2.2796	2.2916	2.3037
2.3157	2.3278							

in Fig. 15. We used these weighting profiles to generate the curves for Weighting System 2 in Figs. 13 and 14.

When the scheme of Section 5.3 is used the $\hat{s/n}$ is computed using eqs. (69) and (29). The word weighting factors are listed in Table IV. The gain in $\hat{s/n}$ when the individual word weighting factor W_i is introduced is substantial, as shown by the performance curves of Weighting System 3. These gains in Figs. 13 and 14 exceed 20 dB compared to unweighted PCM when the input signal power is −40 dB and the channel s/n falls below 12 dB.

VII. DISCUSSION

In another paper[7] we described the effect of transmission errors on μ-law PCM encoded signals transmitted over Gaussian and Rayleigh fading channels. The essential theoretical results of that work are condensed here into Sections 4.6 and 5.4, and are employed as bench marks for measuring the gains in overall s/n when the μ-law PCM

bits are weighted prior to transmission. Weighting System 1 is not novel. It is the original scheme due to Bedrosian[1] that has been analyzed by him and Sundberg.[2] However, the results for transmission of weighted μ-law PCM by System 1 over Rayleigh fading channels are new. Systems 2 and 3 mark a basic departure from previous proposals for weighting. In System 2 we introduce the concept of instantaneous weighting, where the bits are weighted by a profile dependent on the quantization level. Thus there are 2^N different weighting profiles, where N is the number of bits in the PCM words and these weighting profiles can be conveniently stored in a ROM. Observing that the digital noise power is dependent on the actual PCM words generated leads us to the notion of assembling the bits weighted by System 2 into their binary words and then weighting each bit in the word by a value unique to the word.

We have presented theoretical results of overall s/n as a function of channel s/n for all our weighting schemes when the transmission is over Rayleigh and Gaussian channels, the modulation NCFSK and CPSK, and when ISC and IMRC diversity is employed. The overall s/n, i.e., the $\hat{s}/n$ of the recovered signal, is a meaningful objective measure of system performance. By contrast BER is a misleading performance parameter in weighted PCM. Indeed, the overall s/n generally increases when the BER increases. This is because the large contributions to the average bit error probability arise from the least significant bits that contribute least to the digital noise power.

In addition to the provision of theoretical equations and graphs of overall s/n, we have provided simulation results when the input signal was composed of four concatenated speech sentences. The simulations were limited to two-level CPSK modulation and apply to a mobile radio channel. However, the simulations encompassed all the various weighting schemes, unweighted μ-law PCM, no diversity, and ISC, $M = 2$, diversity. The results for speech agree satisfactorily with our theory, and the waveform presentation of Fig. 10 shows that the enhancement of the recovered waveforms has a matching correspondence with the measured gains in $\hat{s}/n$.

In summary we make the following observations. For the Rayleigh fading channel, and in the absence of diversity, Weighting Systems 1, 2, and 3 yielded gains of $\hat{s}/n$ over unweighted μ-law PCM of approximated 3, 4.5, and 6 dB, when the input power was -17 dB. This was irrespective of whether the modulation was NCFSK or CPSK. At the lower input level of -40 dB, Systems 1 and 2 had the same performance with a gain in $\hat{s}/n$ of 6.5 dB. System 3 enhanced the performance by approximately 8 dB. Second-order diversity significantly extends the range of channel s/n before $\hat{s}/n$ begins to deteriorate. This is, of course, well known, as is the ability of IMRC diversity to outperform ISC in

terms of $\hat{s/n}$ for a given channel s/n. What was not known was the behavior of these diversity schemes when weighted PCM was introduced. We found that the relative performance of the three weighting systems with no diversity was repeated with diversity, enabling us to draw the general conclusion that System 3 always performs best, and that at low power levels there is no advantage to using System 2 compared to System 1.

For Gaussian channel the improvement in $\hat{s/n}$ for Systems 1, 2, and 3 compared to unweighted μ-law PCM was 10, 12, and 17 dB, respectively, for a channel s/n of 10 dB, and an input level of −17 dB. Thus a $\hat{s/n}$ for unweighted μ-law PCM of 13 dB was transformed to 30 dB, a value often associated with toll quality $\hat{s/n}$. At the lower input level of −40 dB the gains for Systems 1, 2, and 3, become 20, 21, and 24 dB, respectively, i.e., Systems 1 and 2 had virtually the same performance, while System 3 only yielded a gain of 3 dB over System 2.

REFERENCES

1. E. Bedrosian. "Weighted PCM," IRE Trans. Information Theory, *IT-4* (March 1958), pp. 45–9.
2. C.-E. Sundberg, "Optimum Weighted PCM for Speech Signals," IEEE Trans. Commun., *COM-26,* No. 6 (June 1978), pp. 872–81.
3. N. Rydbeck and C.-E. Sundberg, "Analysis of Digital Errors in Non-linear PCM Systems," IEEE Trans. Commun., *COM-24,* No. 1 (January 1976), pp. 59–65.
4. C.-E. Sundberg and N. Rydbeck, "Pulse Code Modulation with Error-Correcting Codes for TDMA Satellite Communication Systems," Ericsson Technics, *32,* No. 1 (1976) pp. 3–56.
5. C.-E. Sundberg, "The Effect of Single Bit Errors in Standard Nonlinear PCM Systems," IEEE Trans. Commun., *COM-24,* No. 9 (September 1976), pp. 1062–4.
6. W. C. Jakes, Jr., *Microwave Mobile Communications,* New York: Wiley, 1974.
7. R. Steele, C.-E. Sundberg, and W. C. Wong, "Transmission Errors in Companded PCM Over Gaussian and Rayleigh Fading Channels," AT&T Bell Lab. Tech. J., *63,* No. 6 (July–August 1984).
8. M. Schwartz, W. R. Bennett and S. Stein, *Communication Systems and Techniques,* New York: McGraw Hill, 1966.
9. H. W. Arnold and W. F. Bodtmann, "A Hybrid Multichannel Hardware Simulator for Frequency-Selective Mobile Radio Paths," IEEE Trans. Commun., *COM-31,* No. 3 (March 1983), pp. 370–7.
10. W. C. Wong, R. Steele, B. Glance, and D. Horn. "Time Diversity With Adaptive Error Detection to Combat Rayleigh Fading in Digital Mobile Radio," IEEE Trans. Commun., *COM-31,* No. 3 (March 1983), pp. 378–87.
11. J. M. Chambers, *Computational Methods for Data Analysis,* New York: John Wiley & Sons, 1977.

APPENDIX A

Optimum Weighting Profile When System 1 Is Operating Over Rayleigh Fading Channels

Consider Weighting System 1 operating with M-fold ideal maximal ratio diversity and NCFSK. The optimum weights that minimize the digital noise power ϵ_a^2 for this system are found by means of the Lagrange multiplier technique,[11] viz:

$$F = F(\phi_1 \cdots \phi_N, \lambda)$$
$$= \sum_{l=1}^{N} A_l \frac{2^{M-1}}{(2 + \phi_l \Gamma)^M} + \lambda \left(\sum_{l=1}^{N} \phi_l - N \right), \tag{78}$$

where λ is a dummy variable. Partially differentiating F with respect to ϕ_l and λ and setting these derivatives to zero we have

$$A_l \cdot \frac{M 2^{M-1} \Gamma}{(2 + \phi_l \Gamma)^{M+1}} = \lambda. \tag{79}$$

Using the constraint $\sum_{l=1}^{N} \phi_l = N$, the λ value is given by

$$\frac{1}{N} \sum_{l=1}^{N} (A_l)^{\frac{1}{M+1}} = (2 + \Gamma) \cdot \left(\frac{\lambda}{\Gamma M 2^{M-1}} \right)^{\frac{1}{M+1}}. \tag{80}$$

Using expressions (79) and (80), we arrive at the optimum weights (33).

Note that for the reason of simplicity of analysis we did not impose the physical condition $\phi_l \geq 0$. In the solution to the mathematical optimization problem, optimum mathematical weights might be negative for low channel s/n's.

The optimum weights (33) give the minimum digital noise power

$$\epsilon_a^2 = \frac{2^{M-1}}{(2 + \Gamma)^M} \cdot \left(\frac{1}{N} \right)^M \cdot \left(\sum_{l=1}^{N} (A_l)^{\frac{1}{M+1}} \right)^{M+1}, \tag{81}$$

where the optimum weight profile is used at each s/n Γ. For a fixed weight profile, (81) is a lower bound for those Γ's, where the fixed weight profile is not optimized.

The optimum weights for Systems 2 and 3 can also be found by means of the Lagrange multiplier method. In Appendices C and D we have shown the detailed derivations for the Gaussian channel.

APPENDIX B

Optimum Weighting Profile When System 1 Is Operating Over Gaussian Channels

Applying the constraint that the average bit energy is constant, we determine the optimum weights that minimize ϵ_a^2 with the aid of the Lagrange multiplier technique,[11] viz:

$$F = F(\phi_1, \phi_2, \cdots \phi_N, \lambda)$$
$$= \sum_{l=1}^{N} A_l \frac{1}{2} e^{-\phi_l \frac{E}{2N_o}} + \lambda \left[\left(\sum_{l=1}^{N} \phi_l \right) - N \right], \tag{82}$$

where λ is a dummy variable. Partially differentiating F with respect to the lth weight,

$$\frac{\partial F}{\partial \phi_l} = -A_l \frac{E}{4N_o} e^{-\phi_l \frac{E}{2N_o}} + \lambda; \qquad l = 1, 2, \cdots, N, \tag{83}$$

and upon setting $\partial F/\partial \phi_l$ to zero we have

$$\lambda = A_l \frac{E}{4N_o} e^{-\phi_l \frac{E}{2N_o}}, \tag{84}$$

a constant. Writing eq. (84) as

$$\ln(\lambda) = \ln(A_l) + \ln\left(\frac{E}{4N_o}\right) - \frac{\phi_l E}{2N_o}$$

and after considering all N values of l, we get

$$N \ln(\lambda) = \sum_{l=1}^{N} \ln(A_l) + N \ln\left(\frac{E}{4N_o}\right) - \frac{E}{2N_o} \sum_{l=1}^{N} \phi_l. \tag{85}$$

Applying the constraint of eq. (22) yields

$$\lambda = \frac{E}{4N_o} (A_1 A_2 \cdots A_n)^{1/N} e^{-\frac{E}{2N_o}}. \tag{86}$$

Defining

$$A_o \underset{=}{\Delta} \left[\prod_{l=1}^{N} A_l\right]^{\frac{1}{N}} \tag{87}$$

and equating eqs. (84) and (86), we have the optimum fixed word weighting profile,

$$\phi_l = 1 + \frac{\ln\left(\frac{A_l}{A_o}\right)}{\frac{E}{2N_o}}; \qquad l = 1, 2, \cdots, N. \tag{88}$$

APPENDIX C

Optimum Weighting Profile When System 2 Is Operating Over Gaussian Channels

Applying eq. (26) to eq. (56), and upon using the Lagrange multiplier technique, we have the function

$$F = F(\phi_1(x_0) \cdots \phi_l(x_0) \cdots \phi_N(x_0) \cdots \cdots \phi_l(x_i) \cdots \phi_N(x_{2^N-1}), \lambda_0, \lambda_1 \cdots \lambda_l \cdots \lambda_{2^N-1}) \tag{89}$$

$$= \sum_{i=0}^{2^N-1} p_i \sum_{l=1}^{N} a_l(x) \frac{1}{2} e^{-\phi_l(x_i)\frac{E}{2N_o}}$$

$$+ \sum_{i=0}^{2^N-1} \lambda_i \left[\sum_{l=1}^{N} \phi_l(x_i) - N \right]. \tag{90}$$

Upon partially differentiating F with respect to $\phi_l(x_i)$,

$$\frac{\partial F}{\partial \phi_l(x_i)} = p_i - a_l(x_i) \frac{E}{4N_o} e^{-\phi_l(x_i)\frac{E}{2N_o}} + \lambda_i, \tag{91}$$

and setting $\partial F/\partial \phi_l(x_i)$ to zero we get

$$\frac{\lambda_i}{p_i} = a_l(x_i) \frac{E}{4N_o} e^{-\phi_l(x_i)\frac{E}{2N_o}}, \tag{92}$$

a constant for each fixed i and $l = 1, 2, \cdots, N$. Applying the constraint on $\phi_l(x_i)$, and following the procedure used in the derivation of eq. (88), we have the optimum individual word weighting profile,

$$\phi_l(x_i) = 1 + \frac{\ln \left[\frac{a_l(x_i)}{a_o(x_i)} \right]}{\frac{E}{2N_o}}$$

$$l = 1, 2, \cdots, N$$

$$i = 0, 1, 2, \cdots 2^N - 1, \tag{93}$$

where

$$a_o(x_i) = (a_1(x_i)a_2(x_i) \cdots a_N(x_i))^{1/N}$$

$$= \left[\prod_{l=1}^{N} a_l(x_i) \right]^{1/N}. \tag{94}$$

APPENDIX D

The Optimum Word Weighting Factor When System 3 Is Operating Over Gaussian Channels

In this case the Langrange multiplier technique yields

$$F = F(W_0, W_1, W_2, \cdots, W_{2^N-1}, \lambda)$$

$$= \sum_{i=0}^{2^N-1} p_i N a_o(x_i) \frac{1}{2} e^{-\frac{W_i E}{2N_o}}$$

$$+ \lambda \left[\sum_{i=0}^{2^N-1} p_i W_i - 1 \right], \tag{95}$$

whence

$$\frac{\partial F}{\partial W_i} = p_i N a_o(x_i) \frac{1}{2} e^{-\frac{W_i E}{2N_o}} \left(- \frac{E}{2N_o} \right) + \lambda p_i.$$

Upon $\partial F / \partial W_i$ equals zero,

$$\lambda = N a_o(x_i) \frac{E}{4E_o} e^{-\frac{W_i E}{2N_o}}; \qquad i = 0, 1, 2, \cdots, 2^N - 1, \tag{96}$$

a constant. We have assumed that

$$p_i \neq 0; \qquad i = 0, 1, 2, \cdots, 2^N - 1,$$

but if any p_i is zero, the corresponding word weight is set to zero, there being no advantage in reserving energy for an event that never occurs. When some values of p_i are zero the minimization is performed as above, but over those W_i's (fewer than 2^N) that have nonzero p_i.

Taking the natural logarithm of eq. (96) and applying the constraint of eq. (43) yields

$$\ln(\lambda) = \sum_{k=0}^{2^N-1} p_i \ln[N a_o(x_k)] + \ln\left(\frac{E}{4E_o}\right) - \frac{E}{2N_o}. \tag{97}$$

Thus from eqs. (96) and (97), the optimum word weighting factor becomes

$$W_i = 1 + \frac{1}{\frac{E}{2N_o}} \left\{ \ln[N a_o(x_i)] - \sum_{k=0}^{2^N-1} p_k \ln[N a_o(x_k)] \right\}$$

$$i = 0, 1, 2, \cdots, 2^N - 1. \tag{98}$$

AUTHORS

Raymond Steele, (SM '80), B.S. (Electrical Engineering) from Durham University, Durham, England, in 1959, the Ph.D. degree in 1975, and the Doctor of Science Degree (DSc) in 1983. Prior to his enrollment at Durham University, he was an indentured apprenticed Radio Engineer. After research and development posts at E. K. Cole Ltd., Cossor Radar and Electronics, Ltd., and The Marconi Company, all in Essex, England, he joined the lecturing staff at the Royal Naval College, Greenwich, London, England. Here he lectured in telecommunications to NATO and the External London University degree courses. His next post was as Senior Lecturer in the Electronic and Electrical Engineering Department of Loughborough University, Loughborough, Leics., England, where he directed a research group in digital encoding of speech and television signals. In 1975 his book, *Delta Modulation Systems* (Pentech Press, London), was published. He was a consultant to the Acoustics Research Department at Bell Laboratories in the summers of 1975, 1977, and 1978, and in 1979 he joined the company's Communications Methods Research

Department, Crawford Hill Laboratory, Holmdel, N.J. In 1983 he became Professor of Communications in the Electronics Department at the University of Southampton, England.

Carl-Erik W. Sundberg, M.S.E.E., 1966, and Dr. Techn., 1975, Lund Institute of Technology, University of Lund, Sweden; Bell Laboratories, 1981–1982. Mr. Sundberg is an Associate Professor in the Department of Telecommunication Theory, University of Lund, and a consultant in his field. He is Director of the consulting company SUNCOM, Lund. During 1976 he was with the European Space Research and Technology Centre (ESTEC), Noordwijk, The Netherlands, as an ESA Research Fellow. He has been a Consulting Scientist at LM Ericsson and SAAB-SCANIA, Sweden, and at AT&T Bell Laboratories. His research interests include source coding, channel coding (especially decoding techniques), digital modulation methods, fault-tolerant systems, digital mobile radio systems, spread spectrum systems, and digital satellite communication systems. He has published a large number of papers in these areas during the last few years. Senior Member, IEEE; member, SER, Sveriges Elektroingenjörers Riksförening.

Wai Choong Wong, B.Sc. (Electronic and Electrical Engineering), Ph.D. (Electronic Engineering), Loughborough University of Technology, Loughborough, England, in 1976 and 1980, respectively. Since April 1980 he has been a Member of Technical Staff in the Communications Methods Research Department of Bell Laboratories at Crawford Hill, Holmdel, New Jersey. His current interest is in speech signal processing, particularly applied to mobile radio environment, digital modulation techniques, and simultaneous transmission of data and speech signals.

AT&T BELL LABORATORIES TECHNICAL JOURNAL
Vol. 63, No. 4, April 1984
Printed in U.S.A.

On the Use of Hidden Markov Models for Speaker-Independent Recognition of Isolated Words From a Medium-Size Vocabulary

By L. R. RABINER,* S. E. LEVINSON,* and M. M. SONDHI*

(Manuscript received September 19, 1983)

Recent work at AT&T Bell Laboratories has shown how the theories of Vector Quantization (VQ) and Hidden Markov Modeling (HMM) can be applied to the recognition of isolated word vocabularies. The initial experiments with an HMM word recognizer were restricted to a vocabulary of 10 digits. For this simple vocabulary with dialed-up telephone recordings, we found that a high-performance, speaker-independent word recognizer could be implemented, and that the performance was, for the most part, insensitive to parameters of both the HMM and the VQ. In this paper we extend our investigations of the HMM recognizer to the recognition of isolated words from a medium-size vocabulary (129 words), as used in the AT&T Bell Laboratories airlines reservation and information system. For this moderately complex word vocabulary, we have found that recognition accuracy is indeed a function of the HMM parameters (i.e., the number of states in the model and the number of symbols per state). We have also found that a VQ that includes energy information gives better performance than a conventional VQ of the same size (i.e., same number of code-book entries).

I. INTRODUCTION

Vector Quantizers (VQs), Linear Predictive Coding (LPC) coefficients, and Hidden Markov Models (HMMs) have been shown to be useful for a wide range of speech processing problems in the areas of

* AT&T Bell Laboratories.

coding, synthesis, and recognition.[1–12] In the area of speech recognition, there have been two distinctly different ways of applying HMMs. In the earliest work, extremely ambitious large-scale network models were used to model continuous discourse with constrained vocabularies.[5,7,8] For these large networks, HMMs were derived for basic speech sounds (e.g., phonemes), and words were made by coupling together the individual sound HMMs. Similarly, a sentence was made by coupling the models of all the words in the sentence. Solving such large-scale networks (i.e., finding the best path through the network in order to decode the sentence) was a major problem and required very sophisticated network search routines to find good (generally suboptimal) solutions.

More recently, work has been carried out on speech recognition based on HMMs for individual, isolated words.[11,12] For this type of system, an HMM is designed for each word in the vocabulary, and recognition is carried out by evaluating the probability that an unknown test pattern is the output of a given word model. The reference word whose model has the highest probability is chosen as the recognized word. To date, the word-based HMM recognizer has been tested only on a vocabulary of the 10 digits. For this vocabulary, it was found that the overall performance of the HMM recognizer was fairly insensitive to the parameters of both the HMM and the VQ, and that average word recognition accuracy was approximately the same as that obtained from a conventional Dynamic Time Warping (DTW) template approach.

Based on the success of the word-based HMM recognizer for the digits vocabulary, we have attempted to extend the approach to handle a fairly complex, medium-size word vocabulary. The vocabulary we have chosen is the 129-word airlines terms vocabulary, which has been extensively studied in the context of an airlines reservation and information system.[13–16] Table I shows the words in this vocabulary. We have studied the effects of varying several of the parameters of the HMM and the VQ on recognizer performance. Results indicate that a significant degradation in average word recognition accuracy is introduced by the use of a VQ, even with as many as 256 vectors in the code book. Results also show that the HMM/VQ system can and does achieve average word recognition accuracy comparable to a DTW/VQ template-based recognizer. Finally, we have found that, for a given size of code book, VQs using energy, along with LPC shape, give better performance than VQs with LPC shape alone.

The organization of this paper is as follows. In Section II we briefly review the design of the conventional DTW recognizer, the design of a VQ based on either LPC shape alone or LPC shape plus energy, and the operation of the HMM recognizer. In Section III we describe the

Table I—Words in airlines vocabulary

A	A.M.	Afternoon
American	April	Are
Area	Arrival	Arrive
At	August	B.A.C.
Boeing	Boston	By
Card	Cash	Charge
Chicago	Class	Club
Coach	Code	Credit
D.C.	December	Denver
Depart	Departure	Detroit
Diners	Do	Does
Douglas	Eight	Eleven
Evening	Express	Fare
February	First	Five
Flight	Flights	For
Four	Friday	From
Go	Home	How
I	In	Information
Is	January	July
June	Leave	Like
Lockheed	Los-Angeles	Make
Many	March	Master
May	Meal	Miami
Monday	Morning	Much
My	Need	New York
Night	Nine	Non stop
November	Number	O'clock
October	Of	Office
Oh	On	One
P.M.	Pay	Philadelphia
Phone	Plane	Please
Prefer	Repeat	Reservation
Return	Saturday	Seat
Seats	Seattle	September
Served	Seven	Six
Some	Stops	Sunday
Take	Ten	The
Thee	There	Three
Thursday	Time	Times
To	Tuesday	Twelve
Two	Uh	Want
Washington	Wednesday	What
When	Will	Would

experimental evaluation used to measure performance of the various recognizers on the 129-word airlines vocabulary. In particular, we give a detailed analysis (for the two best recognition systems) of the individual talker error rates, the most prevalent types of word errors, and the extent to which errors made by DTW and HMM recognizers are disjoint. Finally, in Section IV we summarize our findings.

II. THE DTW AND HMM/VQ WORD RECOGNIZERS

The two types of word recognition systems that we will be concerned with are:

1. A conventional DTW recognizer (either with or without VQ) based on LPC modeling and using isolated word templates as reference patterns.

2. An HMM recognizer with quantized LPC vectors, using single-word Markov models as parametric representations of the words in the vocabulary.

In this section we briefly review the implementations of the VQ, the DTW recognizer, and the HMM recognizer.

2.1 VQ of LPC parameters

Vector quantization is a technique for coding an LPC vector into one of M^* code-book entries such that the average quantization distortion is minimized over some typical training set of LPC vectors. Vector quantization differs from the more conventional scalar quantization methods in that the entire LPC vector is quantized in a single pass, rather than quantizing each component of the vector by a separate quantizer. Experience indicates a substantial savings in required code-book size (bit rate) for VQ over conventional scalar quantization.[1–4] For HMM recognition purposes, VQ serves as a way of characterizing continuous LPC vectors by a set of discrete symbols (i.e., the indices of the code-book entries that provide best matches to the input LPC vectors to the recognizer). In addition, for the DTW recognizer, VQ provides a simple and straightforward way of trading off storage and computation in the calculation of LPC distances as required in the DTW algorithm.[9,12]

A VQ is designed from a training set of I LPC vectors, $\mathbf{a}_i$, $i = 1, 2, \cdots, I$, which are intended to be a good representation of the range of LPC vectors that occur when the words in the vocabulary are pronounced by a wide range of talkers. The VQ training algorithm determines an optimum set of code-book LPC vectors, $\hat{\mathbf{a}}_m$, $m = 1, 2, \cdots, M^*$, such that, for a given M^*, the average distortion in replacing each of the training set vectors, $\mathbf{a}_i$, by the closest code-book entry, $\hat{\mathbf{a}}_m$, is minimum.

If we define $d(\mathbf{a}_R, \mathbf{a}_T)$ as the conventional LPC distance[17] between the LPC vectors $\mathbf{a}_R$ and $\mathbf{a}_T$, i.e.,

$$d(\mathbf{a}_R, \mathbf{a}_T) = \frac{\mathbf{a}_R' V_T \mathbf{a}_R}{\mathbf{a}_T' V_T \mathbf{a}_T} - 1, \tag{1}$$

where V_T is the autocorrelation matrix of the sequence that gave rise to LPC vector $\mathbf{a}_T$, then the goal of the VQ training algorithm is to find the set (of code-book entries), $\hat{\mathbf{a}}_m$, such that

$$\| D_{M^*} \| = \min_{\hat{a}_m} \left\{ \frac{1}{I} \sum_{i=1}^{I} \min_{1 \le m \le M^*} [d(\hat{\mathbf{a}}_m, \mathbf{a}_i)] \right\} \tag{2}$$

is satisfied. The quantity $\| D_{M^*} \|$ is the (minimum) average distortion of the VQ with M^* code-book entries.

The way in which eq. (2) is solved has been intensively investigated by several researchers[1–4] and will not be described here. As a result of these earlier studies, a highly reliable and robust procedure for the design of a VQ code book exists and can readily be implemented.

Although the conventional VQ (which we call a shape VQ) used only the LPC vector, recent studies have shown how normalized frame energy can be incorporated directly into the local distance [eq. (1)][18] to give a shape plus energy VQ. For these designs we denote the LPC distance of eq. (1) as $d_{\mathrm{LPC}}(\mathbf{a}_R, \mathbf{a}_T)$ and we denote an energy distance as $d_E(\hat{E}_R, \hat{E}_T)$. The total distance is then

$$d(\mathbf{a}_R, \mathbf{a}_T) = d_{\mathrm{LPC}}(\mathbf{a}_R, \mathbf{a}_T) + \alpha d_E(\hat{E}_R, \hat{E}_T), \tag{3}$$

where $\hat{E}_R$ and $\hat{E}_T$ are log energies of the reference and test frames, normalized to the peak energies in the word, and α is a multiplier for giving appropriate weight to the energy distance. Using the modified frame distance of eq. (3), a shape plus energy VQ can be designed according to the criteria of eq. (2) with no further modification.

2.2 The conventional DTW word recognizer

Figure 1 shows a block diagram of the conventional DTW word recognizer based on LPC modeling.[17,19] The input speech signal, $s(n)$, recorded over a standard dialed-up telephone line, is bandpass filtered between 100 and 3200 Hz, and digitized at a 6.67-kHz rate. The first step (preprocessing) consists of a first-order digital network, which provides a high-frequency preemphasis to the speech. The preemphasized signal is blocked into frames of 45 ms (300 samples), with each consecutive frame spaced 15 ms (100 samples) apart. An eight-pole

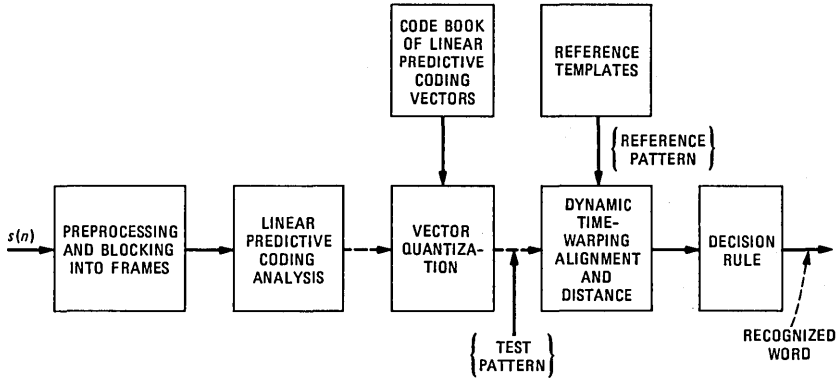

Fig. 1—Block diagram of conventional DTW word recognizer based on LPC modeling.

LPC analysis (autocorrelation method) is performed on each frame of the word (after the word has been isolated by means of an endpoint detector).[20] Each resulting LPC vector is either used directly or vector quantized by means of a code book of size M^*. The resulting sequence of LPC vectors, called the test pattern, is compared with each reference pattern in the reference template set using a DTW alignment algorithm that simultaneously provides a distance score associated with the alignment. The distance scores for all the reference patterns are sent to a decision rule, which provides a classification of the spoken word, and possibly an ordered (by distance) set of the best β candidates.

The word reference patterns for the recognizer of Fig. 1 are created by a training algorithm. For speaker-trained applications, typically a single reference pattern is created for each word in the vocabulary using a robust training algorithm.[21] For speaker-independent applications, a set of Q reference patterns is created for each vocabulary word using a clustering procedure.[22,23] Typically, about 12 templates per word are sufficient for recognizing words from a fairly homogeneous adult population of native American talkers.

If a VQ code book of M^* entries has been designed as in Section 2.1, one can compute and store the table of $M^* \times M^*$ distances between all pairs of code-book entries. In this manner, computation of distance between any pair of VQ code-book entries becomes a simple table lookup. Hence, if we vector quantize the LPC vectors of a test utterance and of all reference patterns, then the computation for distances in the DTW matching becomes trivial. In addition, a novel technique for reducing quantization distortion when using a VQ was proposed by Sakoe.[24] For this technique the test vector is not quantized. Instead, the table of distances between each test vector and all code-book entries is computed once and used in the DTW distance calculation. In this manner there is reduced distortion, reduced storage (over conventional VQ), and essentially no computation for local distance calculation (it is still a table lookup procedure).

2.3 The HMM word recognizer

Figure 2 is a block diagram of the HMM word recognizer. The front-end processing, namely preprocessing, frame blocking, LPC analysis, and vector quantization, is identical to that used in the vector quantized DTW recognizer described above. The test utterance is reduced to an observation sequence, $\{\mathbf{O}\}$, consisting of the indices of the code-book vectors that best match corresponding LPC vectors of the utterance. A Viterbi scoring algorithm determines, for each individual word HMM, the probability that the observation sequence was generated by the given word HMM. A decision rule either chooses the word

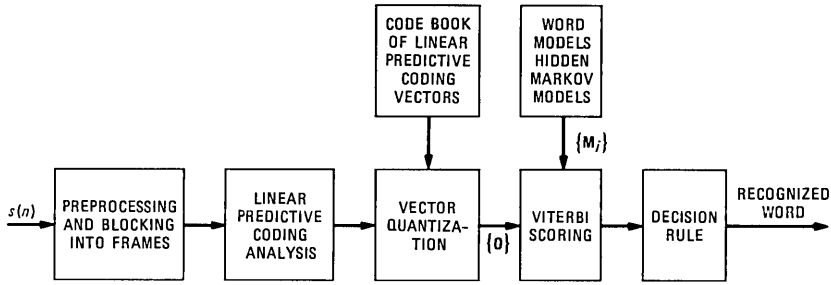

Fig. 2—Block diagram of HMM word recognizer based on LPC modeling and VQ.

whose word model has the highest probability as the recognized word, or gives a list of word candidates ordered by model probability scores.

Model probability scores for each word model are computed as follows. Each word HMM is an N-state model characterized by a state transition matrix, **A**, and a model output symbol probability matrix, **B**. Figure 3 illustrates an $N = 5$ state word model with M^* discrete output symbols for each state. Here we assume that the word models are left-to-right models; i.e., the elements of the transition matrix, a_{ij}, satisfy the relationship

$$a_{ij} = 0 \qquad j < i \tag{4a}$$

and, furthermore, we restrict the range of transitions to the case

$$a_{ij} = 0 \qquad j > i + 2. \tag{4b}$$

That is, we allow transitions between states that are either adjacent or one apart. Previous experimentation has shown these constraints are reasonable.[12]

Based on the above discussion, the scoring procedure for the observation sequence $\mathbf{O} = \{O_1, O_2, \cdots, O_L\}$ (i.e., L indices of code-book entries), given the model $\mathbf{M}(\equiv \mathbf{A}, \mathbf{B})$, is as follows:

1. Initialization: $\delta_1(1) = \log[b_1(O_1)]$

$$\delta_1(i) = \infty, \quad 2 \leq i \leq N$$

2. Recursion: For $2 \leq l \leq L$, $1 \leq j \leq N$

$$\delta_l(j) = \max\{\delta_l - 1(i) + \log[a_{ij}]\} + \log[b_j(O_l)]$$

$$\min(1, j-2) \leq i \leq \max(j, N)$$

3. Termination: $P(\mathbf{M}) = \delta_L(N)$.

The above algorithm is a form of the well-known dynamic programming method and can be shown to have the property of determining the state sequence $\mathbf{i} = i_1, i_2, \cdots, i_L$, which maximizes $P(\mathbf{O},\mathbf{i} \mid \mathbf{M})$. It can be seen that if the entries in the matrices **A** and **B** are stored in

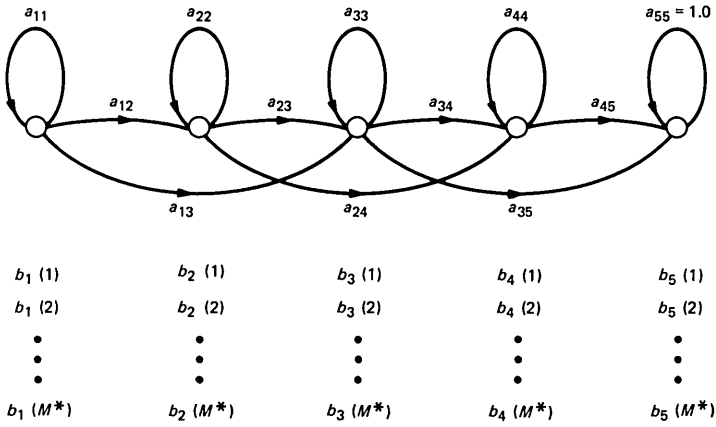

Fig. 3—Typical five-state Markov model for word with transition matrix $\mathbf{A} = \{a_{ij}\}$ and output symbol matrix $\mathbf{B} = \{b_j(k)\}$.

logarithmic format, i.e., $\log[a_{ij}]$, and $\log[b_j(k)]$, then the computation of the Viterbi scoring algorithm requires no multiplications or logarithm computation. Hence, the speed of computation of the Viterbi scoring is quite high.

The **A** and **B** matrices for each word HMM are estimated from a training set consisting of a set of observation sequences for the word. Starting with an initial estimate of the model, the probability, P, of observing the given training sequence **O** given the model **M** is computed. Using the Baum-Welch reestimation algorithm,[25] the model is iteratively adjusted to increase P. The iterations are stopped when P stops increasing significantly or when some other stopping criterion is met (e.g., when the number of iterations exceeds a limit).

III. RECOGNITION EVALUATION OF THE AIRLINES VOCABULARY

A series of recognition tests was run on both the DTW and HMM word recognizers, using the 129-word airlines vocabulary of Table I. A training set consisting of one replication of each word by each of 100 talkers (50 male, 50 female) was used to generate speaker-independent word templates for the DTW recognizer, and speaker-independent word HMMs for the HMM recognizer. The code-book vectors for the VQ were also derived from a subset of the training data. (VQs derived from a digits-only vocabulary were also tried and produced essentially no degradation in system performance.) All word recordings were made over dialed-up local telephone lines, with a new line used for each talker.

An independent test set consisting of one replication of each word by each of 20 talkers (10 male, 10 female) was used. None of the test

talkers had contributed to the training data. Again, all recordings were made over local, dialed-up telephone lines.

A series of 14 separate recognition tests were made on the DTW and HMM recognizers. The runs consisted of the following systems:

Run 1: Conventional DTW recognizer without VQ.

Runs 2 and 3: Conventional DTW recognizer with VQ applied to both test and reference sets.

Runs 4 through 9: HMM recognizer using a shape VQ with different values for N, the number of states, and M^*, the size of the VQ code book.

Run 10: HMM recognizer using a shape plus energy VQ.

Run 11: HMM recognizer using a shape VQ with variable number of states per word.

Run 12: HMM recognizer using a shape VQ with five randomly generated models per word.

Run 13: HMM recognizer using a shape VQ using the average of five randomly generated models per word.

Run 14: HMM recognizer using a shape VQ with both five and eight state models for each word.

Recognition runs 1 through 10 are the standard cases of DTW and HMM recognizers, and they effectively provide performance measurements on the effects of HMM and VQ parameters. Run 11 is used to test the hypothesis that long words (in terms of phoneme count) need bigger models (more states) than short words. For this run the number of states in the Markov model was set equal to the number of phonemes in the word, and a lower limit of 4 states and an upper limit of 10 states were imposed. Runs 12 and 13 examine the effects of generating multiple models (from different random initial model guess) for each word and either using all models in the recognizer (run 12), or the averge model (run 13). Finally, run 14 is used to study the effects of using multiple models with different numbers of states in each model. For this run, models with five and eight states were generated for each word.

3.1 Recognition run results

The performance results, given as a series of average word error rates for the β best word candidates, are shown in Table II and are partially plotted in Figs. 4 and 5. Table II gives the average word error rate scores for each of the 14 runs. Figure 4 shows plots of these results for runs 1, 2, 3, and 10, and Fig. 5 shows plots of the results for runs 4 through 9. An examination of the curves in Fig. 4 shows that the use of the VQ leads to significantly poorer performance in both the DTW and the HMM recognizers (at least 6 percent for $\beta = 1$ and at

Table II—Characteristics of recognizer and average word error rate scores (%) as function of candidate position for individual recognition tests on airlines vocabulary

Run	Recognizer	N	M^*	Number of Word Candidates 1	2	3	4	5
1	DTW	—	—	9.4	4.0	2.4	1.7	1.4
2	DTW/VQ	—	64	20.1	10.7	6.0	4.2	3.5
3	DTW/VQ	—	128	16.4	7.4	4.5	3.6	2.8
4	HMM/VQ	5	64	27.2	15.6	11.1	8.4	6.7
5	HMM/VQ	5	128	22.5	12.3	8.2	6.1	4.8
6	HMM/VQ	8	64	24.0	13.3	8.8	6.6	5.3
7	HMM/VQ	8	128	20.7	10.3	6.4	4.8	3.9
8	HMM/VQ	10	128	19.3	9.9	6.2	4.3	3.6
9	HMM/VQ	10	256	17.6	8.2	5.1	3.8	2.9
10	HMM/VQ.E	10	128	15.5	7.0	4.4	3.1	2.2
11	HMM/VQ	Variable	64	30.5	19.1	13.4	9.9	8.1
12	$(\text{HMM/VQ})_5$	5	64	30.4	18.4	11.9	9.1	7.3
13	$\overline{(\text{HMM/VQ})_5}$	5	64	30.4	18.4	11.9	9.1	7.3
14	HMM/VQ	5 + 8	64	24.3	13.5	8.9	6.7	5.5

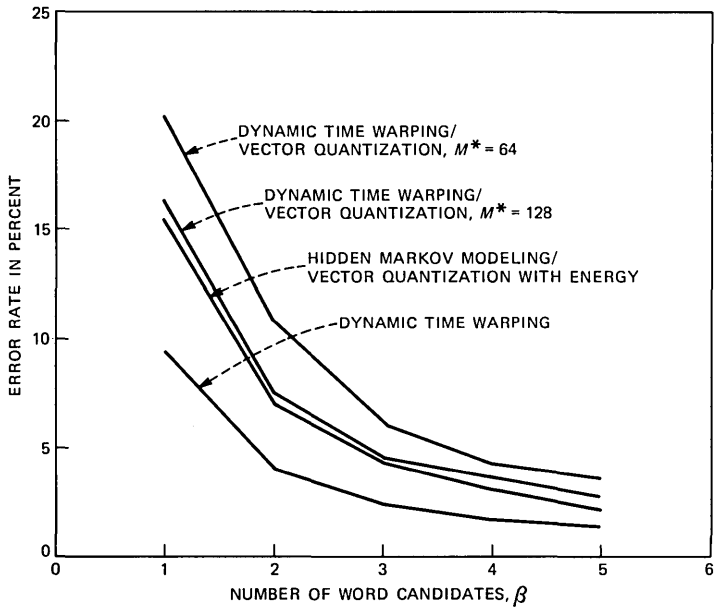

Fig. 4—Average word error rate, in percent, versus number of word candidates for data of runs 1 through 3 and run 10.

least 0.8 percent for $\beta = 5$). However, within the set of recognizers using a VQ, the HMM recognizer with a shape plus energy VQ achieves performance comparable to or better than the DTW recognizer with a shape VQ of the same size.

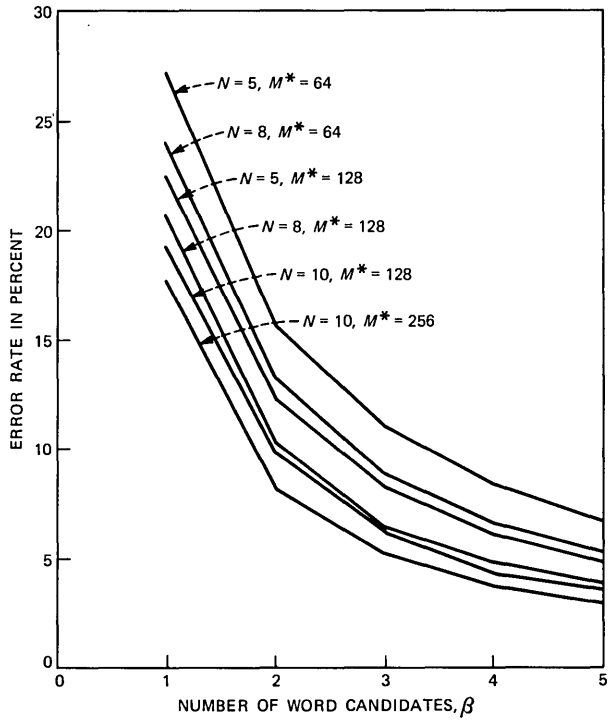

Fig. 5—Average word error rate, in percent, versus number of word candidates for data of runs 4 through 9.

The results in Fig. 5 show that the parameters N and M^* of the HMM (and the VQ) do affect recognizer performance significantly for the airlines vocabulary. The results shown in this figure indicate that increasing both N and M^* leads to improved word recognition accuracy. In fact, a decrease in average word error rate of about 10 percent is obtained in going from $N = 5$, $M^* = 64$ to $N = 10$, $M^* = 256$.

The results of the special runs (11 through 14) have some interesting implications. The results of run 11 (with variable-size Markov models) indicate worse performance than for fixed-size models. This result was anticipated based on experimentation with simulated HMM examples in which a stronger bias was always found for bigger models (more states) than for smaller models. The results of runs 12 and 13, in which five random starting conditions were used to generate five models per word, show a small but consistent improvement in performance when using all five models in the scoring (run 12) and a small but consistent degradation in performance when using the average model in the scoring (run 13). A plausible explanation of this result is that due to large model variability, averaging often results in a poor model because of the outliers.

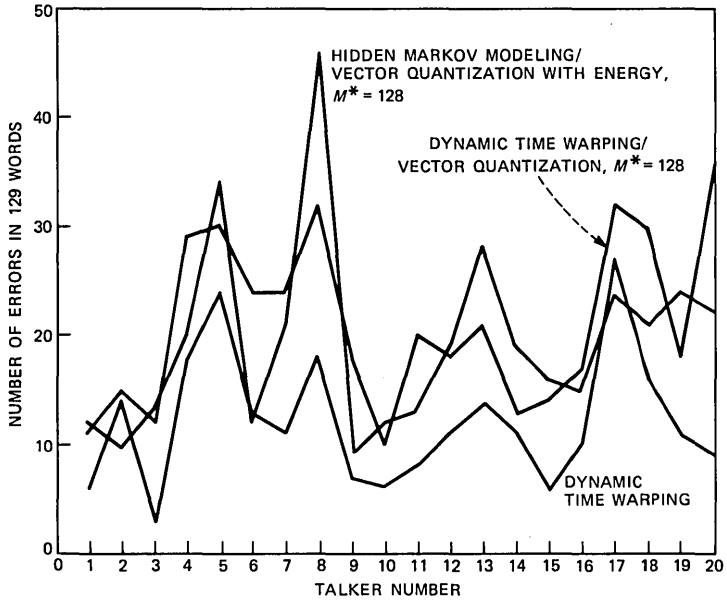

Fig. 6—Number of word errors as function of talker for data of runs 1, 3, and 10.

The results of run 14, in which the five- and eight-state models were combined, show that the performance in this case is essentially identical to the eight-state recognizer alone. Hence, this result again supports the observation that a strong bias exists in favor of bigger models.

3.2 Additional analysis of runs 1, 3, and 10 data

For the data of runs 1, 3, and 10, several additional analyses were performed to determine the correlation of individual talker errors with the recognizer, to examine the most frequent errors made, and to see how similar the errors were in the two recognizers. Figure 6 shows a plot of the number of word errors versus talker number for the recognition systems of runs 1, 3, and 10. It can be seen that there is a high correlation in the individual talker error rates among the three systems. It can also be seen that there is a high degree of variability in individual talker error rates.

Table III shows, for the data of runs 1 and 10, the words with the highest error rates over all talkers, and the words most confused with these words. The numbers in parentheses indicate the total number of errors (across the 20 talkers) and the total number of confusions. For the DTW recognizer the confusions of these 12 words accounted for one-third of the overall word errors; for the HMM recognizer the confusions among the 14 worst words accounted for 30 percent of the

Table III—Major word confusions in data of runs 1 and 10

DTW Recognizer		HMM Recognizer	
Word	Major Confusions	Word	Major Confusions
By (9)	I (5), My (4)	Many (11)	May (6)
Do (8)	To/Two (4)	Oh (10)	Of (3), How (2)
Flight (8)	Flights (6), Like (2)	Time (10)	Times (5), Five (4)
May (7)	Make (2)	Pay (10)	A (5), Take (3)
Oh (7)	How (3), Go (2)	Flight (9)	Flights (6)
Is (6)	In (5)	Do (8)	To/Two (8)
Home (6)	Oh (2), How (2)	On (8)	Of (3), August (2)
Seat (6)	Seats (3)	Please (8)	Leave (4)
Time (6)	Times (4)	Miami (8)	Monday (4), Morning (2)
Some (6)	From (3)	In (7)	Evening (3), A.M. (2)
A (6)	Take (2)	Want (7)	What (4), One (2)
Seats (6)	Seat (4)	Take (7)	Eight (3), Seat (2)
		Seats (7)	Seat (5)
		Three (7)	Three (2), Many (2), May (2)

overall word errors. For the DTW recognizer most of the major confusions are between words that sound similar (e.g., "By," "I," "My"); for the HMM recognizer there are many major confusions between dissimilar words (e.g., "In," "Evening;" "Miami," "Morning," etc.). It is interesting that among the words most confused by both systems, there are only three overlapping words, namely "Do," "Time," and "Seats."

The final check on the data was a comparison of the errors made by the DTW recognizer (run 1) and the HMM recognizer (run 10). In earlier experimentation with the digits vocabulary, it was found that an orthogonality existed between the errors of the DTW and HMM recognizers, in that whenever the DTW recognizer made an error, the HMM recognizer was almost always correct. We have made the same type of orthogonality check on the data of runs 1 and 10. Of the 243 word errors made by the DTW recognizer, 111 (45 percent) were cases in which the HMM recognizer also made an error. Hence, in only 55 percent of the cases is there any potential for error detection and correction. Thus, we conclude that it would not be easy to combine the results of the DTW and HMM recognizers, for this vocabulary, to greatly improve overall word accuracy.

IV. SUMMARY

In this paper we have applied isolated word recognition based on probabilistic modeling (HMMs) to a medium-size vocabulary of airline terms. We have found that the use of a finite-size VQ leads to a significant degradation in performance for both the conventional DTW recognizer and the one based on HMMs. We have also found that after vector quantization the HMM and DTW recognizers can be

designed to give essentially identical performance. We have shown that increasing N, the number of states in the HMM, and/or M^*, the size of the VQ code book, improves performance of the HMM recognizer. Hence, one should use the largest models that can be accommodated in a practical implementation. We have also found that using a VQ based on both LPC shape and energy gives improved recognition performance over a VQ based on LPC shape alone. Hence, the energy contour is extremely helpful in recognizing word vocabularies with many polysyllabic words.

The only discouraging finding was that there was a high degree of overlap between the word errors made by the DTW and HMM recognizers. Hence, there appears to be no simple method for combining these two approaches to give greatly improved performance.

REFERENCES

1. Y. Linde, A. Buzo, and R. M. Gray, "An Algorithm for Vector Quantization," IEEE Trans. Commun., *COM-28,* No. 1 (January 1980), pp. 84–95.
2. B. Juang, D. Wong, and A. H. Gray, Jr., "Distortion Performance of Vector Quantization for LPC Voice Coding," IEEE Trans. Acoustics, Speech, and Signal Processing, *ASSP-30,* No. 2 (April 1982), pp. 294–303.
3. A. Buzo et al., "Speech Coding Based Upon Vector Quantization," IEEE Trans. Acoustics, Speech, and Signal Processing, *ASSP-28,* No. 5 (October 1980), pp. 562–74.
4. D. Wong, B. Juang, and A. H. Gray, Jr., "An 800 Bit/S Vector Quantization LPC Vocoder," IEEE Trans. Acoustics, Speech, and Signal Processing, *ASSP-30,* No. 5 (October 1982), pp. 770–80.
5. J. K. Baker, "The DRAGON System—An Overview," IEEE Trans. Acoustics, Speech, and Signal Processing, *ASSP-23,* No. 1 (February 1975), pp. 24–9.
6. A. B. Poritz, "Linear Predictive Hidden Markov Models and the Speech Signal," Proc. IEEE Int. Conf. Acoustics, Speech, and Signal Processing, Paris, France (May 1982), pp. 1291–4.
7. F. Jelinek, L. R. Bahl, and R. L. Mercer, "Design of a Linguistic Decoder for the Recognition of Continuous Speech," IEEE Trans. Inform. Theory, *IT-21* (May 1975), pp. 250–6.
8. L. R. Bahl, F. Jelinek, and R. L. Mercer, "A Maximum Likelihood Approach to Continuous Speech Recognition," IEEE Trans. Pattern Analysis and Machine Intelligence, *PAMI-5,* No. 2 (March 1983), pp. 179–90.
9. A. Buzo, H. Martinez, and C. Rivera, "Discrete Utterance Recognition Based Upon Source Coding Techniques," Proc. ICASSP-82 (May 1982), pp. 539–42.
10. J. E. Shore and D. Burton, "Discrete Utterance Speech Recognition Without Time Normalization," Proc. ICASSP-82 (May 1982), pp. 907–10.
11. R. Billi, "Vector Quantization and Markov Source Models Applied to Speech Recognition," Proc. ICASSP-82 (May 1982), pp. 574–7.
12. L. R. Rabiner, S. E. Levinson, and M. M. Sondhi, "On the Application of Vector Quantization and Hidden Markov Models to Speaker-Independent Isolated Word Recognition," B.S.T.J., *62,* No. 4 (April 1983), pp. 1075–105.
13. A. E. Rosenberg and F. Itakura, "Evaluation of an Automatic Word Recognition System Over Dialed-Up Telephone Lines," J. Acoust. Soc. Amer., Supplement 1, (1976), p. 60.
14. S. E. Levinson, A. E. Rosenberg, and J. L. Flanagan, "Evaluation of a Word Recognition System Using Syntax Analysis," B.S.T.J., *57,* No. 5 (May–June 1978), pp. 1619–26.
15. S. E. Levinson and A. E. Rosenberg, "A New System For Continuous Speech Recognition—Preliminary Results," Proc. IEEE Int. Conf. Acoustics, Speech, and Signal Processing, Washington, DC (April 1979), p. 239–43.
16. S. E. Levinson and K. L. Shipley, "A Conversational Mode Airline Information and Reservation System Using Speech Input and Output," B.S.T.J., *59,* No. 1 (January 1980), pp. 119–37.

17. F. Itakura, "Minimum Prediction Residual Principle Applied to Speech Recognition," IEEE Trans. Acoustics, Speech, and Signal Processing, *ASSP-23,* No. 1 (February 1975), pp. 67–72.
18. L. R. Rabiner, M. M. Sondhi, and S. E. Levinson, "A Vector Quantizer Combining Energy and LPC Parameters and Its Application to Isolated Word Recognition," AT&T Bell Lab. Tech. J., *63,* No. 5 (May–June 1984).
19. L. R. Rabiner and S. E. Levinson, "Isolated and Connected Word Recognition—Theory and Selected Applications," IEEE Trans. Commun., *COM-29,* No. 5 (May 1981), pp. 621–59.
20. L. F. Lamel et al., "An Improved Endpoint Detector for Isolated Word Recognition," IEEE Trans. Acoustics, Speech, and Signal Processing, *ASSP-29,* No. 4 (August 1981), pp. 777–85.
21. L. R. Rabiner and J. G. Wilpon, "A Simplified Robust Training Procedure for Speaker Trained, Isolated Word Recognition Systems," J. Acoust. Soc. Amer., *68,* No. 5 (November 1980), pp. 1271–6.
22. S. E. Levinson et al., "Iterative Clustering Techniques for Selecting Speaker Independent Reference Templates for Isolated Word Recognition," IEEE Trans. Acoustics, Speech, and Signal Processing, *ASSP-27,* No. 2 (April 1979), pp. 134–41.
23. L. R. Rabiner et al., "Speaker Independent Recognition of Isolated Words Using Clustering Techniques," IEEE Trans. Acoustics, Speech, and Signal Processing, *ASSP-27,* No. 4 (August 1979), pp. 336–49.
24. H. Sakoe, "Device for Recognizing an Input Pattern With Approximate Patterns Used for Reference Patterns on Mapping," U.S. Patent 4,256,924, March 17, 1981.
25. L. E. Baum et al., "A Maximization Techique Occurring in the Statistical Analysis of Probabilistic Functions of Markov Chains," Ann. Math. Statist., *41,* No. 1 (1970), pp. 164–71.

AUTHORS

Stephen E. Levinson, B.A. (Engineering Sciences), 1966, Harvard University; M.S and Ph.D (Electrical Engineering), University of Rhode Island, Kingston, 1972 and 1974, respectively; AT&T Bell Laboratories, 1976—. From 1966 to 1969, Mr. Levinson was a design engineer at Electric Boat Division of General Dynamics in Groton, Connecticut. From 1974 to 1976, he held a J. Willard Gibbs Instructorship in Computer Science at Yale University. As a Member of Technical Staff at AT&T Bell Laboratories, he is pursuing research in the areas of speech recognition and cybernetics. Fellow, Acoustical Society of America; Senior Member, IEEE; Member, Association for Computing Machinery. Mr. Levinson is also a member of the editorial board of Speech Technology and an associate editor of the IEEE Transactions on Acoustics, Speech, and Signal Processing.

Lawrence R. Rabiner, S.B. and S.M., 1964, Ph.D (Electrical Engineering), 1967, Massachusetts Institute of Technology; AT&T Bell Laboratories, 1962—. At AT&T Bell Laboratories Mr. Rabiner is engaged in research on speech communications and digital signal processing techniques. He is coauthor of the books *Theory and Application of Digital Signal Processing* (Prentice-Hall, 1975), *Digital Processing of Speech Signals* (Prentice-Hall, 1978), and *Multirate Digital Signal Processing* (Prentice-Hall, 1983). Fellow, Acoustical Society of America, IEEE; Member, Eta Kappa Nu, Sigma Xi, Tau Beta Pi, the National Academy of Engineering.

Man Mohan Sondhi, B.Sc. (Physics), Honours, 1950, Delhi University, Delhi, India; D.I.I.Sc. (Communications Engineering), 1953, Indian Institute of Science, Bangalore, India; M.S. and Ph.D (Electrical Engineering), University of Wisconsin, Madison, Wisconsin, 1955 and 1957, respectively; AT&T

Bell Laboratories, 1962—. Before joining AT&T Bell Laboratories, Mr. Sondhi worked at the Avionics Division of John Oster Manufacturing Co., Racine, Wisconsin and the Central Electronics Research Institute in Pilani, India. He taught for one year at Toronto University, Toronto, Canada. At AT&T Bell Laboratories his research has included work on speech signal processing; echo cancellation; adaptive filtering; modeling of auditory, speech and visual processing by human beings; acoustical inverse problems; and, more recently, speech recognition based on hidden Markov modeling of speech. From 1971 to 1972 Mr. Sondhi was a guest scientist at the Royal Institute of Technology, Stockholm, Sweden.

AT&T BELL LABORATORIES TECHNICAL JOURNAL
Vol. 63, No. 4, April 1984
Printed in U.S.A.

Probabilistic Analysis of Interframe Tie Requirements for Cross-Connect Systems

By C. L. MONMA* and D. R. SMITH†

(Manuscript received August 26, 1983)

Cross-connect system frames provide the capability for remote access and cross-connection of circuits in digital format. Their usefulness has resulted in a rapidly growing number of existing and planned offices with multiple frames. A key problem in the planning of these offices is the determination of the frame capacity that should be reserved for tying purposes. Ties, or connections between frames, are necessary to cross-connect two-point circuits whose segments are terminated on different frames. This paper provides the theoretical basis for the computation of interframe tie requirements. We describe two scenarios for the assignment of circuits to facilities, and facilities to frames. For each case we derive the mean and variance of the number of tied circuits per frame. These quantities can be used to determine the number of ports that must be reserved for ties so that circuits requiring ties between frames will only be blocked with a prescribed small probability.

I. INTRODUCTION

Automated cross-connect systems, engineered to be effectively nonblocking, are often used in special service applications. Legs of circuits are assigned to transmission facilities that are linked to a cross-connect frame via ports. These frames allow remote access to digital circuits for testing purposes and provide cross-connection of legs of a circuit remotely. Multiframe offices, necessary because of the limited capacity

* AT&T Bell Laboratories; present affiliation Bell Communications Research, Inc. † AT&T Bell Laboratories.

of an individual frame, require planning so that sufficient capacity is reserved for interframe connections. This paper describes a method to compute the capacity required for this purpose.

One such system is the Digital Access and Cross-Connect System (DACS). For an introduction to DACS, see Refs. 1 through 7. The analysis presented here is applicable to similar cross-connect systems.

Each frame has a fixed capacity of ports. Currently, many offices require more than one frame because of their size, and the need for such multiframe offices is growing rapidly. Multiframe offices may be configured in two different ways: fully interconnected and tandem (see Figs. 1 and 2).

Legs of two-point circuits that terminate on different frames must be cross-connected by ties (special connections between the frames). These connections are either made via facilities linked directly between the frames in the fully interconnected case, or through a tandem frame. Since ties consume additional termination capacity on frames (as well as additional hardware), they should be minimized as much as possible. On the other hand, it is also important for planners to reserve enough tie ports on a frame so that circuit legs are not blocked because of lack of ties.

Legs of a multipoint circuit are connected by means of a multipoint bridge, which is external to the frames, eliminating the need for ties. For the remainder of the paper, we assume that all ties are due to two-point circuits. The analysis is easily extended to treat the case of

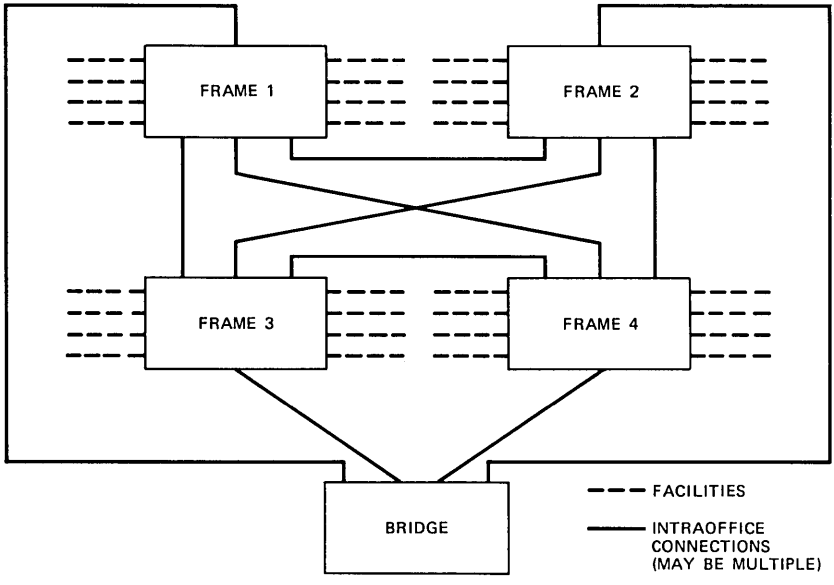

Fig. 1—Fully interconnected office configuration.

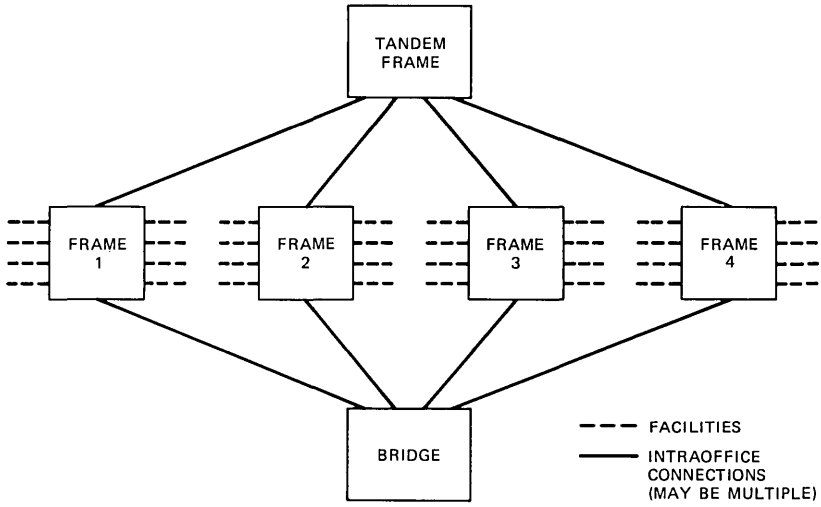

Fig. 2—Tandem office configuration.

multipoint bridges that are inside the frames. When such bridges are available, ties may be necessary to bring the legs of a multipoint circuit to the proper frame for bridging.

This paper describes the theoretical basis for the computation of interframe tie requirements for an office for each of two scenarios. These scenarios assume different procedures for the assignments of circuits to facilities. We have developed a model for an office that incorporates these two scenarios as subcases, and we refer to this model as the "semicontrol model".

1.1 The semicontrol model

In the semicontrol model, destinations are of two types: control destinations, for which the office administrator controls the assignment of circuit legs to facilities; and no-control destinations, for which the assignment of circuit legs to facilities is performed by someone else. It is assumed that circuit legs going to a no-control destination appear at random on facilities with capacity to that destination. This model also assumes that facilities to control destinations are balanced, that is, the numbers of facilities to a given destination that are terminated on different frames are as equal as is possible (they differ by at most one). Each two-point circuit is assumed to connect one control and one no-control destination. Multipoint circuits may connect any combination of destination types. The semicontrol model is consistent with networks of separately administered offices, since the assignment of a circuit leg between two points cannot be controlled by both end offices.

In this paper we analyze two subcases of the semicontrol model. In the first, tie requirements are computed for a mature frame subject to "churn" (circuits are connected and disconnected with time) without the possibility of planned rearrangement. Thus, once a circuit is cross-connected by a tie, it remains in this configuration throughout its lifetime, even if the possibility of a nontied path becomes available later (due to the disconnection of another circuit). In this subcase we develop a stochastic model for tied circuits, and solve for the mean and variance of the number of ties of the equilibrium distribution.

In the second subcase of the semicontrol model, we assume simultaneous assignment of circuit legs to the control facilities after observation of the assignment of circuit legs to the no-control facilities. (We do not use this knowledge in the assignment of facilities to frames.) We compute tie requirements immediately after this assignment—before the effects of churn are felt. This subcase of the model is appropriate immediately after the cutover of a new office (when knowledge of circuits on facilities is not used in assignment of facilities to frames), or immediately after a planned rearrangement of the circuit legs to control destinations within an existing office.

One should note that as time passes, if circuits are not rearranged, the total tie requirement will increase from the value computed assuming the second scenario until it reaches the value computed assuming the first scenario of the model. The speed with which this occurs depends on the value of the disconnect rate (sometimes referred to as churn rate), but the eventual value of the total tie requirement does not.

The present two subcases do not adequately model a third scenario involving a growing office. In this scenario, demand increases, and new frames and facilities are added from time to time. The policies used to select the times for the introduction of new frames and new facilities are crucial in determining tie requirements during growth. It is conceivable that phased introduction of equipment can lead to tie requirements higher than those given by either of the two subcases described earlier. This phenomenon has been verified by simulation work done by P. Soni.[8] Eventual tie requirements for mature offices without planned rearrangements are still given by the first subcase.

For both of the subcases, we compute the mean and variance of the number of tied circuits (on a frame) associated with each control destination. The mean of total tie requirements per frame can be found by summing the previously described means over the control destinations. The variance of total tie requirements per frame can be found by summing the previously described variances over the control destinations, under the assumption that circuits to different control destinations on a frame behave independently. The number of ports

necessary to guarantee that the tie requirement is met with a given probability is then obtained for the various configurations of frames, assuming that total number of tied circuits is normally distributed. It would also be possible to compute tie requirements by the equivalent-random method,[9] but the large number of control destinations typically encountered results in satisfactory accuracy of the normal approximation.

The methodology used here assumes that there is a large number of frames within the office. Care must be taken when interpreting the results for small offices. The calculations described herein will overestimate tie requirements for offices of two or three frames. When four or more frames are involved, the tendency to overestimate tie requirements is probably minimal.

The rest of this paper is organized as follows: Section II describes and analyzes the subcase of a mature frame affected by churn without planned rearrangements, and Section III describes and analyzes the subcase of a frame after an initial assignment of circuits. Section IV contains concluding remarks.

II. THE "MATURE" FRAME UNDER CHURN WITHOUT PLANNED REARRANGEMENTS

Here we consider an individual frame within an office and compute the distribution of the number of tied circuits on that frame when the churn assumption is appropriate. We assume the previously described semicontrol model. That is, there are control and no-control destinations, circuit legs to no-control destinations appear at random on facilities to those destinations, two-point circuits connect one no-control and one control destination, and facilities to control destinations are balanced as much as possible on frames. We also assume that there are no planned rearrangements, i.e., once a circuit is cross-connected, it remains in that configuration for the duration of its lifetime.

The lifetime of a circuit is assumed to be exponentially distributed. We consider a "mature" frame, so that the rate of replacement of circuits on a frame is essentially constant and equal to the long-run rate of circuit disconnects (the disconnect rate per circuit multiplied by the average number of circuits on the frame). The arrivals of connect orders having a leg to a given destination are assumed to be given by a Poisson process. We assume that the long-run average of the proportion of circuits to any given destination is constant, as is the proportion of two-point circuits. We also assume that these proportions are maintained on each of the no-control facilities, independent of their destinations. The last assumption will tend to give higher values for the computed number of ties because it ignores the com-

munities of interest that may exist between the no-control and control destinations.

The entire analysis of this section is concerned with circuits that have a leg to a given control destination and appear on a given frame. The mean and variance of the number of tied circuits on a frame due to these circuits will be determined. The mean (variance) of total tie requirements per frame will be found by summing the means (variances) of the tie requirements for all destinations.

We keep track of four types of circuits (see Fig. 3) for the given control destination on the given frame:

1. Two-point circuits cross-connected through the frame—Here the two legs of the circuit are assigned to facilities appearing on the same frame. Obviously, no ties are used for these circuits.

2. Two-point circuits tied out of the frame—Here the circuit has one leg on a no-control facility terminated on the given frame, but is tied to another frame for cross-connection to a facility going to the proper (control) destination. One tie circuit is needed on this frame for this type of circuit.

3. Two-point circuits tied into the frame—Here the circuit has one leg on a no-control facility terminated on another frame, but is tied to the given frame for cross-connection to a facility going to the proper (control) destination. One tie circuit is needed on this frame for this type of circuit.

4. Multipoint legs on the frame—Here a cross-connection appears on the given frame between a circuit going to the multipoint bridge and a circuit on a facility going to the proper (control) destination.

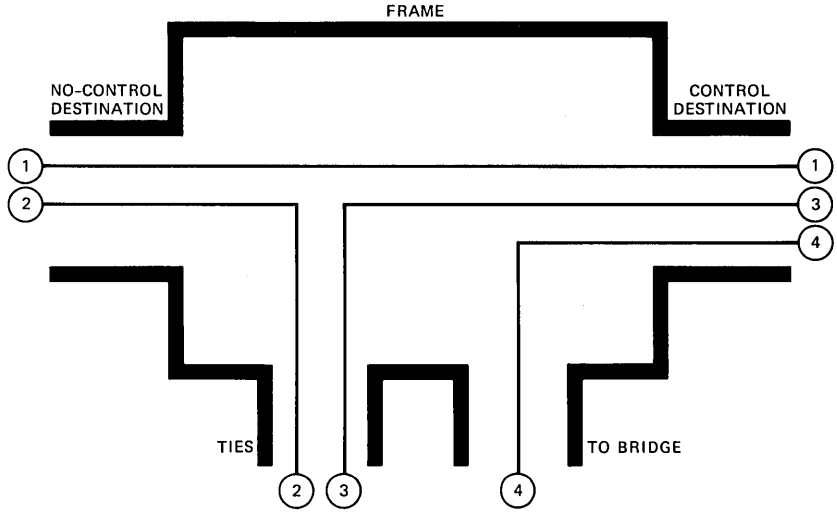

Fig. 3—Circuit types on a given frame.

No ties are needed for circuits of this type, although port capacity is used to connect these circuits to the bridge.

We denote by X_i the number of circuits of type i (described above) to a particular control destination. We show that the evolution of the state vector (X_1, X_2, X_3, X_4) is given by a continuous-time Markov chain that is closely related to the evolution of the state vector for a classical overflow process. The latter has a known solution for the means and variances of its two random variables, which enables us to calculate the mean and variance of the equilibrium tie requirements $(X_2 + X_3)$.

We assume that the total capacity of facilities to the control destination, which are terminated on the given frame, is k circuits. Clearly, $X_1 + X_3 + X_4$ is the number of these circuits in use, which cannot exceed k.

State transitions change one of the components of the state vector by one unit (either up or down). These transitions correspond to the connecting or disconnecting of a circuit of the type represented by that component.

We consider disconnect transitions first. Without loss of generality, we scale time in units of the mean lifetime of a circuit, so that the disconnect rate per circuit is unity. There is a transition corresponding to the disconnection of a circuit of type i at rate X_i for each of the four types of circuits, since the lifetimes are assumed to be exponentially distributed.

Now consider transitions corresponding to the connecting of circuits. There are two kinds of these transitions. The first comprises those two-point circuits that have one leg connected to a no-control destination on the given frame (corresponding to circuits of types 1 and 2). The second comprises those circuits having a leg elsewhere, which we assign to the given frame for cross-connection to the control destination (corresponding to circuits of types 3 and 4).

The first kind corresponds to arrivals of circuit legs on no-control facilities of the given frame that require cross-connection to a particular destination. We assume that these occur according to a Poisson process with rate λ_1. If there is capacity to the destination $(X_1 + X_3 + X_4 < k)$, these circuits are cross-connected through the frame to avoid ties. In this case each such event corresponds to the arrival of a type 1 circuit (X_1 is incremented by 1). If there is no capacity to the destination $(X_1 + X_3 + X_4 = k)$, these must be tied out of the frame. In this case each such event corresponds to the arrival of a type 2 circuit (X_2 is incremented by 1).

Now we consider events that cause type 3 circuits to connect. Every time a circuit is tied out of any frame in the office, it must be tied into another frame with available capacity to the destination. (It would

never be tied into a frame without capacity.) If the frame to be tied into is selected without regard to remaining capacity and without preference for a given frame, then the rate of such tied-in circuit connects should be approximately equal for all frames. Furthermore, this rate should be approximately equal for all states on the frame for which there is available capacity, at least if there are many frames in the office.

Accordingly, we assume that the connects of type 3 circuits correspond to a Poisson process with rate λ_2 (still to be determined) independent of the state, provided that capacity exists to the destination. Later in the section, λ_2 will be determined by a self-consistency requirement. For the present, we assume it is known.

In a similar fashion, it can be reasoned that requests for type 4 circuit connects occur at rate λ_3 (still to be determined) roughly independent of frame and state, provided that capacity to the destination is available at the frame.

To sum up, we assume that the evolution of the state vector (X_1, X_2, X_3, X_4) is given by a continuous-time Markov chain with the following transition rates [all from (x_1, x_2, x_3, x_4)]:

Into State	Rate	
$(x_1 - 1, x_2, x_3, x_4)$	x_1	
$(x_1, x_2 - 1, x_3, x_4)$	x_2	
$(x_1, x_2, x_3 - 1, x_4)$	x_3	
$(x_1, x_2, x_3, x_4 - 1)$	x_4	
$(x_1 + 1, x_2, x_3, x_4)$	λ_1	(if $x_1 + x_3 + x_4 < k$)
$(x_1, x_2 + 1, x_3, x_4)$	λ_1	(if $x_1 + x_3 + x_4 = k$)
$(x_1, x_2, x_3 + 1, x_4)$	λ_2	(if $x_1 + x_3 + x_4 < k$)
$(x_1, x_2, x_3, x_4 + 1)$	λ_3	(if $x_1 + x_3 + x_4 < k$).

Our goal is to find the mean and variance of the number of ties ($X_2 + X_3$) for the ergodic state distribution.

If we introduce another component to the state space, having no effect on the first four components, the resulting ergodic probabilities can be related to the ergodic probabilities of the classical trunk-overflow process. Since the means and variances of the state variables are readily available for the trunk-overflow process,[9] we are easily able to solve for the mean and variance of the required number of ties for a destination on a frame.

We thus add a dummy component, X_5, and also add the following transition rates from (x_1, x_2, x_3, x_4, x_5):

Into State	Rate	
$(x_1, x_2, x_3, x_4, x_5 - 1)$	x_5	
$(x_1, x_2, x_3, x_4, x_5 + 1)$	$\lambda_2 + \lambda_3$	(if $x_1 + x_3 + x_4 = k$).

The other transitions are as before (ignoring the value of X_5), with X_5 unchanged by the transitions.

Define $Y_1 = X_1 + X_3 + X_4$, $Y_2 = X_2 + X_5$, and $\lambda = \lambda_1 + \lambda_2 + \lambda_3$. It is readily seen that the vector (Y_1, Y_2) is a continuous-time Markov chain with transition rate from (y_1, y_2):

Into State	Rate	
$(y_1 - 1, y_2)$	y_1	
$(y_1, y_2 - 1)$	y_2	
$(y_1 + 1, y_2)$	λ	(if $y_1 < k$)
$(y_1, y_2 + 1)$	λ	(if $y_1 = k$).

These are the transition rates for the classical trunk-overflow process. Physically, one may think of offering λ Erlangs of traffic to k primary trunks, with any overflow going to an infinite group of trunks. The first component represents the number of primary trunks occupied, and the second component represents the number of overflow trunks occupied. The moments of the ergodic distribution of these variables are available:[9]

$$E(Y_1 + Y_2) = \lambda, \tag{1}$$

$$\text{var}(Y_1 + Y_2) = \lambda, \tag{2}$$

$$E(Y_1) = \lambda(1 - B(k, \lambda)), \tag{3}$$

$$E(Y_1^2) = (1 + \lambda)E(Y_1) - k\lambda B(k, \lambda), \tag{4}$$

$$E(Y_2) = \lambda B(k, \lambda), \tag{5}$$

and

$$\text{var}(Y_2) = E(Y_2)\left[1 - E(Y_2) + \frac{\lambda}{k + 1 + E(Y_2) - \lambda}\right], \tag{6}$$

where $B(k, \lambda)$ is the classical Erlang blocking formula

$$B(k, \lambda) = \frac{(\lambda^k/k!)}{\sum_{j=0}^{k} (\lambda^j/j!)}. \tag{7}$$

We now relate the ergodic distribution of $(X_1, X_2, X_3, X_4, X_5)$ to the ergodic distribution of (Y_1, Y_2). Let $q_i = \lambda_i/\lambda$. Whenever Y_1 is incremented, X_1 is incremented with probability q_1, X_3 is incremented with probability q_2, and X_4 is incremented with probability q_3. Furthermore, departures from X_1, X_3, and X_4 are proportional to the values of these state variables. Therefore, given Y_1, (X_1, X_3, X_4) is distributed in a multinomial distribution corresponding to Y_1 trials with probabilities of each type q_1, q_2, and q_3, respectively.

Similar reasoning tells us that given Y_2, (X_2, X_5) has a binomial distribution corresponding to Y_2 trials with probabilities of each type q_1 and $1 - q_1$, respectively. Also, given Y_1 and Y_2, (X_1, X_3, X_4) and (X_2, X_5) are independent.

Thus, the ergodic probability of $(x_1, x_2, x_3, x_4, x_5)$, denoted $\pi(x_1, x_2, x_3, x_4, x_5)$, is related to the ergodic probability of (y_1, y_2), denoted $\pi^*(y_1, y_2)$, in the following fashion:

$$\pi(x_1, x_2, x_3, x_4, x_5) = \pi^*(x_1 + x_3 + x_4, x_2 + x_5) \cdot \frac{(x_1 + x_3 + x_4)!(x_2 + x_5)!}{x_1!x_2!x_3!x_4!x_5!} q_1^{x_1} q_2^{x_3} q_3^{x_4} q_1^{x_2} (1 - q_1)^{x_5}. \quad (8)$$

Equation (8) may also be checked by direct substitution into the balance equations, but we omit the details here. The facts stated previously, which allowed us to write equation (8), are sufficient to extract moments of the number of circuits tied. We proceed by conditioning on the values of Y_1 and Y_2:

$$E(X_2 + X_3 \mid Y_1, Y_2) = q_1 Y_2 + q_2 Y_1 \quad (9)$$

and

$$E((X_2 + X_3)^2) \mid Y_1, Y_2) = q_1^2 Y_2^2 + q_1(1 - q_1) Y_2 + 2q_1 q_2 Y_1 Y_2 + q_2^2 Y_1^2 + q_2(1 - q_2) Y_1. \quad (10)$$

Taking expectations with respect to Y_1 and Y_2 in (9) and (10), we obtain (after some algebra)

$$E(X_2 + X_3) = q_1 E(Y_2) + q_2 E(Y_1) \quad (11)$$

and

$$\text{var}(X_2 + X_3) = q_1 q_2 \text{var}(Y_1 + Y_2) + q_2(q_2 - q_1)\text{var}(Y_1) + q_1(q_1 - q_2)\text{var}(Y_2) + q_2(1 - q_2)E(Y_1) + q_1(1 - q_1)E(Y_2). \quad (12)$$

Equations (11) and (12), when combined with eqs. (1) through (6), give the mean and variance of the number of tied circuits to a given control destination on a given frame. These expressions depend implicitly on q_1 and q_2, which depend on λ_2 and λ_3. We will determine q_1 and q_2 in Section 2.1.

2.1 Determination of λ, q_1, and q_2

We have so far analyzed a single frame with available capacity of k circuits to the particular destination considered. It is possible that not all frames in an office have the same number of available circuits to the destination (since the total number of facilities may not be a multiple of the number of frames), and these considerations affect the

determination of λ_2 and λ_3. We will actually find the derived quantities λ, q_1, and q_2. Suppose that there are m types of frames (in terms of circuits to the destination) represented in the office, with available number of circuits to the destination of $k_1, k_2, \cdots k_m$ (m will usually be two). Suppose that the proportions of the frames in the office that are of these types are $p_1, p_2, \cdots, p_m$, respectively. We have argued previously that the values of λ_2 and λ_3 are identical for all the frames, since these represent the rates of arrival of circuits that are selected to be connected to any frame in the office (having capacity) with equal probability.

Denote the expected number of circuit legs to the control destination per frame (including two-point and multipoint circuits) by T. (This is known.) The (random) number of outgoing circuit legs from a frame to the destination is given by Y_1. Consistency in the average number of legs to the destination per frame demands that the average value of the expectation of Y_1 equals T, or

$$\sum_{i=1}^{m} p_i[\lambda(1 - B(k_i, \lambda))] = T, \tag{13}$$

where use has been made of (3). The left-hand side of (13) is increasing in λ, is continuous, and takes all values in the range $[0, c)$ for $\lambda \geq 0$, where $c = \sum_{i=1}^{m} p_i k_i$ is the average capacity to the destination on a frame basis. Therefore, (13) has a unique solution for λ as a function of T in the above quoted range.

We also require, for consistency, that the total number of tied-in circuits in the entire office is equal to the number of tied-out circuits. Recall that X_2 represents tied-out circuits and X_3 represents tied-in circuits, and their expectations are $q_1 E(Y_2)$ and $q_2 E(Y_1)$, respectively, where $E(Y_1)$ and $E(Y_2)$ are given in (3) and (5). This consistency requires that the averages of these values over all frames be equal, or

$$q_1 \sum_{i=1}^{m} p_i B(k_i, \lambda) = q_2 \sum_{i=1}^{m} p_i (1 - B(k_i, \lambda)), \tag{14}$$

where a common factor of λ has been eliminated. Use of (13) in (14) with the identity

$$q_1 = \frac{\lambda_1}{\lambda} \tag{15}$$

yields

$$q_2 = \frac{\lambda_1}{T} - \frac{\lambda_1}{\lambda}. \tag{16}$$

2.2 Computation of the mean and variance of total ties per frame

Equations (14), (15), and (16) allow one to compute the parameters q_1 and q_2 used in eqs. (11) and (12), which give the mean and variance of the total number of tied circuits on a particular frame. Equations (11) and (12) depend on the value of k, the number of circuits to the destination on the frame. When the value of k to a particular destination is not constant over all frames, averaging over the values is necessary. Although the rationale for averaging the mean number of ties is clear, some explanation is necessary for the averaging of the variance (as opposed to taking the average of the second moment minus the square of the average first moment).

The ultimate goal of this process is to obtain a number representing the reserved capacity for tied circuits on a frame, where reserved capacity is sufficient to meet tie requirements with a given (user-specified) probability. It can be argued that if the number of control destinations is large, circuits to each of the destinations behave roughly independently. Now choose a particular frame, which has ℓ_i circuits to control destination i, $i = 1, 2, \cdots, n$, where n is the total number of control destinations. If n is sufficiently large, the total tie requirements for this frame will be approximately normally distributed. The mean is equal to the sum of the means calculated for each destination (given the number of circuits to that destination on the frame). The variance is equal to the sum of the variances calculated for each destination (given the number of circuits to that destination on the frame).

Although the vector $(\ell_1, \ell_2, \cdots, \ell_n)$ will vary from frame to frame, the components are definitely not independent, since the total outgoing capacity from a frame will be more or less fixed. In other words, a frame having a greater than average number of facilities to one destination will tend to have lower than average numbers of facilities to other destinations.

If all destinations have identical characteristics (in terms of the number of frames with given number of circuits to the destination), then the proportion of ℓ_i on a given frame that are equal to a particular value will be very close to the overall proportion (over all frames) of ℓ_i that are equal to that value. In this case, the total variance on the frame will be nearly equal to the sum of the average variances (conditioning on the number of circuits) to each destination.

If all destinations are not identical, there will still be a tendency for the variance of tied circuits to be close to the sum of the average variances over the control destinations.

For this reason it is reasonable to compute the variance of the total number of ties per frame as the sum of the average variance per destination. The latter is equal to the sum of the product of p_i with the value of (12) when k_i replaces k.

2.3 The mean ties for a destination per frame

We obtain a simple expression for the average number of ties per frame.

Equations (11), (3), and (5) give

$$E(X_2 + X_3) = q_1\lambda B(k, \lambda) + q_2\lambda(1 - B(k, \lambda)). \tag{17}$$

The average number of ties per frame, which we denote v, is thus

$$v = \sum_{i=1}^{m} p_i[q_1\lambda B(k_i, \lambda) + q_2\lambda(1 - B(k_i, \lambda))]. \tag{18}$$

Use of (13), (15), and (16) gives

$$v = 2\lambda_1(1 - T/\lambda). \tag{19}$$

Note that λ_1 is the expected number of two-point circuits per frame, so that $2\lambda_1$ is the total ties if all circuits are tied. (Each tied circuit results in one tie in and one tie out.) The factor $(1 - T/\lambda)$ is the proportion of two-point circuits that are tied, where λ is determined by the implicit solution to (13). As T increases, it can be shown that $1 - T/\lambda$ increases. As T approaches c [facility fill goes to one, see definition following (13)], $1 - T/\lambda$ goes to 1.

As stated earlier, the mean total number of ties required per frame can be found by summing expected ties per destination as given by (19) over all destinations.

2.4 Graphical representation of mean tie requirements

It is possible to summarize the mean number of ties needed for a specific destination per frame in several families of graphs, each of which corresponds to a type of facility. These graphs give a value of v from (19) when λ has been determined from (13) based on four inputs. These are

- j = number of circuits per facility (typically $j = 12$ or 24),
- f = average fill on these facilities,
- a = average number of facilities (to the destination) terminated per frame, and
- r = proportion of circuit legs to that destination that are from two-point circuits.

Figure 4 illustrates one set of these graphs, corresponding to analog group facilities ($j = 12$). The average number of tied circuits per frame is plotted versus the average number of facilities per frame (a) for fills (f) of 0.70, 0.75, 0.80, 0.85, 0.90, and 0.95. These curves assume that all circuits are two-point ($r = 1$). If this is not the case, expected ties obtained from the graph should be multiplied by the value of r. The

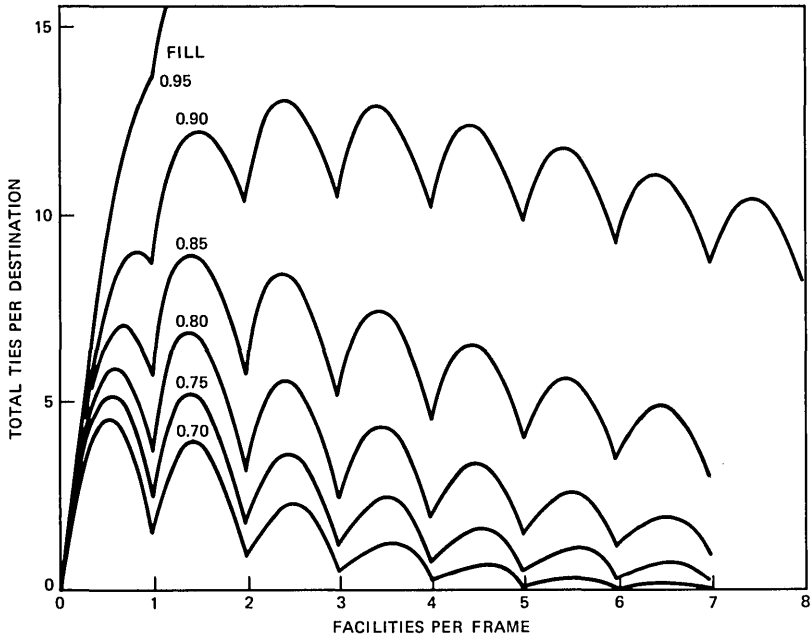

Fig. 4—Ties versus facilities for analog groups; churn model (12 circuits per facility).

"scalloped" nature of the curves is due to the relatively higher mean tie requirement when the mean number of facilities per frame is not integer, forcing uneven spreading of these facilities on the frames.

We now describe the method used to obtain the curves. If facilities are spread as evenly as possible, then $m = 2$, and

$$\left.\begin{aligned} T &= afj, \\ p_1 &= \lceil a \rceil - a, \\ p_2 &= 1 - p_1, \\ k_1 &= (\lceil a \rceil - 1)j, \\ \text{and } k_2 &= \lceil a \rceil j \end{aligned}\right\}. \tag{20}$$

Here $\lceil x \rceil$ represents the smallest integer greater than or equal to x. We can now determine λ by numerical solution of (13) and v, the average number of ties, can be obtained from (19).

III. SIMULTANEOUS ASSIGNMENT OF CIRCUITS

In this section we consider the second subcase of the semicontrol model in which circuits (and ties) are assigned to control facilities after assignment of all facilities to frames and after observation of the

assignment of the no-control legs of the circuits. This scenario excludes the possibility that circuits will be both tied in and tied out to the same destination on the same frame. Here again (as in the last section), there are two types of ties on a frame—those due to circuits tied out and those due to circuits tied in.

We first obtain the distribution of the number of circuits tied out of a frame. By assumption, we know that the distribution of the number of no-control legs of two-point circuits on a frame that require cross-connection to a particular control destination is a Poisson distribution. Ties out are required if this number exceeds the available number of circuits to the destination on the frame. In this case the number required is exactly equal to the excess.

The distribution of the number of tied-in circuits on a frame depends on the methodology used to assign tied-in circuits. The total number of tied-in circuits in an office is equal to the number of tied-out circuits in the same office (this can be determined by the method described in the last paragraph). The specific way that individual frames are assigned these tied-in circuits is up to the office administrator. Of course, the number assigned to any particular frame cannot exceed the remaining capacity (after satisfying through-connects on the frame to the destination). Thus, circuits will never be tied into and tied out of the same frame (unlike the churn model of Section II).

Here we compute distributions of tied-in circuits under each of two assignment policies. In the first, tied-in circuits are assigned to minimize the variance of ties on a frame. In the second, tied-in circuits are assigned to maximize the variance of tied circuits on a frame. The resulting variances provide lower and upper bounds for the variance of any assignment policy.

We obtain first and second moments for the number of circuits tied in and tied out (for a given control destination) per frame. The second (first) moment of the total number of ties per destination per frame equals the sum of the second (first) moments of the number of circuits tied in and the number of circuits tied out. The second moment is additive since circuits are never tied into and tied out of the same frame in the simultaneous assignment case. (This can, however, occur in the churn model of the previous section.)

3.1 Moments of circuits tied out of a frame

Let X be the number of legs of two-point circuits incident on a frame that must be cross-connected to a given control destination, let k be the capacity in circuits to the controlled destination on a frame, let Y be the number of circuits tied out to this destination on the frame, and let Z be the remaining capacity available for tied-in circuits (or multipoints) on the frame. Then,

$$Y = (X - k)^+, \tag{21}$$

and

$$Z = (k - X)^+, \tag{22}$$

where $a^+ = \max[a, 0]$.

Under the assumption that X is a Poisson random variable with mean λ, i.e.,

$$P\{X = i\} = (\lambda^i/i!)e^{-\lambda}, \tag{23}$$

we can compute the first two moments of Y:

$$E(Y) = \lambda S_k - kS_{k+1}, \tag{24}$$

and

$$E(Y^2) = \lambda^2 S_{k-1} + (1 - 2k)\lambda S_k + k^2 S_{k+1}, \tag{25}$$

where

$$S_k = \sum_{j=k}^{\infty} (\lambda^j/j!)e^{-\lambda}. \tag{26}$$

That is, S_k is the tail sum of the Poisson probability distribution.

A good approximation for S_k for large values of k is given by the normal approximation

$$S_k \approx \bar{\Phi}\left(\frac{k - 1/2 - \lambda}{\sqrt{\lambda}}\right), \tag{27}$$

where $\bar{\Phi}$ represents the complement of the standard normal c.d.f.; that is,

$$\bar{\Phi}(y) = \int_y^{\infty} \frac{1}{\sqrt{2\pi}} e^{-x^2/2} dx. \tag{28}$$

When the value of k varies, i.e., a proportion p_i of the frames has k_i circuits to the destination for $i = 1, 2, \cdots, m$, then the appropriate average moments are found by taking the expectations of (24) and (25) with respect to the distribution p.

3.2 Moments of the number of tied-in circuits

We first find the distribution of the available capacity to the destination after the assignment of circuits cross-connected through the frame, but before circuits are tied in (the random variable Z). We obtain

$$P\{Z = i\} = (\lambda^{k-i}/(k - i)!)e^{-\lambda}, \qquad 0 < i \leq k; \tag{29}$$

$$P\{Z = i\} = 0, \qquad i > k; \tag{30}$$

and

$$P\{Z = 0\} = 1 - \sum_{i=1}^{k} P\{Z = i\}. \tag{31}$$

Equations (29) through (31) are based on a given frame with k available circuits to the destination. Let α_i be the overall probability (considering all frames with possibly different values of k) that there is a remaining capacity of i circuits to the destination after the assignment of circuits cross-connected through the frame, but before circuits are tied in. We can compute α_i, $i > 0$, by conditioning on the value of k

$$\alpha_i = e^{-\lambda} \sum_{j:k_j \geq i} p_j \lambda^{(k_j - i)}/(k_j - i)!, \tag{32}$$

where p_j is the proportion of frames in the office with capacity k_j circuits to the control destination under consideration. The maximum subscript i for which $\alpha_i > 0$ is max $\{k_j\}$.

We next compute the average number of circuits that must be tied in per frame, which we denote by B. This must equal the average number of circuits tied out per frame. Using (24) for various k values yields

$$B = \sum_{j=1}^{m} p_j(\lambda S_{k_j} - k_j S_{k_j+1}). \tag{33}$$

Now assume that there is a large number of frames. It is possible to have a proportion Θ_i of frames with i tied-in circuits to the destination under consideration $\forall i$ if and only if

$$\sum_{i=1}^{\infty} i\Theta_i = B \tag{34}$$

and

$$\sum_{i=j}^{\infty} \Theta_i \leq \sum_{i=j}^{\infty} \alpha_i, \qquad \forall j \geq 0. \tag{35}$$

Equation (34) follows from the fact that the expected number of circuits tied in equals the expected number tied out. Equation (35) states that the proportion of frames with i or more circuits tied in has to be no greater than the proportion of frames with capacity for i or more tied-in circuits.

We now determine the values of Θ_i that give minimum and maximum values for the second moment (denoted by V) subject to the constraints (34) and (35), where

$$V = \sum_{i=1}^{\infty} i^2\Theta_i. \tag{36}$$

3.3 Minimum second moment

Choose ℓ such that

$$\sum_{i=1}^{\ell} i\alpha_i + \sum_{i=\ell+1}^{\infty} \ell\alpha_i < B \leq \sum_{i=1}^{\ell+1} i\alpha_i + \sum_{i=\ell+2}^{\infty} (\ell+1)\alpha_i. \tag{37}$$

If $B \leq \sum_{i=1}^{\infty} i\alpha_i$, i.e., if there is average capacity to handle tied-in requirements, then this is always possible. This follows because the left-hand side of (37) is a nondecreasing function of ℓ, with a value of 0 for $\ell = 0$, and a value of $\Sigma_{i=1}^{\infty} i\alpha_i$ for $\ell = \infty$. Note that ℓ is uniquely determined. Define

$$\rho = B - \sum_{i=1}^{\ell} i\alpha_i - \sum_{i=\ell+1}^{\infty} \ell\alpha_i. \tag{38}$$

Now, the minimal value of V is produced by setting

$$\Theta_i = \alpha_i, \qquad i < \ell; \tag{39}$$

$$\Theta_\ell = \sum_{i=\ell}^{\infty} \alpha_i - \rho; \tag{40}$$

$$\Theta_{\ell+1} = \rho; \tag{41}$$

and

$$\Theta_i = 0, \qquad i > \ell + 1. \tag{42}$$

Physically, this distribution is obtained when one assigns tied-in circuits sequentially in the following fashion: Assign the next tied-in circuit to a frame with available capacity having the fewest tied-in circuits already assigned.

Clearly, Θ_i forms a valid probability distribution, since (37) implies that Θ_ℓ and $\Theta_{\ell+1}$ are nonnegative, and also since the sum of the Θ_i's is one. This distribution is also easily seen to satisfy (34) and (35). As a matter of fact, (35) is tight for all $j \leq \ell$.

This last property uniquely specifies Θ, i.e., a probability distribution $\hat{\Theta}$ satisfying (34) and (35) with the property that, for every m, if

$$\hat{\Theta}_{m+1} > 0, \quad \text{then} \quad \sum_{i=j}^{\infty} \hat{\Theta}_i = \sum_{i=j}^{\infty} \alpha_i, \qquad \forall j \leq m \tag{43}$$

must be the distribution Θ given in (39) through (42).

Proof: Choose $n = \sup\{m:\hat{\Theta}_{m+1} > 0\}$. The condition of the last paragraph tells us that $\hat{\Theta}_j = \alpha_j$, $\forall j < n$. The normalization of $\hat{\Theta}$ and its satisfying (34) uniquely determine $\hat{\Theta}_n$ and $\hat{\Theta}_{n+1}$. Also,

$$B = \sum_{i=1}^{n+1} i\hat{\Theta}_i = \sum_{i=1}^{n-1} i\alpha_i + n\hat{\Theta}_n + (n+1)\hat{\Theta}_{n+1}.$$

However,

$$n\hat{\Theta}_n + (n+1)\hat{\Theta}_{n+1} > n \sum_{i=n}^{\infty} \alpha_i,$$

and

$$n\hat{\Theta}_n + (n+1)\hat{\Theta}_{n+1} \leqslant (n+1) \sum_{i=n}^{\infty} \alpha_i \leqslant n\alpha_n + \sum_{i=n+1}^{\infty} (n+1)\,\alpha_i.$$

Comparison with (37) shows that $n = \ell$, and we are done. □

We use this fact to show that the distribution Θ has minimum second moment over all distributions satisfying (34) and (35). Choose $\Theta' \neq \Theta$, which satisfies the constraints; Θ' must violate (43). Thus, we can find m and $j \leqslant m$ with $\Theta'_{m+1} > 0$ and $\sum_{i=j}^{\infty} \Theta'_i < \sum_{i=j}^{\infty} \alpha_i$. Choose the largest such m. Since both Θ' and α sum to one, we can find $k < j$ with $\Theta'_k > 0$. Choose the largest such k. The new distribution Θ'' with

$$\Theta''_k = \Theta'_k - \frac{\epsilon}{j-k},$$

$$\Theta''_j = \Theta'_j + \frac{\epsilon}{j-k},$$

$$\Theta''_m = \Theta'_m + \epsilon,$$

and

$$\Theta''_{m+1} = \Theta'_{m+1} - \epsilon,$$

with $\epsilon = \min[\Theta'_{m+1}, (j-k)\Theta'_k, (j-k)\,(\sum_{i=j}^{\infty}(\alpha_i - \Theta'_i))] > 0$, and other components identical to Θ', is still a probability distribution satisfying (34) and (35) and

$$\sum_{i=1}^{\infty} i^2\Theta''_i = \sum_{i=1}^{\infty} i^2\Theta'_i + \epsilon(j+k-2m-1),$$

or

$$\sum_{i=1}^{\infty} i^2\Theta''_i < \sum_{i=1}^{\infty} i^2\Theta'_i.$$

With a series of such transformations, Θ' can be transformed into Θ. □

3.4 Maximum second moment

We proceed in a similar fashion. In this case choose ℓ such that

$$\sum_{i=\ell+1}^{\infty} i\alpha_i < B \leq \sum_{i=\ell}^{\infty} i\alpha_i. \tag{44}$$

Define

$$\rho^* = B - \sum_{i=\ell+1}^{\infty} i\alpha_i. \tag{45}$$

The maximum value of V is produced by setting

$$\Theta_i = 0, \qquad 0 < i < \ell; \tag{46}$$

$$\Theta_\ell = \rho^*/\ell; \tag{47}$$

$$\Theta_i = \alpha_i, \qquad i > \ell; \tag{48}$$

and

$$\Theta_o = 1 - \sum_{i=1}^{\infty} \Theta_i. \tag{49}$$

Physically, this distribution is obtained when one assigns tied-in circuits in the following sequential fashion: Completely fill the frame with maximum available capacity before assigning to another frame. Here we omit the proof, which is similar to that of the last subsection.

IV. CONCLUDING REMARKS

This paper describes the assumptions of a semicontrol model for facility and circuit assignment in a multiframe office. We compute the mean and variance of the number of ties per frame for each of two subcases. The first scenario assumes that we treat a mature frame in a churn environment without planned rearrangements. The second one assumes a simultaneous assignment of circuits, and is appropriate following the cutover of a new office or a wholesale rearrangement of existing circuits within an office. These computations are incorporated as subroutines in the computer program DACSPET (DACS Planning and Engineering Tool), which computes frame requirements and resulting port usages for a multiframe office.

4.1 Preliminary insights

The previously described computer program has been run on an assortment of sample data. These runs provide preliminary insights into the question of tie requirements for multiframe offices. We summarize these insights below.

1. The effect of fill is clear in all cases. Higher facility fills imply more ties per frame. The reason for this is simply that higher fills imply less spare capacity on fewer facilites, and therefore less flexibility in assigning circuits.

2. Tie requirements under the churn scenario are larger than under the simultaneous circuit assignment scenario. The effect is relatively minor at low facility fills, although it increases rapidly as the fill does.

3. The size of an office, in terms of number of frames or circuits, seems to have less of an effect on tie requirements per frame than other variables, such as the number of control destinations served and the proportion of traffic to each destination. An office with many destinations, each with a small proportion of traffic, will clearly incur more tied circuits than an office with a few large destinations under the semicontrol model.

4. The ratio of two-point and multipoint circuits also affects the number of tied circuits per frame under the assumption of an external multipoint bridge. For the same overall facility fill, the number of tied circuits is roughly proportional to the percentage of two-point circuits, all other factors being equal.

V. ACKNOWLEDGMENTS

This work grew out of a series of meetings on DACS planning issues held at AT&T Bell Laboratories and elsewhere, and benefited from numerous discussions with many people. We would particularly like to thank M. Segal, as well as A. J. Osofsky, of AT&T Bell Laboratories; D. S. Burpee and D. J. Irish of AT&T; T. Bennis of AT&T Communications; and E. J. Anderson and W. E. Symons of Bell Communications Research, Inc. for their help.

REFERENCES

1. J. R. Colton, "Cross-Connections—DACS Makes Them Digital," Bell Lab. Rec., *58*, No. 8 (September 1980), pp. 248–55.
2. R. C. Drechsler, "DACS Cross-Connects—And That's Just the Beginning," Bell Lab. Rec., *58*, No. 9 (October 1980), pp. 305–11.
3. J. R. Colton and A. J. Osofsky, "DACS Features and Applications," Nat. Telecommun. Conf. Rec., *1* (November 1981).
4. R. P. Abbot and D. C. Koehler, "Digital Access and Cross-Connect System Architecture," Nat. Telecommun. Conf. Rec., *1* (November 1981).
5. A. J. Cirillo, L. F. Horney, and J. D. Moore, "DACS Microprocessor System," Nat. Telecommun. Conf. Rec., *1* (November 1981).
6. L. C. Sweeney, "DACS in an Associated Company," Nat. Telecommun. Conf. Rec., *1* (November 1981).
7. G. P. Ashkar, G. A. Ford, and T. Pecsavaradi, "Reshaping the Network for Special Services," Bell Lab. Rec., *61* (September 1983), pp. 4–10.
8. P. Soni, private communication.
9. R. B. Cooper, *Introduction to Queuing Theory*, New York: MacMillan, 1972.

AUTHORS

Clyde L. Monma, B.S. (Computer Science), 1974, Washington State University; M.S. and Ph.D. (Operations Research), 1978, Cornell University; AT&T Bell Laboratories, 1979–1983. Present affiliation Bell Communications

Research, Inc. Mr. Monma's responsibilities have included research in deterministic OR methods, consulting on various scheduling and network planning projects, and developing software tools. His first assignment was to design a Primal Network Flow Code (PNFC), which is now being used in several planning systems. Other projects have included a Packet Network Design and Analysis (PANDA) planning tool, and a Digital Access and Cross-Connect System Planning and Engineering Tool (DACSPET). Recent research topics have been in the areas of scheduling, networks, and graphs. He is professionally active as an Associate Editor for *Operations Research Letters* and *Networks*, and as a referee for numerous OR and Computer Science journals. Member, ORSA, ACM, SIAM, and the Mathematical Programming Society.

Donald R. Smith, A.B. (Physics), 1969, Cornell University; M.S. (Operations Research), 1974, Columbia University; Ph.D. (Operations Research), 1975, University of California, Berkeley; AT&T Bell Laboratories, 1980—. Before joining AT&T Bell Laboratories, Mr. Smith was employed at Adaptive Technology, Inc. (from 1970 to 1974), and was Assistant Professor in the Department of Industrial Engineering and Operations Research, Columbia University (from 1975 to 1979). At Adaptive Technology, Mr. Smith developed mathematical models for new techniques in statistical multiplexing. At AT&T Bell Laboratories he is in the Operations Research Department of the Systems Analysis Center, pursuing interests in applied stochastic processes.

AT&T BELL LABORATORIES TECHNICAL JOURNAL
Vol. 63, No. 4, April 1984
Printed in U.S.A.

A Nonlinear Zero-One Combinatorial, Goal-Programming Model and Constructive Algorithm for Solving Multiobjective Assignment Problems

By K. R. LIPSKE* and J. H. FLETCHER*

(Manuscript received July 18, 1983)

This paper describes a technique for assigning orders against specific reels of inventoried cable to ensure a high level of customer service, efficient labor utilization, highly usable cable lengths in inventory, and minimal scrap. Some orders are interrelated and thus linked, requiring that the assignment of each order be contingent upon the assignment of all linked orders. Due to this contingency, penalties associated with certain assignments, and selection allowances, the problem is quite complex. Our method of solution is formulated as a preemptive, multipriority, zero-one goal programming model used in a constructive initial placement algorithm. The model is primarily linear, but it also contains some nonlinear terms. The goal programming model and initial constructive algorithm run weekly in a production environment that handles up to 100 orders and 150 reels per problem.

I. THE PROBLEM

In 1981 Western Electric began offering 26 types of PULP Cable (Paper Insulated Telephone Exchange Cable) on a short-interval stock basis. Instead of making the cable to order as before, Western Electric would fill customer orders from reels of cable manufactured and inventoried at the stocking locations for weekly shipment. A method was required for selecting the most suitable reel of cable for filling each order while ensuring a high level of customer service, efficient

* AT&T Technologies, Inc.

labor utilization, very usable cable lengths in inventory, and minimal scrap.

Due to the manner in which this cable is installed at the job site, three specific selection requirements exist. First, only one reel of cable may be used to fill each order because the orders are for specific lengths. Henceforth, because of this length requirement, we will refer to the orders as subitems. Second, shipping less than the amount ordered is forbidden and only 10 feet of tolerance is allowed in the amount that can be shipped over the quantity ordered. This corporate shipping policy fortunately provides leeway in the selection process. Finally, in most instances, there exist several subitems for the same cable type, which must be installed at the same time. Subitems of this nature will be referred to as linked subitems in this paper. To this end, it is imperative that if any linked subitem is assigned from inventoried cable, then all subitems to which it is linked must also be assigned to some cable. Also, all linked subitems must be filled from the same stocking location. To accommodate the reader, each subitem/reel of cable possibility will be termed a real variable.

Inventoried cable is cable that has been completely tested and found to meet predetermined electrical requirements. Each time a piece of cable is cut, the newly cut ends must be tested. A 3-foot section of cable is lost in testing each end. This lost footage, henceforth referred to as the cutting allowance, must be considered in the selection process.

Because of the subitem linkage, corporate shipping policy tolerance, and cutting allowance considerations, the method of solution required to solve this assignment problem is quite complex. Since each subitem must be completely filled from a single reel of cable, or left unassigned, a method was sought to provide optimal or near-optimal results in zero-one form, where a value of 1 indicates that the subitem is assigned to the reel of cable, and 0 indicates that the subitem is not assigned to the reel of cable. The problem then is to minimize:

$$Z = \sum_{\substack{\text{ALL CONSTRAINTS} \\ k}} \sum_{\substack{\text{ALL PRIORITY LEVELS} \\ l}} P_{kl}[g(d_k^-, d_k^+)]$$

subject to:

$$U \sum (c_{ij}x_{ij} + d_k^- - d_k^+) - W \sum (c_{ij}x_{ij} + d_k^- - d_k^+) + Y \sum\sum (c_{ij}x_{ij} + d_k^- - d_k^+) < 0,$$

where

P_{kl} = preemptive priority l of constraint k

$g(d_k^-, d_k^+)$ = mathematical operation on slack variables (d_k^-, d_k^+) to be minimized

c_{ij} = various constraint coefficients on real variables X_{ij}

$X_{ij} = 1$ if subitem$_j$ is assigned to reel$_i$, 0 otherwise

$U, W, Y = 0, 1$ based on whether that term is needed in the constraint type (see Appendix A for specific formulation of constraints).

II. HEURISTIC APPROACHES

Zero-one assignment problems traditionally are solved using several techniques, including exhaustive search, branch-and-bound enumeration, and integer linear programming adaptations.[1] These techniques become unusable, however, as the problem grows to large sizes. Since our problems sometimes consist of 1,000 objectives and 1,500 decision variables (for 50 subitems and 150 reels of cable), none of the traditionally small-to-medium solution techniques proved suitable when investigated.

Liggett[1] describes two types of heuristic approaches, which will lead to good if not optimal results with small-to-medium size problems. The first is the iterative improvement approach, which consists of obtaining an initial suboptimal solution by any of several methods and improving this solution in incremental steps. This method is characterized by its quick generation of an initial suboptimal solution with a subsequent step-by-step improvement, which is generally quite time-consuming. This approach has been used with a simplex goal programming algorithm with subsequent heuristic improvements.[2] We attempted to implement this technique; however, due to the many conflicting objectives in our problem, most variables possessed fractional values as a result of the simplex starting solution. Adjusting this solution to zero-one form then tended to defeat the purpose of starting with a simplex-generated solution.

The second method mentioned by Liggett[1] is constructive initial placement. Here a solution is built from scratch by adding variables to the solution set in successive steps that continually improve the results. Because zero-one form can be assumed from the start and each step improves the solution, this approach was more attractive for solving our assignment problem. Parker[3] interestingly compares various approaches of both techniques and concludes that the constructive approach of Graves and Whinston[4] is superior to the iterative improvement method in the solution to the component placement problem, which is somewhat similar but smaller than our problem. Graves and Whinston use conditional probability in their algorithm as a general-purpose enumerative technique to select the next assignment to be added to the partially constructed solution. In lieu of conditional probability, we use a look-ahead feature before generating the model equations to accord high priority to certain assignments. We also restrict certain order-to-reel assignments that could exclude other

assignments that appear preferable. Our specific problem is depicted by the model generated (see the appendix formulation). The algorithm, however, is of a deterministic general-purpose nature and is much less application-oriented.

III. METHOD OF SOLUTION

Our approach to the problem was to develop an algorithm that would produce desirable solutions proceeding under the direction of a model containing the problem formulation. The technique is based on a preemptive multipriority zero-one goal programming model formulation, which is used in a constructive initial placement algorithm.

Goal programming is a multicriteria, problem-solving technique that utilizes mathematical equations and an associated priority scheme to govern its solution. Slack variables (see d_k^-, d_k^+ terms in the equations of the appendix) associated with each equation are ranked and weighted in an achievement function to govern the achievement of the desired results. It is absolutely necessary that higher-ranked objectives are satisfied before lower-ranked objectives, and that the optimality of the overall solution is maintained with higher-ranked objectives as lower-ranked objectives are solved.

The algorithm that we developed to solve this assignment problem does this and with much more flexibility than could be realized using the simplex algorithm. Our algorithm can either maximize and/or minimize variables and, in fact, with this model formulation, makes considerable use of both. Since the algorithm is void of simplex restrictions, it also can perform nonlinear optimization. In this application, we minimize the reciprocal of certain slack variables, implying that if the slack variable cannot be driven to 0, then it should be maximized.

Because we chose the constructive initial placement method, it is imperative that at each iteration, the real variable be chosen that will improve the solution most. To provide this, our algorithm uses the multiphase method of goal programming with entering variable tie logic. With tie logic, if several real variables improve the solution equally at a given priority level, then the improvement of each at the next lower priority level is used to decide which variable to bring into solution. Without tie logic in the algorithm, constructive initial placement would not provide satisfactory results.

3.1 Contingencies

Two conditions exist that involve assigning a set of related variables at the same time. Reel handling can be minimized, in part, by assigning several subitems to a single reel of cable when all or nearly all of the cable on that reel would be used. We adopted a straightforward

technique described by Petersen[5] to solve this type of contingency. Let variables X_{i1}, X_{i2}, and X_{i3} represent three different subitems that in combination would use nearly all the cable on reel$_i$. The variable X_{i4} is generated to represent the assignment of all these variables on that reel. A mutual exclusivity constraint (described in the appendix, Section A.3, item a) ensures that X_{i4} will not be allowed in the solution with X_{i1}, X_{i2}, and X_{i3}. If the combination is selected, then $X_{i4} = 1$ and X_{i1}, X_{i2}, and $X_{i3} = 0$. If the combination is not selected, $X_{i4} = 0$ and X_{i1}, X_{i2}, and $X_{i3} = 0$ or 1.

The second condition, the subitem linkage contingency, is formulated in the model as an absolute set of constraint equalities. A set of constraints for three linked subitems would be:

$$\sum_{p \in R} X_{p1} - \sum_{p \in R} X_{p2} = 0 \tag{1}$$

$$\sum_{p \in R} X_{p2} - \sum_{p \in R} X_{p3} = 0, \tag{2}$$

where X_{p1}, X_{p2}, X_{p3} represent subitems 1, 2, and 3, respectively, assigned to any reel p where p is an element of the reels$_R$ of plant P.

These equality constraints must be satisfied. If any of the three subitems were assigned, then the other two subitems also must be assigned to a reel of cable at the same plant. Bringing an X_{p1} into solution, for instance, would produce an infeasible condition, unless a corresponding X_{p2} and a corresponding X_{p3} were also brought into solution. If this could not be done because of other constraints, then the assignment of subitems 1, 2, or 3 would not be allowed.

3.2 The algorithm

The algorithm incorporates two sets of real variables: (1) those in solution, designated the IS set; and (2) those in the NS set, which are out of solution but candidates for inclusion in the IS set. Using the constructive initial placement method, all variables are initially placed in the NS set and the initial value of the achievement function of the model is calculated. To determine which variable is brought into solution, the net effect on the achievement function is calculated individually for each member of the NS set and assigned to that member. This effect is determined by summing, for each member, the contribution of every slack variable of each objective that would be affected if the member were brought into solution. The NS set is then sorted by these net effects. Next, members are selected individually starting from the top of this set for "fit" within the model formulation. If the variable fits, it is removed from the NS set, placed in the IS set, a new achievement function value is calculated, and the NS set reprioritized. If a member cannot be feasibly fit, it is dismissed from the NS set and the next member is tried. This process continues until

the NS set is exhausted. The feasibility of the problem is then verified by testing the equality constraints. If any equality condition is not met, all real variables with a nonzero coefficient in the violated equality constraint are removed from both the IS set and the NS set to rectify the infeasible constraint violation. The NS set is reconstructed by placing into it all variables that are not in solution or that have not been eliminated because of this or any previously rectified equality constraint violation. The new achievement function value is then calculated and all variables in the NS set are reprioritized. The entire procedure from variable fitting through ensuring equality constraint feasibility is repeated until no equality violation is found.

3.3 The model

The model for this assignment application is formulated from input of a stock cable inventory and customer orders. For each product type we consider a separate problem. There are 14 possible objective types and 12 preemptive priorities. (See the appendix for the mathematical formulation.)

1. Subitem contingency (Priority = absolute)—To guarantee timely shipments, all linked subitems must be assigned at the same time at the same stocking location.

2. Reel capacity (Priority = absolute)—The reel capacity objective type ensures that the total of subitem lengths assigned to a real plus all cutting allowances cannot exceed the length of cable on that reel.

3. Combinations (Priority = 5)—Since a reel of cable is eliminated from inventory and reel handling is greatly minimized, this objective type, which encourages a good fit of multiple subitems to a single reel of cable, is accorded high priority. To further minimize reel handling, the model encourages combinations involving the largest number of subitems rather than smaller combinations.

4. Perfect one-to-one matches (Priority = 4)—This objective type encourages perfect and close (up to 20 feet short of cable length) individual subitem length to cable length matches. The benefits are those of eliminating reels of cable and of minimizing reel handling.

5. Assignment of future subitems (Priority = absolute)—A lateness factor is calculated for every subitem. It is based on when the customer wants the cable and takes into account the amount of time required to process and ship the subitem from the time it is received. Subitems that need to be assigned in this week's processing cycle in order to arrive at the job site on time are considered current subitems. Future subitems need not be assigned yet. Hence, future subitems are not assigned unless their assignment eliminates short remnant pieces that had been generated by the assignment of current and late subitems. Subitem linkage rules also apply to future subitems.

6. Assignment of current and late subitems (Priority = 6)—To guarantee that customers are satisfied, the assignment of current and late subitems is encouraged by this objective type. These objectives are weighted by the lateness factor of the associated subitem and more consideration is given to subitems the later they become. They are also weighted by order length so that the large subitems can be placed on the large reels first, while the large reels of cable are still available.

7. Forced subitems (Priority = 6)—In emergency situations, subitems can be entered with a force code indicating that they should be assigned before all nonforced subitems. Even though the preemptive priority is the same, the weighting factor on this objective type is larger than for any nonforced subitem, hence they receive greater consideration.

8. Use of full reels (Priority = 7)—This objective type encourages using all or almost all the cable on a reel when customer orders are assigned.

9. Minimization of scrap (Priority = 8)—This objective type minimizes assignments that cause cable to be scrapped. If cable must be scrapped, it also minimizes the amount scrapped. It is the only nonlinear objective type in the formulation.

10. Remnants of just over the scrapping limit (Priority = 9)—Since few subitems are desired for an amount less than 50 feet over the scrapping limit, this objective type is formulated to prevent assignments from leaving less than this amount on any reel, thereby keeping carrying costs to a minimum.

11. Remnants of less than 500 feet (Priority = 10)—Since approximately 80 percent of the subitems are for 500 feet or more, assignments that leave remaining cable lengths less than 500 feet are not desirable. This objective type provides this.

12. Use of minimum number of reels and largest reel (Priority = 11, 12)—This objective type encourages using as few reels as possible (Priority 11). The use of the largest reel is also encouraged (Priority 12).

13. Vacation (Priority = 1, 2)—This objective type accommodates shutdowns of stocking location in a multilocation stocking environment. To avoid adversely affecting customer service due to a scheduled shutdown at a particular location, subitems will be assigned against inventories at locations that are not shut down because of vacation or other causes.

14. Transportation (Priority = 3)—Transportation charges differ depending on the distance from the stocking location to the customer job site. Overall transportation charges are minimized by this objective type.

IV. PROCESSING IMPROVEMENTS

The algorithm has undergone considerable enhancement since the initial form was coded. Because it began producing good results using the constructive initial placement technique alone, the need to perform subsequent time-consuming iterative improvements was eliminated.

After we obtained good results with the algorithm, the problem of computer core size and run time was looked at extensively. The amount of core required was quickly reduced by trimming what was unnecessary in Lee's goal programming simplex tableau.[6] Because the simplex tableau is not executed, the sparse simplex tableau was replaced by dense lists. This allowed us to handle a much larger number of variables and objectives.

Reprioritizing the members of the NS set requires the largest segment of run time. This area was improved with several enhancements. When reprioritizing each member of the NS set, we found that many members could not be feasibly fit, given the set of variables already fit. Since constructive initial placement is a "block building" approach (once a variable is fit, it will never leave the solution at any time before the feasibility of the equality constraints is tested), we enhanced the procedure by removing the members from the NS set during reprioritizing. This considerably cut the size of the NS set. For instance, after a subitem is assigned, all associations of that subitem with other reels can be dropped from the NS set. Another large reduction was realized when we decided to recalculate the effect on the achievement function only for members of the NS set that are affected by the real variable just fit.

A further reduction in the execution time was realized in the handling of future subitems. Since a future subitem is only fit to prevent a remnant cable length less than 500 feet from being generated, the futures only need to be considered after all the current and late subitems have been considered. Also, only future subitems less than 500 feet need be considered since those over 500 feet will not improve the solution.

Run time for solving all 26 problems has varied based on the weekly mix, from 30 seconds to 30 minutes in the central processing unit (CPU) on an IBM 3033.

V. OPTIMALITY CONSIDERATIONS

This algorithm is constructive initial placement in the strict sense. Each iteration is performed without knowledge of its effect on other iterations. Also, once a variable is brought into solution, it will never be removed unless equality conditions are not met. Even though each iteration improves the result, the optimum may not, of course, be

obtainable without a subsequent exchange of in-solution with out-of-solution real variables. A method of variable exchanging was not implemented because, with our subitem linkage restrictions, it would call for exchanges of the magnitude of 26/15 (26 variables in-solution exchanged for 15 variables out-of-solution) or more. An exchange algorithm would require a tremendous amount of time just to decide that a 26/15 exchange was necessary. Fortunately, due to our methods of eliminating certain assignments and identifying combinations of good fit prior to model generation, suboptimal solutions have been found empirically in only 2 percent of the solutions.

VI. EASE OF USE

This method of solution comprises the model and the algorithm. The model provides direction for the algorithm in its attempt to find an optimal solution.

If new objectives are added or existing ones are changed, the model can easily be modified and the algorithm need not be changed. The algorithm can operate on any objective with zero-one real variables in which either maximization or minimization of the slack or real variables is desired. The result of the exponentiation operation on variables can also be maximized or minimized. Variable interaction (i.e., $d_1^- d_2^- = 10$), however, is not provided for.

Since its initial implementation in August 1981, the model has undergone one revision. It was changed to handle two types of subitems: (1) the subitems as previously described, and (2) subitems with a shipping policy tolerance and cutting allowance different from those previously described. Some objective types in the model required modification to provide for this but the algorithm has not required modification to accommodate model changes.

It is also important that the algorithm was coded in such a way that our use of multiple preemptive priorities has only a minimal effect on computer processing time.

VII. CONCLUSION

Assignment problems of large size are difficult to solve. Hence, a great deal of attention among operations researchers has been devoted to the subject. To our knowledge, as yet no usable technique guarantees optimal solutions to large problems. Large assignment problems with the additional complexities of this particular assignment problem are even more difficult to solve. The nonlinear zero-one combinatorial goal programming model with constructive initial placement algorithm that we developed solves large and complex assignment problems satisfactorily. It is efficient, easy to modify, and produces good results.

REFERENCES

1. R. S. Liggett, "The Quadratic Assignment Problem: An Experimental Evaluation of Solution Strategies," Manage. Sci., *27*, No. 4 (April 1981), pp. 442–58.
2. J. P. Ignizio, *Goal Programming and Extensions*, Lexington, MA: D. C. Heath and Co., 1976, pp. 202–6.
3. C. S. Parker, "An Experimental Investigation of Some Heuristic Strategies for Component Placement," Oper. Res. Quart., *27*, No. 1, i (1976), pp. 71–81.
4. G. W. Graves and A. G. Whinston, "An Algorithm for the Quadratic Assignment Problem," Manage. Sci., *16*, No. 7 (March 1970), pp. 453–71.
5. C. C. Petersen, "A Capital Budgeting Heuristic Algorithm Using Exchange Operations," AIEE Trans., *6*, No. 2 (June 1974), pp. 143–50.
6. S. M. Lee, *Goal Programming for Decision Analysis*, Philadelphia, PA: Auerback Publishers Inc., 1972.

APPENDIX

The Mathematical Formulation (Initial Implementation Formulation—August 1981)

Let:

R_i = Reel$_i$ of cable large enough to hold subitem$_j$
S_j = Subitem$_j$ that can be taken from reel$_i$ of cable
X_{ij} = 1 if subitem$_j$ assigned to reel$_i$, 0 otherwise
CA = 2 (Cutting Allowance)
SA_j = Amount ordered on subitem$_j$
RC_i = Amount of cable on reel$_i$
$LATENESS_j$ = Degree of lateness of subitem$_j$
SP = Shipping policy (assignment) tolerance
SL = Maximum amount allowed to scrap
$d^-, d^+ \geq 0$

A.1 Subitem contingency

$$\sum_{\substack{\text{ALL } R_i \\ \text{ON PLANT}_p \\ \text{OF LINKUP}_k}} X_{ij} = \sum_{\substack{\text{ALL REELS}_i \\ \text{ON PLANT}_p \\ \text{LARGE ENOUGH FOR} \\ \text{SUBITEM}_{j+1} \text{ OF} \\ \text{LINKUP}_k}} X_{ij+1}$$

$$\cdot \forall \text{ LINKUP}_k, \text{ SUBITEM}_j \text{ OF LINKUP}_k, \text{ PLANT}_p$$

where $1 \leq j <$ number of subitems in LINKUP$_k$,

where LINKUP$_k$ = subitem contingency of subitems involving SUBITEM$_j$.

A.2 Reel capacity

$$\sum_{\text{ALL } S_j} (SA_j + CA)X_{ij} + d_{2i}^- = RC_i + CA \ \forall \text{ REEL}_i$$

A.3 Combinations

a. $$\sum_{\substack{\text{ALL SUBITEMS}_j \\ \text{IN GOOD MATCH} \\ \text{ON REEL}_i}} X_{ij} + (\text{NOSUBFIT}_i)X_g + d_{3i}^- = \text{NOSUBFIT}_i$$

$\cdot \forall$ REEL$_i$ where a MATCH$_g$ exists

b. $X_g + d_{3Bi}^- = 1 \; \forall$ MATCH$_g$

$$WEIGHT = 500 - \text{FITDIFF}_i + (\text{NOSUBFIT}_i 1000),$$

where FITDIFF$_i$ = the footage short of an absolutely perfect match

NOSUBFIT$_i$ = the number of subitems in the fit on REEL$_i$

X_g is a variable generated to represent MATCH$_g$

Minimize at Priority 5: $(d_{3Bi}^- \; WEIGHT) \; \forall_i$.

A4. Perfect one-to-one matches

$X_{ij} + d_{4ij}^- = 1 \; \forall$ REEL$_i$, SUBITEM$_j$ where a one-to-one match exists

$$WEIGHT = (10{,}000{,}000 - (SA_j 1000) + (1000 - \text{REELRANK}_i),$$

where REELRANK$_i$ = ranking of REEL$_i$ relative to other reels by amount of cable on reel

Minimize at Priority 4: $(d_{4ij}^- \; WEIGHT) \; \forall_{i,j}$.

A.5 Assignment of future subitems

$$\sum_{\substack{\text{ALL FUTURE} \\ S_j}} X_{ij} - \infty \sum_{\substack{\text{ALL CURR.} \\ \text{AND LATE} \\ S_j}} X_{ij} + d_{5i}^- = 0 \; \forall \text{ REEL}_i$$

A.6 Assignment of current and late subitems

$$\sum_{\text{ALL } R_i} X_{ij} + d_{6j}^- = 1 \; \forall \text{ SUBITEM}_j$$

$WEIGHT$ = [(LATENESS$_j$ + 1)100,000] + SA_j, if SUBITEM$_j$ not future; 0, if SUBITEM$_j$ is future

Minimize at Priority 6: $(d_{6j}^- \; WEIGHT) \; \forall_j$.

A.7 Forced subitems

$$\sum_{\substack{\text{ALL FORCED} \\ \text{SUBITEMS}_j}} \sum_{\text{ALL } R_i} X_{ij} + d_7^- = \infty$$

$WEIGHT = 1{,}000{,}000$

Minimize at Priority 6: $(d_7^- \ WEIGHT)$.

A.8 Use of full reels

$$\sum_{\text{ALL } S_j} (SA_j + CA + SP)X_{ij} + d_{8i}^- - d_{8i}^+ = RC_i + CA - 51 \ \forall \ \text{REEL}_i$$

Maximize at Priority 7: $d_{8i}^+ \ \forall_i$.

A.9 Minimization of scrap

$$\sum_{\text{ALL } S_j} (SA_j + CA + SP)X_{ij} + d_{9i}^- - d_{9i}^+ = RC_i - SL + CA \ \forall \ \text{REEL}_i$$

Minimize at Priority 8: $(1/d_{9i}^+) \ \forall_i$.

A.10 Remnants of just over the scrapping limit

$$\sum_{\text{ALL } S_j} (SA_j + CA)X_{ij} + d_{10i}^- - d_{10i}^+ = RC_i - SL - 50 \ \forall \ \text{REEL}_i$$

Minimize at Priority 9: $d_{10i}^+ \ \forall_i$.

A.11 Remnants of less than 500 feet

$$\sum_{\text{ALL } S_j} (SA_j + CA)X_{ij} + d_{11i}^- - d_{11i}^+ = RC_i - 500 \ \forall \ \text{REEL}_i$$

Minimize at Priority 10: $d_{11i}^+ \ \forall_i$.

A.12 Use of minimum number of reels and largest reel

$$\sum_{\text{ALL } S_j} X_{ij} + d_{12i}^- - d_{12i}^+ = 1 \ \forall \ \text{REEL}_i$$

Maximize at Priority 11: $d_{12i}^- \ \forall_i$
Minimize at Priority 12: $(RCd_{12i}^-) \ \forall_i$.

A.13 Vacation

a. $$\sum_{\substack{\text{ALL CURRENT} \\ \text{AND LATE} \\ S_j}} \ \sum_{\substack{\text{ALL REELS}_i \\ \text{OF PLANTS} \\ \text{NOT ON} \\ \text{VACATION} \\ \text{DURING} \\ \text{PREPARATION} \\ \text{OF SUBITEM}_j}} X_{ij} + d_{13a}^- = \infty$$

Minimize at Priority 1: d_{13a}^-.

b. $$\sum_{\substack{\text{ALL CURRENT} \\ \text{AND LATE} \\ S_j}} \ \sum_{\substack{\text{ALL REELS}_i \\ \text{OF PLANTS} \\ \text{ON VACATION} \\ \text{ONE WEEK} \\ \text{DURING} \\ \text{PREPARATION} \\ \text{OF SUBITEM}_j}} X_{ij} + d_{13b}^- = \infty$$

Minimize at Priority 2: d_{13b}^{-}.

A.14 Transportation

$$\sum_{\text{ALL SUBITEMS}_j} \sum_{\text{ALL } R_i} \{[1{,}000{,}000(LATENESS_j + 1)]/$$

$$(TRANSPRT_{ij}SA_j) + 1\}X_{ij} + d_{14}^{-} = \infty,$$

where $TRANSPRT$ = transportation rate from stocking location of REEL_i to job site of SUBITEM_j

Minimize at Priority 3: d_{14}^{-}.

Note: For generated variables representing a combination of good match, $LATENESS_j$ is the largest degree of lateness of all orders represented by the generated variable.

AUTHORS

Julian H. Fletcher, B.S. (Industrial Engineering), 1970, Georgia Institute of Technology; AT&T Technologies, Inc., 1970—. Mr. Fletcher's assignments include design and implementation of aggregate plant loading and inventory management systems for products manufactured within the Cable and Wire Division of AT&T Technologies, Inc. He is in the Information Systems Development Organization at the Atlanta Works. Member, the Institute of Management Sciences (TIMS).

Kenneth R. Lipske, B.S. (Mathematics), 1970, University of Wisconsin, Eau Claire; AT&T Technologies, Inc., 1970—. Mr. Lipske's assignments entail optimizing the aggregate plant loading and inventory management functions for the various product lines manufactured by the Cable and Wire Division of AT&T Technologies, Inc. He is in the Information Systems Development Organization at the Atlanta Works. Member, The Institute of Management Sciences (TIMS).

PAPERS BY AT&T BELL LABORATORIES AUTHORS

COMPUTING/MATHEMATICS

Adleman L. M., Odlyzko A. M., **Irreducibility Testing and Factorization of Polynomials.** Math Comput 41(164):699–709, 1983.

Allen R. B., Scerbo M. W., **Details of Command-Language Keystrokes.** ACM T Offic 1(2):159–178, 1983.

Barmish B. R., Petersen I. R., Feuer A., **Linear Ultimate Boundedness Control of Uncertain Dynamical Systems.** Automatica 19(5):523–532, 1983.

Barron E. N., Jensen R., **A Nonlinear Evolution System With Two Subdifferentials and Monotone Differential Games.** J Math Anal 97(1):65–80, 1983.

Bentley J., **Cracking the Oyster (Editorial).** Comm ACM 26(8):550–552, 1983.

Borkovitz D., Hwang F. K., **Multiplicative Magic Squares.** Discr Math 47(1):1–11, 1983.

Brown M. K., Ganapathy S., **Preprocessing Techniques for Cursive Script Word Recognition.** Patt Recog 16(5):447–458, 1983.

Chung F. R. K., **Unavoidable Stars in Three Graphs.** J Comb Th A 35(3):252–262, 1983.

Conway J. H., Sloane N. J. A., **A Fast Encoding Method for Lattice Codes and Quantizers.** IEEE Info T 29(6):820–824, 1983.

Erdos P., Mullin R. C., Sos V. T., Stinson D. R., **Finite Linear Spaces and Projective Planes.** Discr Math 47(1):49–62, 1983.

Fishburn P. C., **Interval Lengths for Interval Orders—A Minimization Problem.** Discr Math 47(1):63–82, 1983.

Garey M. R., **Combinatorial Optimization—Algorithms and Complexity—Papadimitriou C. H., Steiglitz K. (Book Review).** Am Scient 71(6):658, 1983.

Garey M. R., Johnson D. S., **Crossing Number is NP-Complete.** Siam J Alg 4(3):312–316, 1983.

Gershenfeld N. A., Schadler E. H., Bilaniuk O. M., **APL and the Numerical Solution of High-Order Linear-Differential Equations.** Am J Phys 51(8):743–746, 1983.

Johnson D. S., Klug A., **Optimizing Conjunctive Queries That Contain Untyped Variables.** SIAM J Comp 12(4):616–640, 1983.

Larson R. G., **Elongational-Flow Predictions of the Leonov Constitutive Equation.** Rheol Act 22(5):435–448, 1983.

Levy L. S., **A Walk Through AWK.** Sigplan Not 18(12):69–85, 1983.

Lu P. M., Yau S. S., Hong W., **A Formal Methodology Using Attributed Grammars for Multiprocessing-System Software Development. 1. Design Representation.** Inf Sci 30(2):79–105, 1983.

Lu P. M., Yau S. S., Hong W., **A Formal Methodology Using Attributed Grammars for Multiprocessing-System Software-Development. 2. Validation.** Inf Sci 30(2):107–123, 1983.

Luss H., **An Extended Model for the Optimal Sizing of Records.** J Oper Res 34(11):1099–1105, 1983.

Mitra D., Morrison J. A., **Asymptotic Expansions of Moments of the Waiting Time in a Shared-Processor of an Interactive System.** Siam J Comp 12(4):789–802, 1983.

Petersen W. P., **Vector FORTRAN for Numerical Problems on CRAY 1.** Comm ACM 26(11):1008–1021, 1983.

Vo K. P., Whitney R., **Tableaux and Matrix Correspondences.** J Comb Th A 35(3):328–359, 1983.

ENGINEERING

Agrawal G. P., Dutta N. K., **Effect of Auger Recombination on the Threshold Characteristics of Gain-Guided InGaAsP Lasers.** Electr Lett 19(23):974–976, 1983.

Alferness R. C., Joyner C. H., Buhl L. L., Korotky S. K., **High-Speed Traveling-Wave Directional Coupler Switch Modulator for Lambda = 1.32 μm.** IEEE J Q El 19(9):1339–1341, 1983.

Bhatt R. N., Lee P. A., **Low-Temperature Conductivity of Doped Semiconductors—Mass Anisotropy and Intervalley Effects.** Sol St Comm 48(9):755–759, 1983.

Chraplyvy A. R., Kaminow I. P., Dentai A. G., **Evaluation of InGaAsP Laser Material by Optical Pumping.** IEEE J Q El 19(9):1342–1344, 1983.

Citrin P. H., Rowe J. E., **Local-Structure of Adsorbates on Semiconductor Surfaces Using SEXAFS—A Brief Summary.** Surf Sci 132(1–3):205–211, 1983.

Dupuis R. D., Hartman R. L., Nash F. R., **Facet-Coated Graded-Index Separate-Confinement-Heterostructure Single-Quantum-Well Lasers Having Low Degradation Rates (L1 Percent/kh) at 70 Degrees C.** IEEE Elec D 4(8):286–288, 1983.

Engelmaier W., **Fatigue Life of Leadless Chip Carrier Solder Joints During Power Cycling.** IEEE Compon 6(3):232–237, 1983.

Gans M. J., Amitay N., **Narrow Multibeam Satellite Ground Station Antenna Employing a Linear Array With a Geosynchronous Arc Coverage of 60 Degrees. 2. Antenna Design.** IEEE Antenn 31(6):966–972, 1983.

Haskell B. G., **High Definition Television (HDTV)—Compatibility and Distribution (Letter).** IEEE Commun 31(12):1308–1317, 1983.

Heimann P. A., **An Operational Definition for Breakdown of Thin Thermal Oxides of Silicon.** IEEE Device 30(10):1366–1368, 1983.

Henry C. H., **Theory of the Phase Noise and Power Spectrum of a Single-Mode Injection Laser.** IEEE J Q El 19(9):1391–1397, 1983.

Hsu F. C., Muller R. S., Hu C. M., Ko P. K., **A Simple Punchthrough Model for Short-Channel MOSFETs.** IEEE Device 30(10):1354–1359, 1983.

Johnson A. M., Simpson W. M., **Continuous-Wave Mode-Locked Nd:YAG-Pumped Subpicosecond Dye Lasers.** Optics Lett 8(11):554–556, 1983.

Kaminow I. P., Ko J. S., Linke R. A., Stulz L. W., **High-Speed 1.55 μm Single-Longitudinal-Mode Ridge Wave-Guide C3 Laser.** Electr Lett 19(19):784–785, 1983.

Kavehrad M., **Adaptive Decision Feedback Cancellation of Intersymbol Interference Over Multipath Fading Radio Channels.** ICC 2: C8.5.1–C8.5.3, 1983.

Knausenberger W. H., Teneketges N. A., **High Pinout-IC Packaging and the Density Advantage of Surface Mounting.** IEEE Compon 6(3):298–304, 1983.

Kuo W., Kuo Y., **Facing the Headaches of Early Failures—A State-of-the-Art Review of Burn-In Decisions (Review).** P IEEE 71(11):1257–1266, 1983.

Lamorte M. F., Abbott D. H., **Influence of Band-Gap Span on Cascade Solar-Cell Efficiency.** Solar Cells 10(1):33–48, 1983.

Leheny R. F., Liao A., Tell B., Mayer L., **Integrated Photoreceivers for Long Wavelength Communications Systems—Is the Technology Ready?** P Soc Photo 408:115–120, 1983.

Linke R. A., Kasper B. L., Ko J. S., Kaminow I. P., Vodhanel R. S., **1 Gbit/s Transmission Experiment Over 101 km of Single-Mode Fiber Using a 1.55 μm Ridge Guide C^3 Laser.** Electr Lett 19:775–776, 1983.

Liu P. L., Fencil L. E., Ko J. S., Kaminow I. P., Lee T. P., Burrus C. A., **Amplitude Fluctuations and Photon Statistics of InGaAsP Injection Lasers.** IEEE J Q El 19(9):1348–1351, 1983.

Manheimer M. A., Bhagat S. M., Chen H. S., **Reentrant Magnetism—A Low Field Study.** J Magn Magn 38(2):147–158, 1983.

Marcuse D., Lee T. P., **On Approximate Analytical Solutions of Rate-Equations for Studying Transient Spectra of Injection Lasers.** IEEE J Q El 19(9):1397–1406, 1983.

Netravali A. N., Pirsch P., **Character Display on a CRT.** IEEE Broadc 29(3):106–110, 1983.

Ross I. M., **Technology for Tomorrow (Editorial).** IEEE Comm M 21(9):42–45, 1983.

Schaper L. W., Amey D. I., **Improved Electrical Performance Required for Future MOS Packaging.** IEEE Compon 6(3):283–289, 1983.

Schwab T. F., Yau S. S., **An Algebraic Model of Fault-Masking Logic Circuits.** IEEE Comput 32(9):809–825, 1983.

Sproles E. S., Sharma S. P., **Effect of HCl and Cl_2 on Pd-Inlay Coupons and Pd-Connector Contacts.** IEEE Compon 6(3):343–348, 1983.

Stolen R. H., **Applications of Nonlinear Phenomena in Optical Fibers.** P Soc Photo 408:156–162, 1983.

Tsang W. T., Olsson N. A., Logan R. A. Ditzenberger J. A., Kaminow I. P., Ko J. S., **Single-Longitudinal Mode Performance—Characteristics of Cleaved-Coupled-Cavity Lasers.** Appl Phys L 43(11):1003–1005, 1983.

Worlock J. M., **Wave Vector Dependent Magneto-Optical Interband Transitions in Semiconductors.** Sol St Comm 48(12):1067–1070, 1983.

MANAGEMENT/ECONOMICS

Fishburn P. C., **Transitive Measurable Utility.** J Econ Theo 31(2):293–317, 1983.

Gilstein C. Z., Leamer E. E., **Robust Sets of Regression Estimates.** Econometric 51(2):321–333, 1983.

Gordon R. H., **An Optimal Taxation Approach to Fiscal Federalism.** Q J Econ 98(4):567–586, 1983.

Norman A. L., Lasdon L. S., Hsin J. K., **A Comparison of Methods for Solving and Optimizing a Large Nonlinear Econometric Model.** J Econ Dyn 6(1–2):3–24, 1983.

Stiglitz J. E., Weiss A., **Incentive Effects of Terminations—Applications to the Credit and Labor Markets.** Am Econ Rev 73(5):912–927, 1983.

PHYSICAL SCIENCES

Abrahams S. C., Liminga R., Marsh P., Schrey F., Albertsson J., Svensson C., Kvick A., **Thermal Expansivity of α-$LiIO_3$ Between 20 and 520K.** J Appl Crys 16(OCT):453–457, 1983.

Aeppli G. et al., **Spin Correlations and Reentrant Spin-Glass Behavior in Amorphous Fe-Mn Alloys—Statics.** Phys Rev B 28(9):5160–5172, 1983.

Aharonshalom E., Heller A., **Injection Electro-Luminescence of N-InP in Dilute Nitric Acid.** J Phys Chem 87(24):4913–4918, 1983.

Aspnes D. E., Heller A., **Photoelectrochemical Hydrogen Evolution and Water-Photolyzing Semiconductor Suspensions—Properties of Platinum Group Metal Catalyst Semiconductor Contacts in Air and in Hydrogen.** J Phys Chem 87(24):4919–4929, 1983.

Bacon D. D., English A. T., Nakahara S., Peters F. G., Schreiber H., Sinclair W. R., Vandover R. B., **Properties of NbN Thin Films Deposited on Ambient-Temperature Substrates.** J Appl Phys 54(11):6509–6516, 1983.

Bondybey V. E., English J. H., **Electronic Structure and Spectra of SnBi.** J Chem Phys 79(10):4746–4748, 1983.

Bondybey V. E., English J. H., **Observation and Characterization of a New Electronic State of Cu-2 in Solid Neon.** J Phys Chem 87(23):4647–4650, 1983.

Bowmer T. N., Vroom W. I., **Radiation Crosslinking of Poly(vinyl-Chloride) With Trimethylolpropanetrimethacrylate. 4. Effect of Diundecyl Phthalate—Dependence of Physical Properties on Composition.** J Appl Poly 28(11):3527–3548, 1983.

Brasen D., Bonner W. A., **Effect of Temperature and Sulfur Doping on the Plastic Deformation of InP Single Crystals.** Mater Sci E 61(2):167–172, 1983.

Braun C. L., Scott T. W., **Picosecond Measurements of Time-Resolved Geminate Charge Recombination (Letter).** J Phys Chem 87(24):4776–4778, 1983.

Broughton J. Q., Gilmer G. H., **Molecular-Dynamics Investigation of the Crystal Fluid Interface. 1. Bulk Properties.** J Chem Phys 79(10):5095–5104, 1983.

Broughton J. Q., Gilmer G. H., **Molecular-Dynamics Investigation of the Crystal Fluid Interface. 2. Structures of the FCC (111), (100), and (110) Crystal Vapor Systems.** J Chem Phys 79(10):5105–5118, 1983.

Broughton J. Q., Gilmer G. H., **Molecular-Dynamics Investigation of the Crystal Fluid Interface. 3. Dynamical Properties of FCC Crystal Vapor Systems.** J Chem Phys 79(10):5119–5127, 1983.

Brus L. E., **A Simple Model for the Ionization Potential, Electron Affinity, and Aqueous Redox Potentials of Small Semiconductor Crystallites.** J Chem Phys 79(11):5566–5571, 1983.

Burton R. H., Hollien C. L., Marchut L., Abys S. M., Smolinsky G., Gottscho R. A., **Etching of Gallium-Arsenide and Indium-Phosphide in RF Discharges Through Mixtures of Trichlorofluoromethane and Oxygen.** J Appl Phys 54(11):6663–6671, 1983.

Capasso F., Alavi K., Cho A. Y., Foy P. W., Bethea C. G., **New Long Wavelength $Al_{0.48}In_{0.52}As/Ga_{0.47}In_{0.53}As$ Avalanche Photo-Diode Grown by Molecular-Beam Epitaxy.** Appl Phys L 43(11):1040–1042, 1983.

Capasso F., Luryi S., Tsang W. T., Bethea C. G., Levine B. F., **New Transient Electrical-Polarization Phenomenon in Sawtooth Super Lattices.** Phys Rev L 51(25):2318–2321, 1983.

Capasso F., Tsang W. T., Hutchinson A. L., Bethea C. G., Levine B. F., **Novel Graded Band-Gap Photodetectors With Ultrahigh Speed of Response (t_r = 20 ps, FWHM = 40 ps) and Phototransistors with Graded Gap Base.** Inst Phys C1983(65):225–231, 1983.

Cava R. J., Murphy D. W., Zahurak S. M., **Lithium Insertion in Wadsley-Roth Phases Based on Niobium Oxide.** J Elchem So 130(12):2345–2351, 1983.

Cava R. J., Santoro A., Murphy D. W., Zahurak S. M., Roth R. S., **The Structures of the Lithium Inserted Metal-Oxides $Li_{0.2}ReO_3$ and $Li_{0.36}WO_3$.** J Sol St Ch 50(1):121–128, 1983.

Chance B., Kumar C., Powers L., Ching Y., **Peroxidatic Form of Cytochrome-Oxidase as Studied by X-Ray Absorption Spectroscopy.** Biophys J 44(3):353–363, 1983.

Chen C. H., Fleming R. M., **Strandlike Microstructures in the Charge-Density Wave States of Orthorhombic TaS_3.** Sol St Comm 48(9):777–779, 1983.

Chen H. S., Kurkjian C. R., **Sub-Sub-T_g Enthalpy Relaxation in a B_2O_3 Glass.** J Am Ceram 66(9):613–619, 1983.

Chu S. N. G., Jodlauk C. M., Johnston W. D., **Morphological Study of Thermal Decomposition of InP Surfaces.** J Elchem So 130(12):2398–2405, 1983.

Cohen R. L., West K. W., **Intrinsic Cycling Degradation in $LaNi_5$ and Annealing Procedures for Reforming the Material.** J Lessc Met 95(1):17–23, 1983.

Coppersmith S. N., **Scaling Behavior Near the Pinning Transition of the Discrete Frenkel-Kontorova Model.** J Physique 44(NC-3):1579–1582, 1983.

Digiuseppe M. A., Temkin H., Peticolas L., Bonner W. A., **Quantum Well Structures of $In_{0.53}Ga_{0.47}As/InP$ Grown by Hydride Vapor-Phase Epitaxy in a Multiple Chamber Reactor.** Appl Phys L 43(10):906–908, 1983.

Duncan T. M., Winslow P., Bell A. T., **C-13 NMR Spectra of Carbonaceous Deposits on Silica-Supported Ruthenium Catalysts.** Chem P Lett 102(2–3):163–167, 1983.

Fleming R. M., Chen C. H., Moncton D. E., **Electric-Field-Induced Structural Changes in $NbSe_3$.** J Physique 44(NC-3):1651–1658, 1983.

Forrest S. R., Kim O. K., Smith R. G., **Analysis of the Dark Current and Photoresponse of $In_{0.53}Ga_{0.47}As/InP$ Avalanche Photodiodes.** Sol St Elec 26(10):951–968, 1983.

Graedel T. E., Franey J. P., Kammlott G. W., **The Corrosion of Copper by Atmospheric Sulfurous Gases.** Corros Sci 23(11):1141+, 1983.

Gross B., Von Seggern H., Berkley D. A., **Long-Term Behavior of Radiation-Induced Currents in Fluorinated Ethylene Propylene Co-Polymer.** Phys St S-A 79(2):607–615, 1983.

Guntherodt G., Jayaraman A., Batlogg G., Croft M., Melczer E., **Raman Scattering From Coupled Phonon and Electronic Crystal-Field Excitations in $CeAl_2$.** Phys Rev L 51(25):2330–2332, 1983.

Habbal F., Bevk J., **Interface Flux Pinning in Insitu Formed Superconducting Composites.** J Appl Phys 54(11):6543–6548, 1983.

Hayes J. R., Capasso F., Malik R. J., Gossard A. C., Wiegmann W., **Optimum Emitter Grading for Heterojunction Bipolar Transistors.** Appl Phys L 43(10):949–951, 1983.

Heiney P. A. et al., **X-Ray-Scattering Study of the Structure and Freezing Transition of Monolayer Xenon on Graphite.** Phys Rev B 28(11):6416–6434, 1983.

Hemenway B. R., Bowers J. E., Miller B. I., **Anisotropic Undercutting in (100) Indium-Phosphide.** Electr Lett 19(24):1049–1051, 1983.

Henein G. E., Wagner W. R., **Stresses Induced in GaAs by TiPt Ohmic Contacts.** J Appl Phys 54(11):6395–6400, 1983.

Henkel C., Wilson T. L., Walmsley C. M., Pauls T., **Formaldehyde Towards Compact H-II Regions—Densities and Isotope Ratios.** Astron Astr 127(2):388–394, 1983.

Hensel J. C., Halperin B. I., Dynes R. C., **Dynamical Model for the Absorption and Scattering of Ballistic Phonons by the Electron Inversion Layer in Silicon.** Phys Rev L 51(25):2302–2305, 1983.

Hilinski E. F., Milton S. V., Rentzepis P. M., **Picosecond Spectroscopy and Applications to Chemical and Biological Systems (Review).** ACS Symp S 1983(236):201–220, 1983.

Hou T. W., Mogab C. J., Wagner R. S., **Ion Milling Planarization for Magnetic-Bubble Devices.** J Vac Sci A 1(4):1801–1805, 1983.

Inoue A., Masumoto T., Hagiwara M., Chen H. S., **The Structural Relaxation Behavior of $Pd_{48}Ni_{32}P_{20}$, $Fe_{75}Si_{10}B_{15}$ and $Co_{72.5}Si_{12.5}B_{15}$ Amorphous Alloy Wire and Ribbon.** Scrip Metal 17(10):1205–1208, 1983.

Jindal R. P., **A Normalized Analytical Solution for the Capacitance Associated With Uniformly Doped Semiconductors at Equilibrium.** Sol St Elec 26(10):1005–1008, 1983.

Johnson D. W., Rabinovich E. M., Macchesney J. B., Vogel E. M., **Preparation of High-Silica Glasses from Colloidal Gels. 2. Sintering.** J Am Ceram 66(10):688–693, 1983.

Kastalsky A., Dingle R., Cheng K. Y., Cho A. Y., **Two-Dimensional Electron-Gas at an MBE-Grown, Selectively-Doped, $In_{0.53}Ga_{0.47}As/In_{0.52}Al_{0.48}As$ Interface.** Inst Phys C1983(65):181–185, 1983.

Kevan S. D., **Design of a High-Resolution Angle-Resolving Electron-Energy Analyzer.** Rev Sci Ins 54(11):1441–1445, 1983.

Kohl P. A., Wolowodiuk C., Ostermayer F. W., **The Photoelectrochemical Oxidation of (100), (111), and (111) N-InP and N-GaAs.** J Elchem So 130(11):2288–2293, 1983.

Lester M. I., Zegarski B. R., Miller T. A., **Laser-Induced Fluorescence Studies of Large and Small Molecular Cations Produced by Using Electron Bombardment in a Free Jet Expansion.** J Phys Chem 87(25):5228–5233, 1983.

Levinson M., Stavola M., Benton J. L., Kimerling L. C., **Metastable M-Center in InP—Defect-Charge-State Controlled Structural Relaxation.** Phys Rev B 28(10):5848–5855, 1983.

Lifshitz N., **Solubility of Implanted Dopants in Polysilicon—Phosphorus and Arsenic.** J Elchem So 130(12):2464–2467, 1983.

Meiboom S., Sammon M., Berreman D. W., **Lattice Symmetry of the Cholesteric Blue Phases.** Phys Rev A 28(6):3553–3560, 1983.

Miller R. C., Gossard A. C., **Some Effects of a Longitudinal Electric Field on the Photoluminescence of Paradoped GaAs-$Al_xGa_{1-x}As$ Quantum Well Heterostructures.** Appl Phys L 43(10):954–956, 1983.

Mitchell J. W. et al., **Microscale Homogeneity and Compositional Profiling of Borosilicate Glass Materials.** Mikroch Act 3(3–4):253–261, 1983.

Murphy D. W., Dye J. L., Zahurak S. M., **Alkali-Metal Insertion in the Pyrochlore Structure (Letter).** Inorg Chem 22(25):3679–3681, 1983.

Nakahara S., Abys J. A., Abys S. M., **Room-Temperature Diffusion-Induced Grain-Boundary Migration in the Fine-Grained Pd Side of Cu-Pd Diffusion Couples.** Mater Lett 2(2):155–159, 1983.

Paalanen M. A., Tsui D. C., Hwang J. C. M., **Parabolic Magnetoresistance From the Interaction Effect in a Two-Dimensional Electron Gas.** Phys Rev L 51(24):2226–2229, 1983.

Pearson D. S. et al., **Comparison of the Rheological Properties of Linear and Star-Branched Polyisoprenes in Shear and Elongational Flows.** J Pol Sc PP 21(11):2287–2298, 1983.

Pfeiffer L., Celler G. K., Kovacs T., Robinson M., **Suppression of Low-Angle Grain-**

Boundaries in Seeded Thick Si Films Recrystallized Between SiO_2 Layers. Appl Phys L 43(11):1048–1050, 1983.

Phillips J. M., Feldman L. C., Gibson J. M., McDonald M. L., **Epitaxial Growth of Alkaline-Earth Fluorides on Semiconductors.** Thin Sol Fi 107(3):217–226, 1983.

Pini R., Salimbeni R., Matera M., Lin C. L., **Wideband Frequency Conversion in the UV by Nine Orders of Stimulated Raman Scattering in a XeCl Laser Pumped Multimode Silica Fiber.** Appl Phys L 43(6):517–518, 1983.

Rabinovich E. M., Johnson D. W., Macchesney J. B., Vogel E. M., **Preparation of High-Silica Glasses from Colloidal Gels. 1. Preparation for Sintering and Properties of Sintered Glasses.** J Am Ceram 66(10):683–688, 1983.

Roth H. D., Schilling M. L., **Radical Cations of Tetraalkylcyclopropanes—The Cyclopropane Moiety as an Electron Donor.** J Am Chem S 105(23):6805–6808, 1983.

Schleyer P. V. et al., **The 1,2-Hydride Shift Barrier in the Phenyl Cation—An Abinitid Study.** J Chem S CH1983(22):1296–1298, 1983.

Seidel T. E., **Rapid Thermal Annealing of BF_2^+ Implanted, Preamorphized Silicon (Letter).** IEEE Elec D. 4(10):353–355, 1983.

Smith C. G., Okinaka Y., **High-Speed Gold Plating—Anodic Bath Degradation and Search for Stable Low Polarization Anodes.** J Elchem So 130(11):2149–2157, 1983.

Smith N. V., **Inverse Photoemission and Related Techniques.** Vacuum 33(10-1): 803–811, 1983.

Swaminathan V., Wagner W. R., Anthony P. J., **Effect of N-Type and P-Type Doping on the Microhardness of GaAs, (Al,Ga)As and Ga(As,Sb) Active Layers in 0.82 and 0.87 μm Injection Lasers.** J Elchem So 130(12):2468–2472, 1983.

Tarcha P. J., Fitch R. M., Dumais J. J., Jelinski L. W., **Particle Morphology of Self-Hydrolyzed Acrylate Polymer Colloids—A C-13 NMR and DSC Study.** J Pol Sc PP 21(11):2389–2402, 1983.

Teo B. K., **A Simple Electron Counting Rule for Close-Packed High Nuclearity Metal Clusters.** J Chem S CH1983(22);1362–1364, 1983.

Tonelli A. E., Belfiore L. A., **Solution Dipole Moments of Atactic Poly(Para-Chlorostyrene) and Poly(Para-Bromostyrene) and Their Dependence on Temperature and Solvent.** Macromolec 16(11):1740–1743, 1983.

Trimble L. E., Celler G. K., **Novel Laser Scanning Techniques for Si-on-Insulator Devices.** P Soc Photo 385:8–15, 1983.

Tu C. W., Forrest S. R., Johnston W. D., **Epitaxial InP/Fluoride/InP(001) Double Heterostructures Grown by Molecular Beam Epitaxy.** Appl Phys L 43(6):569–571, 1983.

Vasile M. J., **The Reaction Probability of XeF_2 With Silicon.** J Appl Phys 54(11):6697–6704, 1983.

Venkatesan T., Wolf T., Allara D., Wilkens B. J., Taylor G. N., **Synthesis of Novel Inorganic Films by Ion-Beam Irradiation of Polymer Films.** Appl Phys L 43(10):934–936, 1983.

Werner A., Hochheimer H. D., Strössner K., Jayaraman A., **High-Pressure X-Ray Diffraction Studies on H_gT_e and H_gS to 20 GPa.** Phys Rev B 28(6):3330–3334, 1983.

Wernick J. H., Hull G. W., Geballe T. H., Bernardini J. E., Waszczak J. V., **Superconductivity in Ternary Heusler Intermetallic Compounds.** Mater Lett 2(2):90–92, 1983.

Wertheim G. K. et al., **Unit Charge on Supported Gold Clusters in Photoemission Final State.** Phys Rev L 51(25):2310–2313, 1983.

Wilson B. A., Hu P., Jedju T. M., Harbison J. P., **Subnanosecond Radiative and Nonradiative Processes in Alpha-Si-H.** Phys Rev B 28(10):5901–5907, 1983.

Wilson R. J., Petroff P. M., **Cryopump and Sample Holder for Clean Reconstructed Surface Observations in a Transmission Electron Microscope.** Rev Sci Ins 54(11):1534–1537, 1983.

Wood D. L., Rabinovich E. M., Johnson D. W., Macchesney J. B., Vogel E. M., **Preparation of High-Silica Glasses from Colloidal Gels. 3. Infrared Spectrophotometric Studies.** J Am Ceram 66(10):693–699, 1983.

Yachandra V., Powers L., Spiro T. G., **X-Ray Absorption Spectra and the Coordi-**

nation Number of Zn and Co Carbonic Anhydrase as a Function of pH and Inhibitor Binding. J Am Chem S 105(22):6596–6604, 1983.

Yafet Y., **Conduction Electron-Spin Relaxation in the Superconducting State.** Phys Lett A 98(5–6):287–290, 1983.

SOCIAL AND LIFE SCIENCES

Scott T. W. et al., **Subunit Heterogeneity in the Structure and Dynamics of Hemoglobin—A Transient Raman Study.** FEBS Letter 158(1):68–72, 1983.

Wieland S. J., Gelperin A., **Dopamine Elicits Feeding Motor Program in *Limax maximus*.** J Neurosc 3(9):1735–1745, 1983.

SPEECH/ACOUSTICS

Duttweiler D. L., **Subsampling to Estimate Delay with Application to Echo Canceling.** IEEE Acoust 31(5):1090–1099, 1983.

CONTENTS, MAY–JUNE 1984

AT&T BELL LABORATORIES TECHNICAL JOURNAL is abstracted or indexed by *Abstract Journal in Earthquake Engineering, Applied Mechanics Review, Applied Science & Technology Index, Chemical Abstracts, Computer Abstracts, Current Contents/Engineering, Technology & Applied Sciences, Current Index to Statistics, Current Papers in Electrical & Electronic Engineering, Current Papers on Computers & Control, Electronics & Communications Abstracts Journal, The Engineering Index, International Aerospace Abstracts, Journal of Current Laser Abstracts, Language and Language Behavior Abstracts, Mathematical Reviews, Science Abstracts (Series A, Physics Abstracts; Series B, Electrical and Electronic Abstracts; and Series C, Computer & Control Abstracts), Science Citation Index, Sociological Abstracts, Social Welfare, Social Planning and Social Development,* and *Solid State Abstracts Journal.* Reproductions of the Journal by years are available in microform from University Microfilms, 300 N. Zeeb Road, Ann Arbor, Michigan 48106.

AT&T
Bell Laboratories